
[All ETDs from UAB](#)

[UAB Theses & Dissertations](#)

2002

Double cemented carbide: Microstructure-property relationships.

Xin Deng

University of Alabama at Birmingham

Follow this and additional works at: <https://digitalcommons.library.uab.edu/etd-collection>

Recommended Citation

Deng, Xin, "Double cemented carbide: Microstructure-property relationships." (2002). *All ETDs from UAB*. 5057.

<https://digitalcommons.library.uab.edu/etd-collection/5057>

This content has been accepted for inclusion by an authorized administrator of the UAB Digital Commons, and is provided as a free open access item. All inquiries regarding this item or the UAB Digital Commons should be directed to the [UAB Libraries Office of Scholarly Communication](#).

INFORMATION TO USERS

This manuscript has been reproduced from the microfilm master. UMI films the text directly from the original or copy submitted. Thus, some thesis and dissertation copies are in typewriter face, while others may be from any type of computer printer.

The quality of this reproduction is dependent upon the quality of the copy submitted. Broken or indistinct print, colored or poor quality illustrations and photographs, print bleedthrough, substandard margins, and improper alignment can adversely affect reproduction.

In the unlikely event that the author did not send UMI a complete manuscript and there are missing pages, these will be noted. Also, if unauthorized copyright material had to be removed, a note will indicate the deletion.

Oversize materials (e.g., maps, drawings, charts) are reproduced by sectioning the original, beginning at the upper left-hand corner and continuing from left to right in equal sections with small overlaps.

**ProQuest Information and Learning
300 North Zeeb Road, Ann Arbor, MI 48106-1346 USA
800-521-0600**

UMI[®]

**DOUBLE CEMENTED CARBIDE:
MICROSTRUCTURE-PROPERTY RELATIONSHIPS**

by

XIN DENG

A DISSERTATION

**Submitted to the graduate faculty of the University of Alabama and the University of
Alabama at Birmingham,
in partial fulfillment of the requirements for the degree of
Doctor of Philosophy**

BIRMINGHAM, ALABAMA

2002

UMI Number: 3078524

UMI[®]

UMI Microform 3078524

Copyright 2003 by ProQuest Information and Learning Company.

**All rights reserved. This microform edition is protected against
unauthorized copying under Title 17, United States Code.**

**ProQuest Information and Learning Company
300 North Zeeb Road
P.O. Box 1346
Ann Arbor, MI 48106-1346**

**ABSTRACT OF DISSERTATION
GRADUATE SCHOOL, UNIVERSITY OF ALABAMA AT BIRMINGHAM**

Degree: Ph.D. **Program:** Materials Engineering
Name of Candidate: Xin Deng
Committee Chairman: Burton R. Patterson
Title: Double Cemented Carbide: Microstructure-Property Relationships

Double cemented (DC) carbide is a creative and new dual composite composed of spherical cemented carbide granules embedded in a continuous metal-matrix. This 'composite-in-composite' structure contributes to the special mechanical property combinations of DC carbide and allows more flexible composite design. In the present study, the relationships between microstructure and mechanical properties of DC carbide were investigated. For DC carbide with cobalt matrix, WC particle size and cobalt content within the granules strongly influence the mechanical properties. Higher cobalt content inside granules leads to higher toughness and flexural strength with the sacrifice of hardness and wear resistance. Finer WC particle achieves higher hardness and wear resistance with limited sacrifice of toughness and flexural strength.

Granule size is another important factor influencing mechanical properties of DC carbide. At the same metal-matrix content, toughness and high stress wear resistance increase with granule size, and there is a critical granule size at which low stress wear resistance is minimized. At constant total cobalt content (including both the cobalt within the granules and the cobalt in the metal-matrix), direct mechanical property comparison between DC carbide and conventional cemented carbide is possible, showing DC carbide to have higher toughness and high stress wear resistance, similar hardness, low stress wear resistance and Young's modulus and lower flexural strength.

Mean free path of metal-matrix is the main factor controlling the toughness of DC carbide and the most important microstructural parameter relating DC carbide to conventional cemented carbide. Conventional cemented carbide can be regarded as a special DC carbide with a very small mean free path through the metal-matrix and hence low toughness. In high stress wear, granule protrusion enhances wear resistance. In low stress wear, cobalt, both in the metal-matrix and within the granule, is preferentially removed, giving DC carbide no significant advantage over conventional cemented carbide.

ACKNOWLEDGEMENTS

First, I would like to express my gratitude to my advisor, Dr. Burton R. Patterson, for his inspiration and encouragement throughout this research program at the University of Alabama at Birmingham (UAB). Without his great patience, kindness, consideration and wisdom, nothing is possible for me. I am very fortunate to have had such an excellent advisor.

I would like to thank my committee members, Drs. Krishan K. Chawla, Richard C. Bradt, Gregg M. Janowski, Alan W. Eberhardt, and Zhigang Fang, for their advice and encouragement during the whole research process.

I would especially like to thank my external committee member, Dr. Zhigang Fang, Smith International, Inc., for taking time to be on my committee, for many helpful discussions and for much support.

The financial support from the National Science Foundation (DMR 9904352) and Smith International, Inc., is greatly appreciated.

Special thanks go to Mr. Jonathan W. Bitler, Rogers Tool Works, Inc., for granule supply and many meaningful suggestions and discussions during the research. I also want to express my great gratitude to Osram, RTW, BASF and ISP for powder supply.

My sincere appreciation goes to Mr. Greg Lockwood, Smith International, Inc., for his training, consideration and inspiring discussion. Without his help, much of the research work could not have been done smoothly. I also thank Dr. Anthony Griffo and

Mr. Harry from Smith International, Inc., for their significant help and meaningful suggestions.

Without the assistance from the faculty and staff at the Department of Materials Science and Engineering at UAB, much of the research work could not have been done. I would like to express my appreciation to Mr. Mark Koopman, Mr. Robin Crowe, Ms. Cheri Moss and Dr. Robin Griffin. Also greatly appreciated are the excellent secretarial and administrative supports.

My thanks also go to Dr. Shanghua Wu, Mr. Chao Li, Dr. Malesela Jones Papo, Mr. Naiyu Sun, Dr. Hanjun Li and Mr. Haibin Ning for their assistance and friendship throughout the research effort.

Finally, I will thank my family - my parents and my brothers for - their important spiritual support. Especially, I give my greatest gratitude to my late aunt, Ms. Weijie Deng. Without her encouragement and enlightenment, I would not have done anything.

TABLE OF CONTENTS

| | <u>Page</u> |
|---|-------------|
| ABSTRACT | ii |
| ACKNOWLEDGMENTS | iv |
| LIST OF TABLES | viii |
| LIST OF FIGURES | ix |
| CHAPTER | |
| 1 INTRODUCTION – DOUBLE CEMENTED (DC) CARBIDE | 1 |
| 2 LITERATURE REVIEW | 5 |
| 2.1 Conventional cemented carbide | 5 |
| 2.1.1 Development of cemented carbide system | 5 |
| 2.1.2 Fabrication of cemented carbide | 7 |
| 2.1.3 Mechanical properties of cemented carbide | 7 |
| 2.2 DC carbide | 16 |
| 3 EXPERIMENTAL PROCEDURE | 22 |
| 3.1 DC carbide system | 22 |
| 3.2 Fabrication process | 22 |
| 3.3 Mechanical testing | 23 |
| 3.3.1 Hardness and toughness testing | 23 |
| 3.3.2 Wear testing | 24 |
| 3.3.3 Flexural strength and Young's modulus test | 26 |
| 3.3.4 Microstructure parameter measurement | 27 |
| 4 EFFECT OF GRANULE COBALT CONTENT ON MECHANICAL PROPERTIES OF DC CARBIDE | 34 |
| 4.1 Toughness | 35 |
| 4.2 Wear resistance | 36 |
| 4.2.1 High stress wear resistance | 36 |

TABLE OF CONTENTS (Continued)

| | | <u>Page</u> |
|----------------|---|-------------|
| CHAPTER | | |
| 4.2.2 | Low stress wear resistance | 37 |
| 4.2.3 | Flexural strength..... | 38 |
| 4.2.4 | Hardness | 41 |
| 4.2.5 | Young's modulus | 42 |
| 4.2.6 | Relationship between toughness and wear resistance of DC carbide..... | 43 |
| 5 | EFFECT OF GRANULE WC SIZE ON MECHANICAL PROPERTIES OF DC CARBIDE | 61 |
| 5.1 | Toughness..... | 62 |
| 5.2 | Wear resistance | 62 |
| 5.3 | Hardness and flexural strength..... | 63 |
| 6 | EFFECT OF GRANULE SIZE ON MECHANICAL PROPERTIES OF DC CARBIDE..... | 71 |
| 6.1 | Toughness..... | 71 |
| 6.2 | Wear resistance | 72 |
| 6.2.1 | High stress wear resistance | 72 |
| 6.2.2 | Low stress wear resistance | 72 |
| 6.3 | Flexural strength..... | 73 |
| 6.4 | Hardness | 74 |
| 6.5 | Relationship between toughness and wear resistance of DC carbide | 74 |
| 7 | WEAR MECHANISM AND TOUGHNESS MODELING OF DC CARBIDE | 88 |
| 7.1 | Wear resistance mechanism of DC carbide..... | 88 |
| 7.1.1 | High stress wear mechanism..... | 88 |
| 7.1.2 | Low stress wear mechanism..... | 89 |
| 7.2 | Toughness modeling | 90 |
| 8 | CONCLUSIONS | 97 |
| | LIST OF REFERENCES | 99 |

LIST OF TABLES

| <u>Table</u> | | <u>Page</u> |
|--------------|--|-------------|
| 1 | The development of cemented carbide (after [6]) | 6 |
| 2 | Comparison between DC carbide and conventional cemented carbide of the same total cobalt content (after [5]) | 17 |
| 3 | Mechanical properties of granules | 35 |
| 4 | Toughness comparison between experimental data and calculation from eqs. (48) and (49)..... | 93 |

LIST OF FIGURES

| <u>Figure</u> | <u>Page</u> |
|--|-------------|
| 1 Typical microstructures of (a) conventional cemented carbide and (b) DC carbide, showing that the granule microstructure in DC carbide is the same as in conventional cemented carbide | 3 |
| 2 The comparison of toughness and wear resistance between DC carbide and conventional cemented carbide (after [5]) | 4 |
| 3 Schematic diagram of crack tip region in cemented carbide (after [19])..... | 19 |
| 4 The effect of (a) WC grain size on hardness and (b) mean free path of binding phase on strength of cemented carbide (after [31])..... | 20 |
| 5 Relationship between toughness and mean free path of metal-matrix (after [5]) . | 21 |
| 6 Morphology of (a) typical granules and (b) cobalt powder | 28 |
| 7 Chevron-notched bar for toughness test (after [45]) | 29 |
| 8 High stress abrasive wear test apparatus (after [46]) | 30 |
| 9 Low stress abrasive wear test apparatus (after [47]) | 31 |
| 10 Abrasive wear particles for (a) low stress wear test (SiO_2 , 212-300 μm) and (b) high stress wear test (Al_2O_3 , about 590 μm) | 32 |
| 11 Rectangular specimen for dynamic Young's modulus measurement with impulse excitation of vibration (after [49]) | 33 |
| 12 Granule size histogram and cumulative curve for the 10 vol.% cobalt granule, typical of the three granule types with about 3 μm WC and 10, 18 and 25 vol.% cobalt..... | 45 |
| 13 Microstructure of granules with similar WC size (3 μm) but different cobalt content: (a) 10, (b) 18 and (c) 25 vol.%. | 46 |

LIST OF FIGURES (Continued)

| <u>Figure</u> | <u>Page</u> |
|--|-------------|
| 14 Microstructure of DC carbide with (a) 70, (b) 80, and (c) 90 vol.% granule, granule cobalt content 10 vol.%, granule WC size 3 μm | 47 |
| 15 Toughness of DC carbide with different granule cobalt contents but similar WC size (3 μm) as a function of (a) cobalt metal-matrix content and (b) total cobalt content (including the cobalt inside the granule and the cobalt in the metal-matrix) | 48 |
| 16 Microstructure development from (a) DC carbide with low cobalt content granules, (b) DC carbide with high cobalt content granules to (c) conventional cemented carbide..... | 49 |
| 17 Fracture surface of DC carbide with 10 vol.% granule cobalt and 3 μm WC but different metal-matrix content, (a) 30, (b) 20 and (c) 10 vol.% after toughness test, always showing flat fracture surface for DC carbide with different metal-matrix contents | 50 |
| 18 Effect of (a) metal-matrix content and (b) total cobalt content on the high stress wear resistance of DC carbide with different granule cobalt content varying from 10 to 25 vol.% but the same WC size of 3 μm | 51 |
| 19 Wear surface of DC carbide with 30 vol.% metal-matrix but different granules-(a) hard granules (10 vol.% cobalt in the granules) and (b) soft granules (25 vol.% cobalt in the granules)-and wear surface of (c) conventional cemented carbide with 30 vol.% cobalt, showing that the harder granule protrusion is the main reason DC carbide has higher high stress wear resistance than conventional cemented carbide | 52 |
| 20 Effect of (a) metal-matrix content and (b) total cobalt content on the low stress wear resistance of DC carbide with different granule cobalt content varying from 10 to 25 vol.% but the similar WC size-3 μm | 53 |
| 21 Wear surface of DC carbide with 30 vol.% cobalt matrix, 10 vol.% granule cobalt and 3 μm WC | 54 |
| 22 Effect of (a) metal-matrix content and (b) total cobalt content on flexural strength of DC carbide with different granule cobalt content varying from 10 to 25 vol.% but the same WC size of 3 μm | 55 |
| 23 Load-displacement curve of flexural strength test for (a) DC carbide with 30 vol.% cobalt matrix, 10 vol.% granule cobalt and 3 μm WC, and (b) conventional cemented carbide with 40 vol.% cobalt and 3 μm WC | 56 |

LIST OF FIGURES (Continued)

| <u>Figure</u> | <u>Page</u> |
|--|-------------|
| 24 Vickers hardness of DC carbide with 3 μm WC inside the granules but different granule cobalt content varying from 10 to 25 vol.%, as a function of (a) metal-matrix content and (b) total cobalt content..... | 57 |
| 25 Young's modulus and Hashin-Shtrikman boundaries for DC carbide with different granule cobalt content (10-25 vol.%) but the same WC size (3 μm) as a function of (a) granule content and (b) total WC content | 58 |
| 26 Relationship between toughness and high stress wear resistance of DC carbide and conventional cemented carbide. | 59 |
| 27 Relationship between toughness and low stress wear resistance of DC carbide with 3 μm WC inside the granules but different granule cobalt content varying from 10 to 25 vol.% compared with this relationship in conventional cemented carbide | 60 |
| 28 Microstructure of granules with different WC particle sizes, (a) 0.98 μm , (b) 1.56 μm , (c) 3.3 μm , and (d) 5.8 μm , but the same granule cobalt content, 10 vol.% | 65 |
| 29 Effect of WC particle size on the toughness of pure granule and DC carbide with 30 vol.% cobalt matrix, granule cobalt content 10 vol.% and granule size -80+120mesh | 66 |
| 30 Effect of WC particle size on (a) high stress wear resistance and (b) low stress wear resistance of pure granule and DC carbide with 30 vol.% cobalt matrix, granule cobalt content 10 vol.% and granule size -80+120 mesh..... | 67 |
| 31 High stress wear surface of DC carbide with 70 vol.% granule (granule cobalt content 10 vol.%, granule size -80+120 mesh) and 30 vol.% cobalt matrix, (a) WC size 0.98 μm , (b) WC size 1.56 μm , (c) WC size 3.3 μm and (d) WC size 5.8 μm | 68 |
| 32 Low stress wear surface of DC carbide with 70 vol.% granule (granule cobalt content 10 vol.%, granule size -80+120 mesh) and 30 vol.% cobalt; (a) WC size 0.98 μm ; (b) WC size 1.56 μm ; (c) WC size 3.3 μm ; and (d) WC size 5.8 μm | 69 |
| 33 Effect of WC particle size on (a) hardness and (b) flexural strength of pure granule and DC carbide with 30 vol.% cobalt matrix, granule cobalt content 10 vol.% and granule size -80+120 mesh..... | 70 |

LIST OF FIGURES (Continued)

| <u>Figure</u> | <u>Page</u> |
|---|-------------|
| 34 The morphology of granules with 18 vol.% cobalt and 3 μm WC but different granule sizes, (a) +80 mesh, (b) -120+170 mesh and (c) -325 mesh | 76 |
| 35 The microstructure of DC carbide with 30 vol.% metal-matrix but different average granule size, (a) 130 μm , (b) 90 μm , and (c) 60 μm ; granule cobalt content 18 vol.% and WC size 3 μm | 77 |
| 36 Effect of (a) granule size and (b) mean free path of metal-matrix on toughness of DC carbide with 30 vol.% cobalt matrix, granule cobalt content 18 vol.% and WC size 3 μm | 78 |
| 37 Microstructure development of DC carbide from (a) large granule to (b) small granule to (c) conventional cemented carbide..... | 79 |
| 38 Effect of granule size on high stress wear resistance of DC carbide with 70 vol.% granules (18 vol.% Co and 3 μm WC in granule) | 80 |
| 39 Wear surface of DC carbide with 30 vol.% metal-matrix and 3 μm WC inside the granule but different granule sizes: (a) large granules (133 μm , 18 vol.% Co in granule) and (b) small granules (57 μm , 18 vol.% Co in granule). Larger granule size makes more granule protrusion, leading to greater high stress wear resistance | 81 |
| 40 Effect of granule size on low stress wear resistance of DC carbide | 82 |
| 41 Low stress wear surface of DC carbide with 30 vol.% cobalt matrix, 18 vol.% granule cobalt content and 3 μm WC but different granule sizes: (a) 130 μm , overview; (b) 130 μm , sideview; (c) 90 μm , overview; (d) 90 μm , sideview; (e) 60 μm , overview; and (f) 60 μm , sideview..... | 83 |
| 42 Effect of (a) granule size and (b) mean free path of metal-matrix on flexural strength of DC carbide with 30 vol.% cobalt matrix, 18 vol.% granule cobalt content and 3 μm WC | 84 |
| 43 Effect of (a) granule size and (b) mean free path of metal-matrix on the hardness of DC carbide with 30 vol.% cobalt matrix, 18 vol.% granule cobalt content and 3 μm WC | 85 |

LIST OF FIGURES (Continued)

| <u>Figure</u> | <u>Page</u> |
|---|-------------|
| 44 Relationship between toughness and high stress wear resistance for both conventional cemented carbide and DC carbide with 30 vol.% cobalt matrix, 18 vol.% granule cobalt content and 3 μm WC but granule size varying from 55 to 133 μm | 86 |
| 45 Relationship between toughness and low stress wear resistance for both conventional cemented carbide and DC carbide with 30 vol.% cobalt matrix, 18 vol.% granule cobalt content and 3 μm WC but granule size varying from 55 to 133 μm | 87 |
| 46 High stress wear mechanism of DC carbide | 94 |
| 47 Low stress wear mechanism of DC carbide | 95 |
| 48 Critical energy release rate as a function of mean free path of metal-matrix | 96 |

CHAPTER 1

INTRODUCTION-DOUBLE CEMENTED (DC) CARBIDE

Cemented carbide, a hard material with limited toughness, has been used widely in cutting tools, drilling bits and high wear resistance parts. Ever since its development [1], conventional cemented carbide microstructure has remained the same: carbide (WC) particles dispersed homogeneously in a metal binding phase (typically cobalt) as shown in Fig. 1a. More recently, several 'dual property' grade cemented carbides were developed to obtain the combinations of wear resistance and toughness not obtainable by the conventional microstructure [2-5].

Double cemented (DC) carbide is one of these dual property grade materials with a microstructure as shown in Fig. 1 b, with spherical granules of conventional cemented carbide surrounded by a metal-matrix. This 'composite-in-composite' structure results in special mechanical property combinations and makes composite design more flexible, which means not only the whole composite but also every component in the composite are designable. This composite design concept of DC carbide applies to many other composite systems such as cermets and polycrystalline diamond, exhibiting high potential for future applications.

When compared with conventional cemented carbide, DC carbide demonstrates a superior combination of wear resistance and toughness as shown in Fig. 2 (after [5]), demonstrating the great potentials of dual property composites and explaining its promising application in oil field drill bit inserts. In real field drilling tests, DC carbide

inserts did show greater wear resistance and toughness compared to conventional cemented carbide inserts.

Because DC carbide is a relatively unexplored composite system, several important questions remain to be answered:

1. Why does DC carbide have higher toughness than conventional cemented carbide?
2. What is the effect of granule properties on the properties of DC carbide?
3. What is the effect of metal-matrix properties on the properties of DC carbide?
4. What are the controlling mechanisms of deformation and fracture for DC carbide?

Answering these questions is the main goal of the present study.

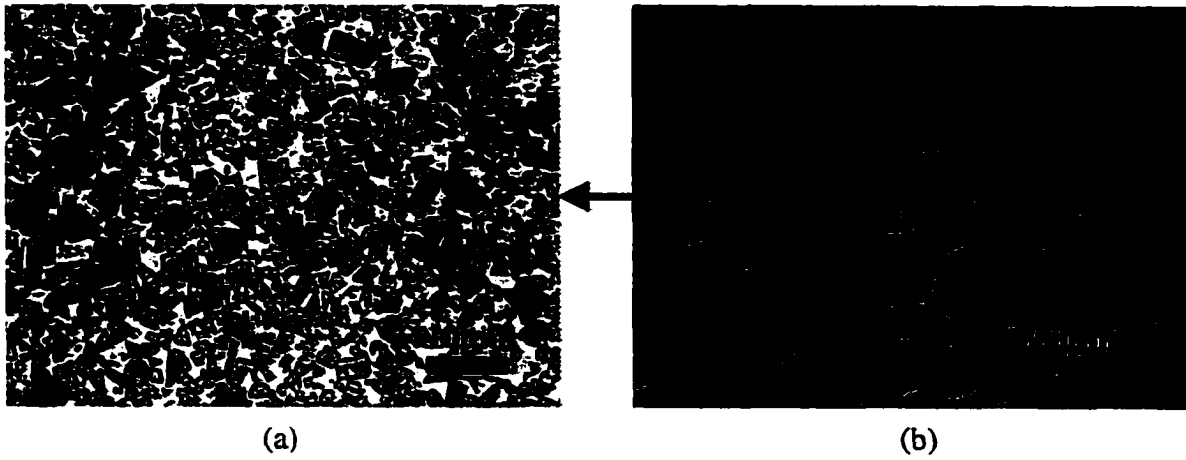


Fig. 1. Typical microstructures of (a) conventional cemented carbide and (b) DC carbide, showing that the granule microstructure in DC carbide is the same as in conventional cemented carbide.

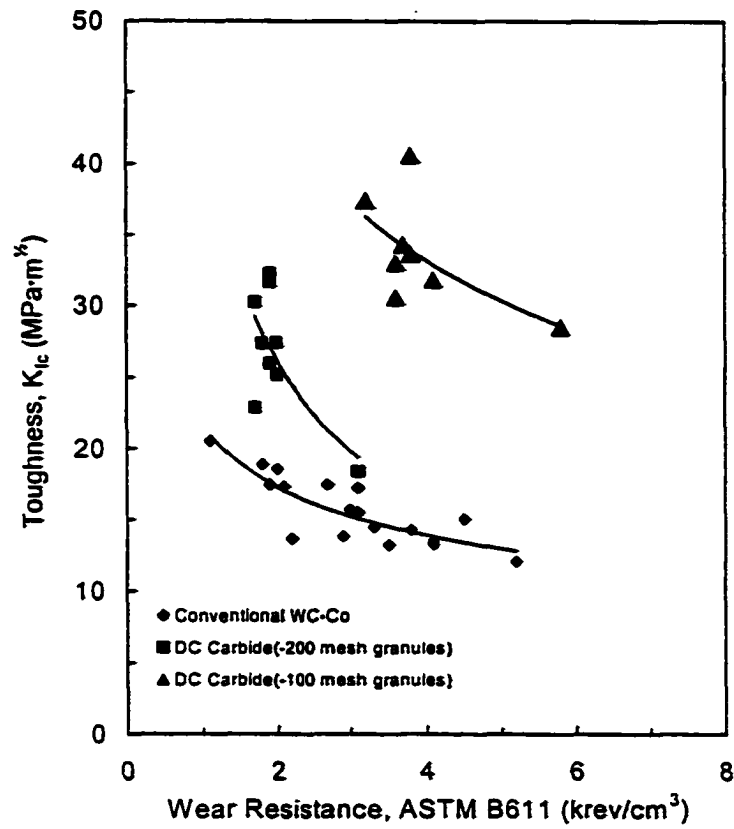


Fig. 2. The comparison of toughness and wear resistance between DC carbide and conventional cemented carbide (after [5]).

CHAPTER 2

LITERATURE REVIEW

2.1. Conventional cemented carbide

2.1.1. Development of cemented carbide system

Cemented carbide was introduced by Karl Schroter [1] as a die material to draw tungsten filament wire for incandescent lamps. The potential of this material for cutting tools was not recognized until later. As shown in Table 1 (after [6]), WC-Co was the very first cemented carbide system and is still employed widely for drilling bits and wear resisting parts. Because WC-Co is subject to crater wear when machining steels, other systems were developed to reduce the reaction between cemented carbide and iron [7-9].

Many efforts have been made to replace the cobalt matrix material with other metals because of this material's high price and limited sources. Nickel, iron and even steels have been investigated [10-14], and some of these have yielded promising results. However, cobalt is still irreplaceable as a binding phase in many cases for the following reasons [15]:

1. The cobalt matrix forms a strong bond with the carbide grains because of the high solubility of WC in cobalt binding phase and prevents carbide particle pullout during wear. Carbide particles also form a skeleton structure that makes it difficult to remove cobalt by plastic extrusion.
2. The cobalt matrix contracts much more on solidification than the carbide grains tendency to crack.

3. Cobalt can form an effective lubrication film on the cemented carbide surface, resulting in lower wear rates.

4. The cobalt matrix may contain very fine precipitates of WC grains, which results in a reduced effective mean free path and aids low stress abrasion resistance.

Table 1. The development of cemented carbide (after [6])

| | |
|-----------|---|
| 1923-1925 | WC-Co |
| 1929-1931 | WC-TiC-Co |
| 1930-1931 | WC-TaC(VC,NbC)-Co |
| 1938 | WC-Cr ₃ C ₂ -Co |
| 1948-1970 | Submicron WC-Co |
| 1956 | WC-TiC-Ta(Nb)C-Cr ₃ C ₂ -Co |
| 1959 | WC-TiC-HfC-Co |
| 1965-1975 | HIP |
| 1965-1978 | TiC, TiN, Ti(C,N), HfC, HfN and Al ₂ O ₃ CVD coatings on WC base |
| 1968-1969 | WC-TiC-Ta(Nb)C-HfC-Co |
| 1968-1969 | WC-TiC-Nb(Ta)C-HfC-Co |
| 1969-1971 | Thermochemical surface hardening |
| 1974-1977 | Polycrystalline diamond on WC-base hardmetal |
| 1973-1978 | Multicarbide, carbonitride/nitride and multiple carbide/carbonitride/nitride/oxide coatings |
| 1981 | Many thin coatings with ALON layers |
| 1983-1992 | Sinter-HIP |
| 1992-1995 | Plasma CVD diamond coating |
| 1993-1995 | Coating complex carbonitrides |
| 1994 | Fine-grain WC/Co agglomerates in tougher WC/Co matrix |
| 1994 | Nanocrystalline cemented carbides |

2.1.2. *Fabrication of cemented carbide*

The sequence of powder milling, spray drying, cold pressing, dewaxing and liquid phase sintering is the most common processing method for cemented carbide, yielding sufficient strength and nearly full density [16]. Hot pressing and hot isostatic pressing (HIP) [17,18] are also employed to eliminate defects and achieve better mechanical properties that cannot be obtained by simple liquid phase sintering. Sinter-HIP [18] combines vacuum sintering with HIP in a single heat cycle. During conventional vacuum sintering, 20-100 bar inert gas is applied to the work pieces to reach full density. The cost can be reduced dramatically with apparent property improvement.

2.1.3. *Mechanical properties of cemented carbide*

Mean free path of binding phase and carbide particle size are two critical factors influencing the mechanical properties of cemented carbide and are also the main concern for mechanical property modeling. In fact, the two factors are related as [19]:

$$\frac{\overline{\lambda}_\beta}{D_\alpha} = \frac{V_v^\beta}{V_v^\alpha} \frac{1}{1-C} \quad (1)$$

where $\overline{\lambda}_\beta$ is the mean free path of matrix, \overline{D}_α is the mean intercept length of carbide, V_v^α and V_v^β are the volume fractions of carbide and binding phase, respectively, and C is the contiguity of carbide. The contiguity of carbide, the fraction of contact area between carbide grains divided by the total surface area of carbide grains if no contact occurred, can be expressed as [20]:

$$C = \frac{2S_{cc}}{2S_{cc} + S_{cm}} \quad (2)$$

where S_{CC} is the area between carbide grains and S_{CM} is the area between carbide grain and matrix in unit volume.

For conventional cemented carbide, carbide particle size or mean free path of binding phase has an apparent effect on wear resistance, toughness, hardness and strength. Hardness and wear resistance of cemented carbide decrease with carbide particle size or mean free path of binding phase, while toughness increases with mean free path of binding phase. At constant binding phase content, there is a critical mean free path for peak strength of cemented carbide. The mechanisms of these effects are discussed below.

2.1.3.1. Wear mechanism

Cemented carbide is widely used for metal machining and rock drilling because of its high wear resistance. The wear mechanism of cemented carbide differs with service conditions. Upadhyaya [21] has summarized the wear mechanisms of cemented carbide during metal machining as abrasive wear, attrition wear and diffusion wear. Hack and Peters [22] found that hardness is not the only factor determining wear resistance and that abrasive wear resistance increases when the fracture toughness of cemented carbide increases. Larsen-Basse [23] summarized the wear mechanisms for rock drilling as gross fracture, impact spalling, impact-fatigue spalling, thermal fatigue and abrasive wear. The abrasion wear resistance of cemented carbide decreases with the increased binder mean free path.

Wayne et al. [24] investigated abrasion and erosion mechanism of cemented carbide with controlled microstructures and found:

$$\text{abrasion resistance} \propto \left(\frac{K_{IC}^{3/8} H^{1/2}}{\bar{D}_{WC}} \right) \quad (3)$$

and

$$\text{erosion resistance} \propto \left(K_{IC}^{3/8} H^{1/2} \right) \frac{\lambda}{\bar{D}_{WC}} \quad (4)$$

where K_{IC} , H , λ and \bar{D}_{WC} are the toughness, hardness, mean free path of binder phase and WC particle size, respectively. Eqs. (3) and (4) give the two most important factors influencing the wear resistance of cemented carbide-toughness and hardness. Factors increasing both toughness and hardness will increase wear resistance. Fang et al. [25] showed that, compared with conventional cemented carbide, DC carbide demonstrates greater toughness with little sacrifice of hardness, making an excellent candidate for oil well drilling bit inserts for high wear resistance and drilling efficiency, as proved by actual field drilling tests.

2.1.3.2. *Toughening mechanisms*

Toughening is an important aspect of cemented carbide because of its brittle nature. Sigl and Exner [26] defined four types of fracture paths in cemented carbide:

1. transgranular fracture through the binder phase, B;
2. fracture close to the carbide/binder interface, B/C;
3. Intergranular fracture along carbide grain boundaries, C/C; and
4. Transgranular fracture through carbide crystals, C.

Sigl and Fischmeister [19] observed the process of crack propagation and found ligament bridging by the binding phase to be the main toughening mechanism of cemented carbide. These authors found that cracks initiate first at path (3) with the

binding phase becoming bridging ligaments to prevent the propagation of crack, as shown in Fig. 3 (after [19]).

Two types of toughening models have been developed for cemented carbide. Both types consider the energy of crack propagation, either through both matrix and WC particles or through just the matrix.

The first type of 'energy balance' model is based on the energy consumed by the four possible crack propagation paths. Summing up the energies spent in the four crack paths, Sigl and Fischmeister [19] developed the fracture resistance R of cemented carbide as:

$$R = (\bar{r}_B A_A^B + r_{B/C} A_A^{B/C}) \bar{\sigma}_f + (A_A^{C/C} + A_A^C) G_{IC}^a \quad (5)$$

where \bar{r}_B is the mean free path of the cobalt binding phase; $r_{B/C}$ is the dimple size of the WC/Co interface; $\bar{\sigma}_f$ is the effective mean flow stress of the binding phase; G_{IC}^a is the critical energy release rate of carbide; and A_A^B , $A_A^{B/C}$, $A_A^{C/C}$ and A_A^C are the fracture area fractions through binding phase, carbide/binder interface, carbide grain boundary and carbide grains, respectively.

Ravichandran introduced a similar energy release model for toughness of cemented carbide [27]:

$$G_C = (1 - V_f) G_{WC} + V_f \sigma_o \lambda \chi \quad (6)$$

where G_C is the critical strain energy release rate of cemented carbide; G_{WC} is the critical strain energy release rate of the brittle phase; and V_f , σ_o , λ and χ are, respectively, the volume fraction, the bulk flow stress, the mean free path and the work of rupture parameter of ductile phase. The value of χ varies from 4 to 16.

Nakamura and Gurland [28] developed an expression of strain energy release rate of cemented carbide as:

$$G = 2\gamma_{\text{eff}} V_h^{2/3} + \alpha \lambda_c V_h^{2/3} \frac{1 - V_h^{2/3}}{1 - V_h} \int_0^{\epsilon_f} \sigma(\epsilon) d\epsilon \quad (7)$$

where γ_{eff} is the effective binding energy of WC, V_h is the volume fraction of WC, α is a constant, λ_c is the mean free path of cobalt binding phase, $\sigma(\epsilon)$ is the flow stress of the cobalt binding phase as a function of strain and ϵ_f is the failure strain.

The second type of toughness model ignores the work consumed to break brittle WC particles and considers only the energy absorbed by the matrix. One simple model is expressed as [29]:

$$\sigma_y \lambda = \alpha G_{\text{lc}} \quad (8)$$

where σ_y is the in situ yield strength of binding phase, α is a constant, λ is the mean free path of binding phase and G_{lc} is the critical strain energy release rate of cemented carbide.

Hong and Schwarzkopf [30] developed a toughness expression for cemented carbide as:

$$K_{\text{lc}} = \sqrt{c \sigma_y \frac{\lambda_c}{d + \lambda_c} \lambda_c} \quad (9)$$

where c is a constant, λ_c is the mean free path of cobalt, σ_y is the in-situ yield stress of cobalt and d is the mean free path of carbide.

From all the models above, we can see the mean free path of matrix phase has a significant effect on the toughness. At the same binding phase content, increased mean free path of binding phase increases toughness of cemented carbide.

2.1.3.3. *Hardness and strength*

Fig. 4a (after [31]) shows that hardness decreases linearly with the increase of WC grain size. The effect of mean free path on strength is somewhat complicated. When mean free path is low, strength increases with increased binder layer thickness (Fig. 4b; after [31]). The main reasons are that the increased binder layer thickness makes plastic flow easier, local stress concentrations are relieved and both crack initiation and crack propagation are impeded. When mean free path increases to a certain degree, further increase will reduce the strength according to dispersion strengthening theory.

Chermant and Osterstock [32] found the flow stress in compression at 0.2% plastic strain of WC-Co hardmetals can be expressed as:

$$\sigma_{0.2} = k' + k'' d_{WC}^{-1/2} \quad (10)$$

where k' and k'' are constants and k' is also a function of V_{Co} .

Lee and Gurland [33] experimentally determined an expression for hardness and yield strength of cemented carbide:

$$H = H_{WC} C \cdot V_{WC} + H_{Co} (1 - C \cdot V_{WC}) \quad (11)$$

where H , H_{WC} and H_{Co} are the hardness or yield strength of cemented carbide, WC and cobalt, respectively; C is the contiguity of WC; and V_{WC} is the volume fraction of WC.

Cobalt hardness, H_{Co} , can be expressed as [33]:

$$H_{Co} = 304 + 12.7\lambda^{-1/2} \quad (12)$$

where λ is the mean free path of binding phase.

Considering microstructure defect and residual stress in cemented carbide leads to the work of Liu et al. [34]. These authors presented a more complicated strength model, where, for cemented carbide with a certain cobalt content, there exists a critical WC size,

R_c , and a critical mean free path of binding phase, M_c . When mean free path M is less than M_c or WC size R is less than R_c , the crack expands mainly across cobalt binding phase, and fracture strength of cemented carbide is:

$$\sigma_f = \left[\frac{1}{\phi_c} \left(\frac{2\pi E_{Co} K' (1-V) M}{3AV(M-2S)(1-\nu^2)} \right)^{1/2} - BP \frac{\phi_t}{\phi_c} \right] C_1 C_2 \quad (13)$$

where S is the length of microstructure defect, M is the mean free path of binder, B is a constant, ν is Poisson's ratio, $A = 1 + S/R$ (R is radius of WC grain size), E_{Co} is the elastic modulus of cobalt binder, K' is a constant and V is the volume fraction of WC.

The terms ϕ_c , ϕ_t , C_1 and C_2 are related to microstructure defect and are given by:

$$\phi_c = \left(1 - \frac{1}{A^2}\right)^{1/2} \left[1 + \frac{1}{4A^2} + \frac{3}{4A^4} \left(1 + \frac{A^2 - 1}{3}\right) \right] \quad (14)$$

$$\phi_t = 1 - \left(1 - \frac{1}{A^2}\right)^{1/2} + \frac{1}{2A^{3/2}} \left(1 - \frac{1}{A^2}\right)^{1/2} \quad (15)$$

$$C_1 = \left[\frac{\pi A}{2(A + 2(1-V)/3V)} \right]^{1/2} \quad (16)$$

$$C_2 = \left[\tan \frac{\pi A}{2(A + 2(1-V)/3V)} \right]^{-1/2} \quad (17)$$

P is the residual thermal stress:

$$P = \frac{2E\Delta\alpha\Delta T}{3(1-V)} \quad (18)$$

where $\Delta\alpha$ is the difference of thermal expansion between binding phase and WC and ΔT is differential temperature. Eq. (18) applies only to isotropic composites and therefore can only give approximate values for cemented carbide because of the anisotropic nature of

WC. Eq. (13) indicates that the strength of cemented carbide increases with WC size or mean free path of binding phase.

When mean free path M is larger than M_c , or WC size R is larger than R_c , crack expands mainly through WC, and the fracture strength of cemented carbide is given by:

$$\sigma_f = \left[\frac{1}{\phi_c} \left(\frac{\pi E_{wc} \gamma_{wc}}{3A(1-\nu^2)V(M-2S)} \right)^{1/2} - BP \frac{\phi_t}{\phi_c} \right] C_1 C_2 \quad (19)$$

where E_{wc} is the elastic modulus of WC and γ_{wc} is the average surface energy of WC grains. Eq. (19) shows that the strength decreases with WC size or mean free path of binding phase.

The combination of eqs. (13) and (19) demonstrates that the critical WC size and mean free path of binding phase correspond to the peak strength, just as shown in Fig. 4b.

2.1.3.4. *Young's modulus*

Young's modulus is the basic elastic property of cemented carbide. Both theoretical and practical investigations and modeling have been performed. Hashin and Shtrikman [35] derived a general model for the composite with a matrix in which spherical inclusions are embedded. Rather than giving the exact elastic modulus, the model consists the upper and lower bounds:

$$K_1^* = K_1 + \frac{\nu_2}{\frac{1}{K_2 - K_1} + \frac{3\nu_1}{3K_1 + 4G_1}} \quad (20)$$

$$K_2^* = K_2 + \frac{\nu_1}{\frac{1}{K_1 - K_2} + \frac{3\nu_2}{3K_2 + 4G_2}} \quad (21)$$

$$G_1^* = G_1 + \frac{v_2}{\frac{1}{G_2 - G_1} + \frac{6(K_1 + 2G_1)v_1}{5G_1(3K_1 + 4G_1)}} \quad (22)$$

$$G_2^* = G_2 + \frac{v_1}{\frac{1}{G_1 - G_2} + \frac{6(K_2 + 2G_2)v_2}{5G_2(3K_2 + 4G_2)}} \quad (23)$$

where K_1^* and K_2^* are upper and lower bounds of bulk modulus of the composite, respectively; G_1^* and G_2^* are upper and lower bounds of shear modulus, respectively; K_1 , K_2 , G_1 , and G_2 are the bulk and shear modulus of the two phases, respectively; $K_2 > K_1$, and $G_2 > G_1$; and v_1 and v_2 are the volume fractions of the two phases.

Paul [36] presented the theoretical expressions for the elastic modulus of two-phase materials:

$$\bar{E} = \frac{E_1 + (E_2 - E_1)v_1^{2/3}}{E_1 + (E_2 - E_1)v_2^{2/3}(1 - v_2^{1/3})} E_1 \quad (24)$$

where E_1 and E_2 are the Young's modulus of two phases, $E_2 > E_1$ and v_1 and v_2 are the volume fraction of the two phases.

Doi et al. [37] measured Young's modulus, shear modulus and Poisson's ratio on WC-(1-30 wt.%) Co alloys by dynamic resonance method. These authors investigated the effects of volume fraction of WC, the carbon content and the WC size and found that Young's modulus depended solely on volume fractions of WC. All the Young's modulus data fell within Hashin and Shtrikman's bounds [35] and close to Paul's [36] model.

Jaensson and Sundstrom [38] calculated Young's modulus and Poisson's ratio by finite element method. The calculated value is just inside Hashin and Strikman's bonds.

Jaensson and Sundstrom [38] also investigated the effect of cracks and found that a reasonable number of cracks have only a small influence on Young's modulus.

2.2. *DC carbide*

In a broad sense, DC carbide is a hybrid composite because one of the components is a composite itself. One example of such is microstructurally toughened composite (MTC) [39-41]. Nardone and Strife [39] fabricated an MTC consisting of continuous tubular 304 stainless steel toughening regions embedded in a matrix of B₄C particle-reinforced NiAl. This MTC has higher impact resistance than the NiAl material alone. Nardone [40] found this kind of MTC also has higher toughness. A hybrid composite of Al-SiC rods surrounded by an Al matrix was also produced that had higher impact resistance than conventional Al-SiC composite [41,42].

Angers et al. [43] developed a new wear resistant composite material containing WC-Co granules in a steel matrix infiltrated with a copper alloy. In this case, WC-Co granules were added to the steel matrix as a dispersed second phase (30 vol.%) to improve the abrasive wear resistance of the steel. Champagne et al. [44] hot isostatically pressed a composite with WC-Co granules in steel matrix and found a thin interdiffusion zone forms at the interface of WC-Co granule/steel matrix. Mechanical tests showed that good properties were obtained in this composite containing less than 30 vol.% of WC-Co granules.

For cemented carbide, 'functional gradient' approaches have been developed and commercialized successfully in the last 20 years [2-5]. Krall and Olsson [2] described a method to produce functionally graded cemented carbide, where unsintered nodules of a

preblended hard metal powder are uniformly dispersed into unsintered nodules of a preblended hard metal composite of a second grade. After liquid-phase sintering, the overall properties benefit from the two grades of component.

Fang et al. [5] made a detailed investigation of typical DC carbide with WC-Co granules containing 10 vol.% Co and granule volume fraction varying from 62 to 77%. At the same cobalt content, DC carbide had higher toughness and abrasive wear resistance but lower flexural strength than conventional cemented carbide. The main reason for improved toughness is the increased mean free path between granules as shown in Fig. 5 (after [5]).

Table 2 (after [5]) shows directly the advantage and disadvantage of DC carbide compared with conventional cemented carbide of the same cobalt content, which indicates that DC carbide has higher toughness and high stress abrasion resistance but lower hardness and flexural strength.

Table 2. Comparison between DC carbide and conventional cemented carbide of the same total cobalt content (after [5])

| Property | DC carbide | WC-27Co |
|---|------------|---------|
| Hardness, HRC | 59 | 60 |
| Flexural Strength (MPa) | 2110 | 3040 |
| Toughness, K_{Ic} (MPa m ^{1/2}) | 32 | 21 |
| Mean Free path, λ (μm) | 11 | 1.5 |
| High stress abrasion resistance (krev/cm ³) | 2.2 | 1.1 |

An expression of fracture energy release rate for DC carbide was presented [5]:

$$-G_{IC} = R = (\overline{r_m} A_A^m + \overline{r_{m/g}} A_A^{m/g}) \overline{\sigma_f} + (A_A^{g/g} + A_A^g) G_{IC}^g \quad (25)$$

where superscript or subscript g stands for the granules and m stands for the matrix, $\overline{r_m}$ is the mean size of the plastic zone, $\overline{\sigma_f}$ is the flow stress for the matrix and A_A^i is the area fraction of fracture path.

Based on the study of DC carbide, the following chapters are devoted to the investigation of the effect of granule cobalt content, granule WC particle size and granule size on mechanical properties of DC carbide. The relationship between mechanical properties of DC carbide and microstructure parameters was investigated, and the toughness model for DC carbide was set up necessarily.

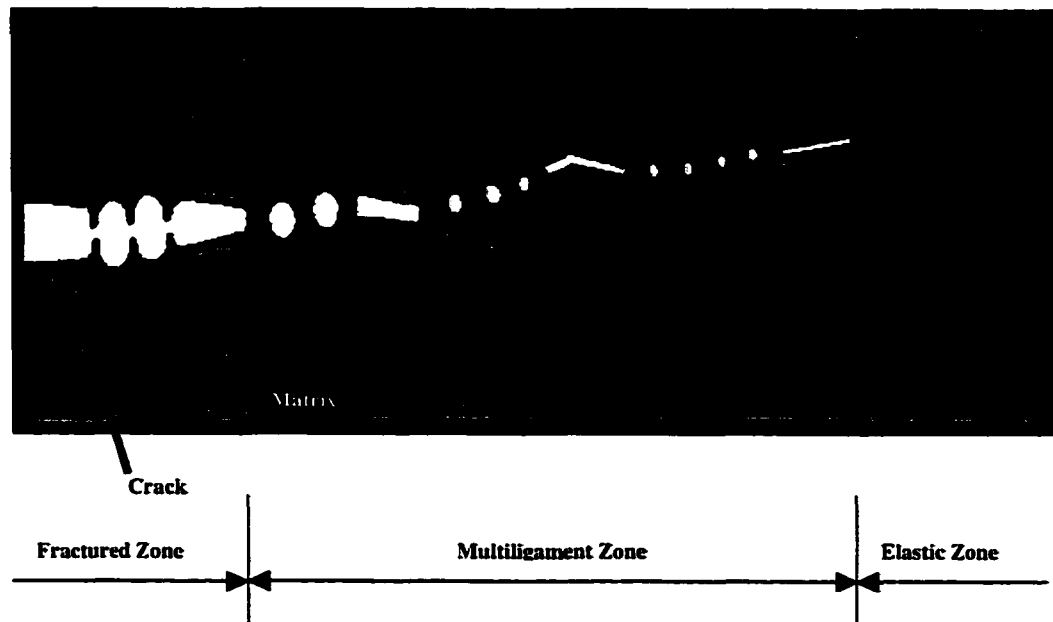


Fig. 3. Schematic diagram of crack-tip region in cemented carbide (after [19]).

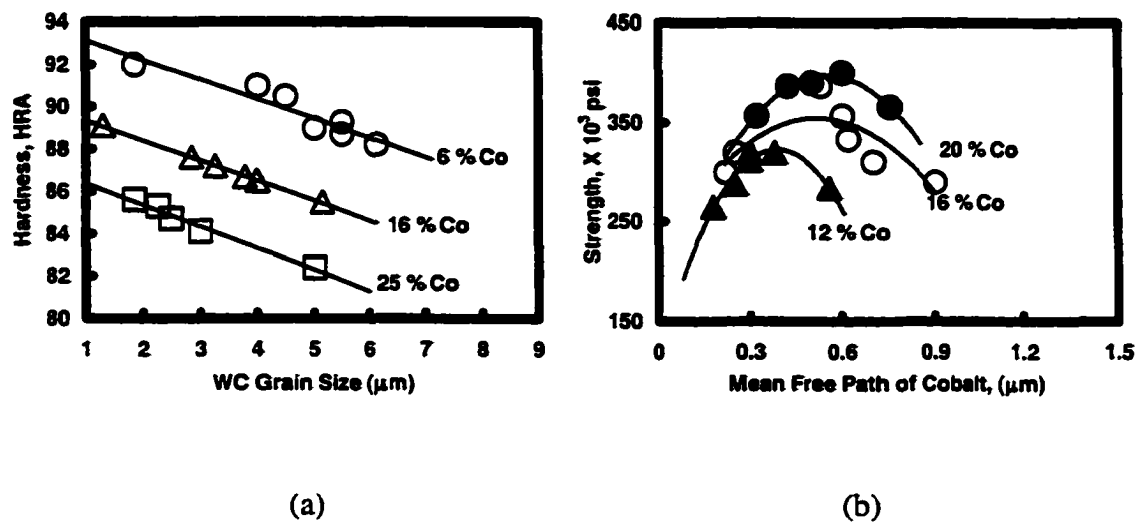


Fig. 4. The effect of (a) WC grain size on hardness and (b) mean free path of binding phase on strength of cemented carbide (after [31]).

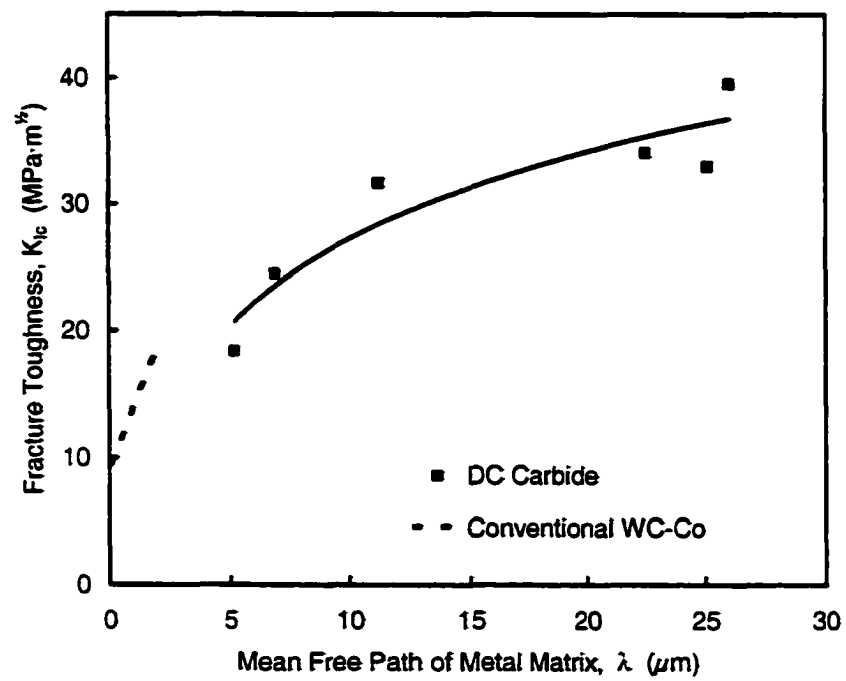


Fig. 5. Relationship between toughness and mean free path of metal-matrix (after [5]).

CHAPTER 3

EXPERIMENTAL PROCEDURE

3.1. DC carbide system

In the present study, DC carbide with different cobalt matrix contents (0, 10, 20 and 30 vol.%) and different granule cobalt contents (10, 18 and 25 vol.%), but similar WC particle size inside the granules (3 μm) and granule size distribution were employed for the investigation of the effect of granule cobalt content on mechanical property of DC carbide.

DC carbide with different WC particle sizes inside the granules (0.98, 1.56, 3.3 and 5.8 μm) and different cobalt matrix contents (0 and 30 vol.%) but the same granule size (-80+120 mesh) and granule cobalt content (10 vol.%) was fabricated for the investigation of the effect of WC size.

DC carbide with different granule sizes but the same cobalt matrix content (30 vol.%), granule cobalt content (18 vol.%) and granule WC size (3 μm) was used for the investigation of the effect of granule size.

3.2. Fabrication process

The fabrication of DC carbide includes dewaxing and presintering green granules, wet mixing granules and metal-matrix powder, drying and hot pressing. The raw granules are spherical pellets produced by spray drying, where the mixture of WC, cobalt and wax is heated to 200°C, at which point the wax melts and the fluid is sprayed vertically

through a nozzle, atomizing the fluid to droplets. On cooling during free fall in the high pressure gas chamber, the mixture solidifies into spherical granules. Green granules are dewaxed at lower temperature (250-500°C) and presintered at higher temperature (1200°C) in hydrogen for future mixing with metal powder. The morphologies of granule and matrix cobalt powder are shown in Fig. 6.

Ball milling with cemented carbide milling balls and heptane as a liquid medium is employed to mix presintered granules and metal powder. The milling time (8 hr) is critical because if the time too short, the mixture is not homogeneous and because if the time too long, the granules will be broken. Full density of DC carbide is achieved by hot pressing at 1250°C, which is below the liquid-phase sintering temperature, in a graphite die in vacuum; the pressure is 35 MPa.

3.3. Mechanical testing

Five mechanical tests were employed to evaluate mechanical properties of DC carbide, including hardness, toughness, wear resistance, flexural strength and elastic modulus tests. All tests were performed with loading in the hot press direction for consistency.

3.3.1. Hardness and toughness testing

Vicker's hardness tests were performed with 100 kg load. Eight tests were made for each sample, and the average value and standard deviation (<7.8% of the average value) were calculated.

Due to the hot press limitation for specimen size, the toughness test cannot be made according to ASTM standards. In this experiment, toughness (K_{Ic}) testing by using three-point bending of the chevron-notched bars shown in Fig. 7 was based on the method of Wu [45]:

$$K_{Ic} = \frac{P_{max}}{B\sqrt{W}} Y_C(\alpha_o, \alpha_i) \quad (26)$$

where $\alpha_o = a_o/W$; $\alpha_i = a_i/W$; Y_C is the coefficient determined by the ratio among S , W and B ; and P_{max} is the peak load during bending test. Although Wu [45] stated that K_{Ic} value can be obtained directly from this method, direct comparison between this method and the ASTM standard is not made; therefore, the ' K_Q ' is used for the toughness value of DC carbide only to indicate this specific test method. Five tests were made for each DC carbide composition. Average and standard deviation (<8.6% of average) were calculated.

3.3.2. *Wear testing*

Wear testing includes high stress wear test and low stress wear test. High stress wear tests were performed according to ASTM B611 as shown in Fig. 8 (after [46]) by using wet, coarse Al_2O_3 particles (about 590 μm) as the abrasive. After 1000 revolutions of a steel wheel (100 rpm), the mass loss of sample was measured and the wear number of sample was obtained by:

$$\text{Wear Number} = \frac{\text{Density}}{\text{Mass Loss}} \quad (27)$$

The physical meaning of wear number is the number of revolutions to remove a unit volume of sample. The higher the wear number, the higher the wear resistance of DC carbide becomes.

Low stress wear tests were performed according to ASTM G65 as shown in Fig. 9 (after [47]), where dry quartz sand (-50+70 mesh, 212-300 μm) is employed as the abrasive. The main difference between the high and low stress wear tests is that in the low stress test, a rubber wheel is employed and SiO_2 (Fig. 10a), which is softer and finer than the Al_2O_3 particle (Fig. 10b) used in high stress tests, is used as the abrasive. Thus, the low stress wear test evaluates the wear resistance of DC carbide under a soft abrasive environment, while the high stress wear test evaluates the wear resistance of DC carbide under a hard abrasive environment. After 0.5 hr at the 200 rpm wheel rotation speed, the volume loss of DC carbide per 1000 revolutions is obtained as:

$$\text{Volume Loss} = \frac{\text{Mass Loss}}{6 \times \text{Density}} \quad (28)$$

Although the right number of revolutions was used in this experiment, volume loss was reported as one sixth of the ASTM value for comparison with other commercial DC carbide values.

The lower the volume loss, the higher the low stress wear resistance becomes. In some cases, wear number is also used to express low stress wear resistance of DC carbide:

$$\text{Wear Number} = \frac{1}{\text{Volume Loss}} \quad (29)$$

For both high and low stress wear tests, only one test was made for each DC carbide composition.

3.3.3. Flexural strength and Young's modulus test

Flexural strength is measured according to ASTM C1161 [48], employing the four-point-bend test.

The flexural strength is given by:

$$S = \frac{3PL}{4bd^2} \quad (30)$$

where P is breakload, L is outer (support) span, b is specimen width and d is specimen thickness. Five tests were made for each DC carbide composition, and average and standard deviation (<5.8% of average) value were calculated.

Young's modulus of DC carbide is measured by impulse excitation of vibration according to ASTM E1876 [49]. As shown in Fig. 11 (after [49]), when the specimen is excited mechanically by a singular elastic strike with an impulse tool, the fundamental resonant frequency is obtained by microphone, and dynamic Young's modulus can be calculated:

$$E = 0.9465(mf_f^2/b)(L^3/t^3)T_1 \quad (31)$$

where E is the Young's modulus; m is the mass of specimen; b, L and t are the width, length and thickness of the specimen, respectively; f_f is the fundamental resonant frequency of specimen; and T_1 is the correction factor:

$$T_1 = 1 + 6.585(1 + 0.0752\mu + 0.8109\mu^2)(t/L)^2 - 0.868(t/L)^4 - \left[\frac{8.340(1 + 0.2023\mu + 2.173\mu^2)(t/L)^4}{1.000 + 6.338(1 + 0.1408\mu + 1.536\mu^2)(t/L)^2} \right] \quad (32)$$

where μ is Poisson's ratio, which was previously determined [50]. One test was made for each DC carbide composition.

3.3.4. Microstructure parameter measurement

Microstructure parameter measurement is necessary for the investigation of the relationship between mechanical properties and microstructure of DC carbide. For DC carbide, volume fraction of granule and metal-matrix, V_V^g and V_V^m ; granule size, D_g ; and mean free path of metal-matrix, λ_m , are the main parameters to be measured [51,52].

$$D_g = \frac{3}{2}L_g = \frac{3}{2} \left[\frac{4V_V^g}{2S_V^{g/g} + S_V^{g/m}} \right] \quad (33)$$

$$\lambda_m = \frac{4V_V^m}{S_V^{g/m}} \quad (34)$$

where superscript g and m stand for the granules and matrix, respectively, and S_V is the surface area of different phases in unit volume of composite. The measurement of V_V and S_V is based on eqs. (35)-(38) [51,52]:

$$V_V^m = P_p^m \quad (35)$$

$$V_V^g = P_p^g \quad (36)$$

$$S_V^{g/g} = 2P_L^{g/g} \quad (37)$$

$$S_V^{g/m} = 2P_L^{g/m} \quad (38)$$

For every parameter, 60 measurements were made to control the coefficient of variation CV ($CV = \frac{S.E.}{\bar{X}}$, where \bar{X} is the sample mean and S.E. is the standard error of the sample mean) between 0.01 and 0.05.

Scanning electron microscopy was used for microstructure, fracture surface and wear surface observation. An optical microscope was used for microstructure observation and quantitative metallography measurement.

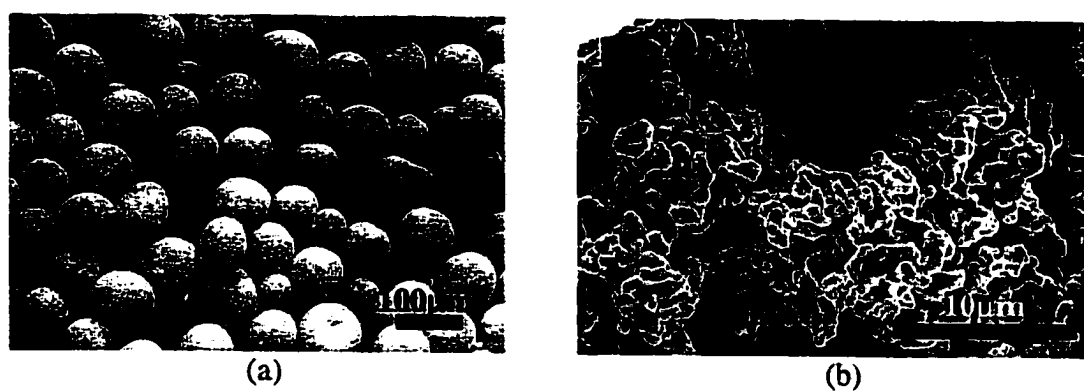


Fig. 6. Morphology of (a) typical granules and (b) cobalt powder.

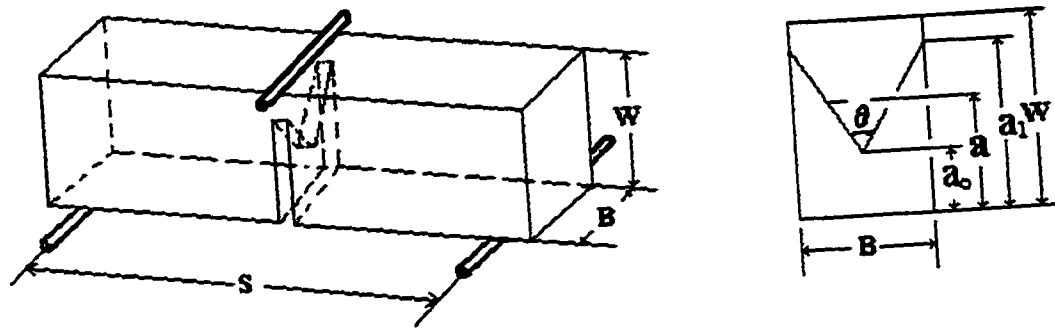


Fig. 7. Chevron-notched bar for toughness test (after [45]).

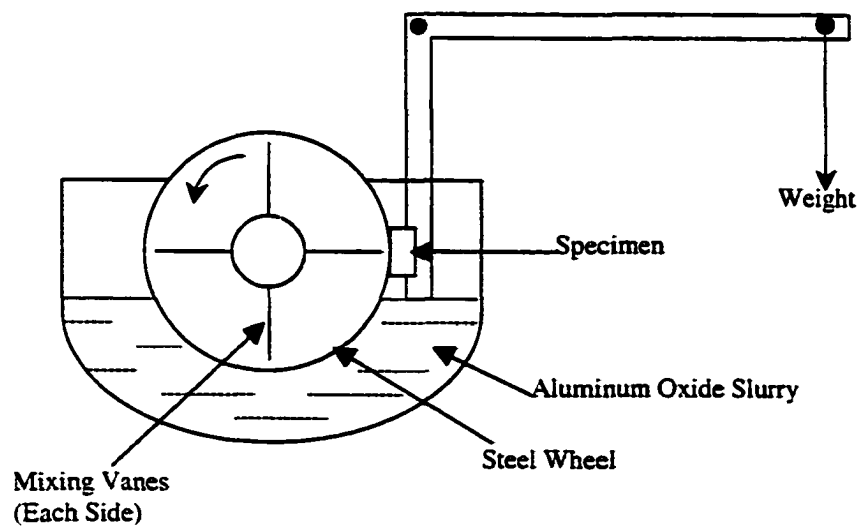


Fig. 8. High stress abrasive wear test apparatus (after [46]).

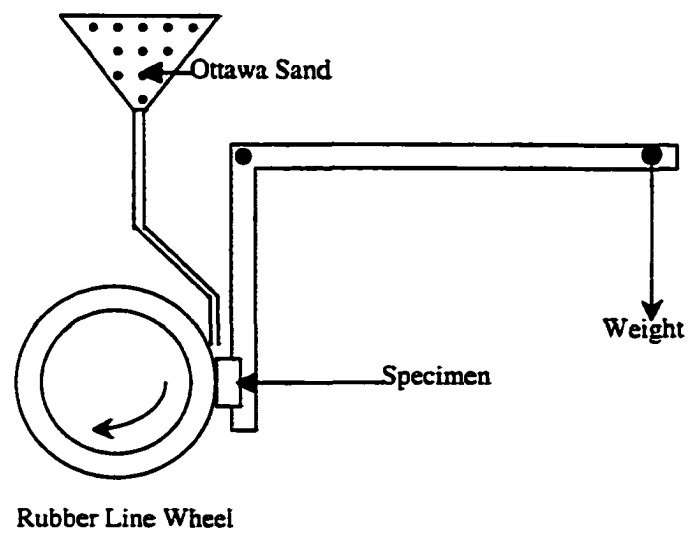


Fig. 9. Low stress abrasive wear test apparatus (after [47]).

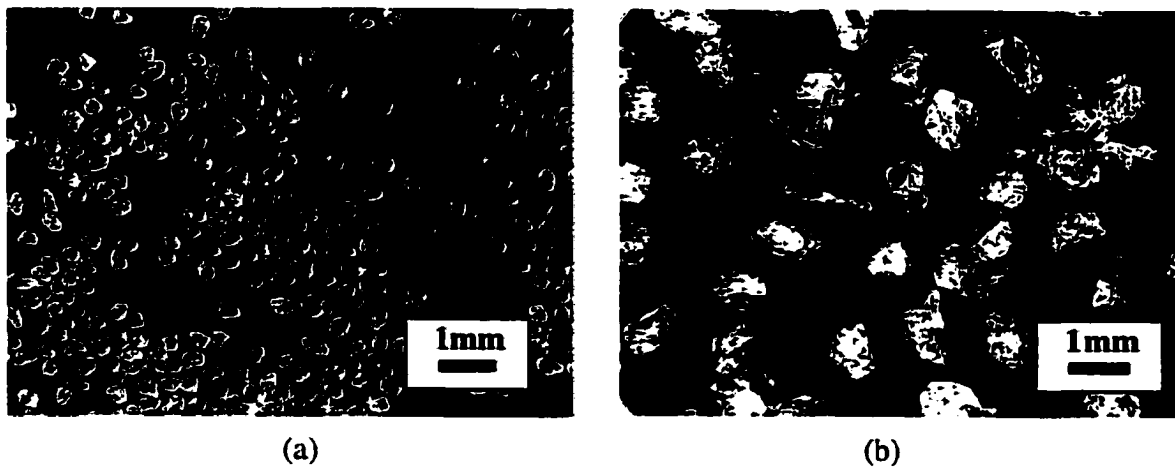
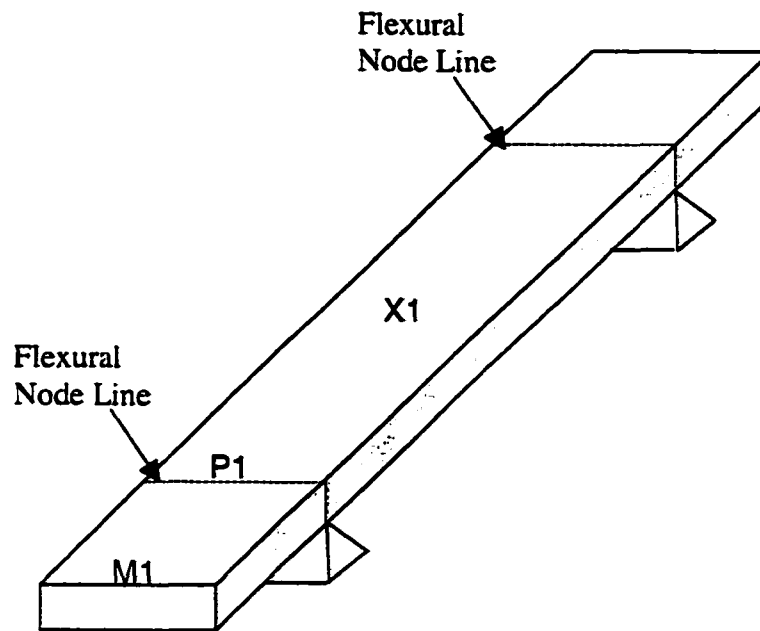


Fig. 10. Abrasive wear particles for (a) low stress wear test (SiO_2 , 212-300 μm) and (b) high stress wear test (Al_2O_3 , about 590 μm).



X1-OUT-OF-PLANE IMPULSE POINT
 P1-OUT-OF-PLANE CONTACT SENSOR POINTS
 M1-OUT-OF-PLANE MICROPHONE SENSOR POINT

Fig. 11. Rectangular specimen for dynamic Young's modulus measurement with impulse excitation of vibration (after [49]).

CHAPTER 4

EFFECT OF GRANULE COBALT CONTENT ON MECHANICAL PROPERTIES OF DC CARBIDE

In DC carbide, the granule is the reinforcement phase (>70 vol.%); therefore, the mechanical properties of DC carbide are controlled strongly by the granule properties. Three types of granules with similar WC size (3 μm) and granule size distribution but different cobalt binder levels (10, 18 and 25 vol.%) were selected for the investigation of the effect of granule cobalt content. Fig. 12 shows the typical granule size distribution for these three granules; the arrow indicates the upper size limit of the granules was not determined. The mechanical properties of three granules, which were obtained from hot-pressed pure granules (0 vol.% metal-matrix content) are shown in Table 3. With increased granule cobalt content, granule hardness decreases and toughness increases. The internal microstructures of granules with different cobalt contents are shown in Fig. 13. Here, it can be seen that the mean free path of binding phase within the granules increases from 1 μm (10 vol.% cobalt in granule) to 3 μm (25 vol.% cobalt in granule) with increased cobalt content.

Cobalt was selected as the metal-matrix throughout these studies, with content varying from 0 to 30 vol.%. The DC carbide with 0 vol.% metal-matrix, similar to conventional cemented carbide, was produced for comparison by hot pressing granules with no intergranular cobalt. Three additional conventional cemented carbides with 30, 40 and 50 vol.% cobalt were produced, with WC particle size of 3 μm . Fig. 14 shows the

microstructure of DC carbide with different metal-matrix content. With decreased metal-matrix content, contiguity of granule increases and the mean free path of metal-matrix decreases.

Table 3. Mechanical properties of granules

| Granule Co content | | Average WC | | |
|--------------------|--------|---------------------------------|---------------|--|
| wt. % | vol. % | particle size (μm) | Hardness (HV) | K_{Ic} ($\text{MPa}\cdot\text{m}^{1/2}$) |
| 6 | 10 | 3 | 1659 | 10.9 |
| 11 | 18 | 3 | 1340 | 13.4 |
| 16 | 25 | 3 | 1139 | 16.7 |

4.1. Toughness

Fig. 15a shows the toughness of DC carbide with different granule cobalt contents as the function of cobalt metal-matrix content. Toughness increases with the increased metal-matrix content; at the same matrix content, tougher granules yield higher DC carbide toughness, as expected.

When the total cobalt content in DC carbide, including the cobalt in the metal-matrix as well as the cobalt in the granules, is considered, Fig. 15a transforms to Fig. 15b. At the constant total cobalt content, the arrow direction indicates that DC carbide has higher toughness than conventional cemented carbide and harder granules (lower cobalt content in the granules) and larger mean free path of metal-matrix in DC carbide (more cobalt in metal-matrix) result in the higher toughness of the overall material.

Fig. 16 shows the microstructure development from typical DC carbide to conventional cemented carbide in the reverse direction of the arrow in Fig. 15b. At the same total cobalt content, as more cobalt is transferred from the metal-matrix to the granules (granule size remains constant but the number of granules increases), the

granules become tougher; however, the mean free path of the metal-matrix decreases. When all the cobalt in the metal-matrix is transferred to the granules, DC carbide becomes conventional cemented carbide with zero mean free path of intergranular metal-matrix and has very low toughness. Fig. 15b shows directly that DC carbide has higher toughness than conventional cemented carbide with the same total cobalt content. Figs. 15b and 16 indicate the more significant effect of mean free path of metal-matrix on the toughness of DC carbide compared to the effect of granule toughness.

The fracture surface of DC carbide after the toughness test is basically flat (Fig. 17), where the granules show brittle fracture and the metal-matrix shows ductile dimples, indicating the crack prefers to go across the granules rather than along the granule/matrix interface. Because of the composite nature of the granules and the strong binding condition between cobalt matrix and WC, it is difficult to form a weak and smooth granule/matrix interface, and fracture along the granule/matrix interface is not common.

4.2. *Wear resistance*

4.2.1. *High stress wear resistance*

Fig. 18a shows the high stress wear resistance of DC carbide as the function of metal-matrix content. At the same metal-matrix content, harder granules yield higher wear resistance. Increased metal-matrix content decreases wear resistance.

When the total cobalt content (granule + matrix) is considered, Fig. 18a becomes Fig. 18b. At constant total cobalt content, harder granules yield higher wear resistance as shown by the arrow in Fig. 18b, which also demonstrates the greater high stress wear resistance of DC carbide over conventional cemented carbide.

The wear surface of DC carbide in Fig. 19a and Fig. 19b is quite different from that of conventional cemented carbide (Fig. 19c). The DC carbide wear surface shows granule protrusion while the conventional cemented carbide wear surface is basically flat. In addition, the harder the granules, the more convex the granules and the more concave the metal-matrix becomes. Harder granule protrusion forms discontinuous hard facing of DC carbide, which enhances the high stress wear resistance of DC carbide.

4.2.2. *Low stress wear resistance*

Fig. 20a shows the low stress wear resistance of DC carbide as a function of metal-matrix content. At constant metal-matrix content, harder granules give higher wear resistance (lower volume loss); for each granule type, increased metal-matrix content decreases wear resistance. This tendency is quite similar to that of high stress wear resistance as shown in Fig. 18a.

Fig. 20b gives the low stress wear resistance of both DC carbide and conventional cemented carbide as a function of the total cobalt content. When the total cobalt content is over 30 vol.%, conventional cemented carbide has higher low stress wear resistance than DC carbide. For a total cobalt content less than 30 vol.%, DC carbide has wear resistance similar to the wear resistance of conventional cemented carbide. DC carbide has no advantage over conventional cemented carbide in low stress wear resistance, which is also caused by its special double structure.

Fig. 21 shows the DC carbide wear surface for the high and low stress wear tests. The low stress wear surface (Fig. 21a) shows more smooth granules and concave metal-matrix than the high stress wear surface shows (Fig. 21c). The low stress wear surface of

granules (Fig. 21b) shows that the cobalt binding phase was removed first, increasing the possibility of the WC particles being pulled out, while the high stress wear surface of granules (Fig. 21d) shows that WC and Co were removed from the granule all together.

Fig. 21e and 21f show further the difference between high and low stress wear tests with the side view, where the low stress wear surface shows more metal-matrix removal and fracture of granule caps (Fig. 21f) compared with the high stress wear surface (Fig. 21e).

Because of the double structure of DC carbide, which results in a larger mean free path of metal-matrix ($\sim 20\text{-}40\text{ }\mu\text{m}$) than the path found in conventional cemented carbide (about several micrometers); in addition, because of the rubber wheel and SiO_2 abrasive (smaller and softer than the Al_2O_3 abrasive in the high stress wear test) employed in the low stress wear test, DC carbide is subjected to more metal-matrix and cobalt-binding-phase removal than conventional cemented carbide in the low stress wear test condition. When the metal-matrix or cobalt binding phase is removed to a certain degree, granules or WC particles are easily pulled out. The preferred metal-matrix removal and granule cap fracture are the main reasons DC carbide has no advantage over conventional cemented carbide in the low stress wear test.

4.2.3. *Flexural strength*

Fig. 22a shows the effect of metal-matrix content on the flexural strength of DC carbide. Flexural strength increases with the increased metal-matrix content. At the same metal-matrix content, DC carbide with 25 vol.% cobalt granules has the highest flexural strength. All DC carbides (10 to 30 vol.% metal-matrix) have higher flexural strength

than pure granules (0 vol.% metal-matrix). Compared with toughness of DC carbide or conventional cemented carbide, flexural strength of DC carbide is more sensitive to sample surface finishing quality, microstructure defects and test conditions. Microstructure defects play an especially important role on flexural strength of DC carbide and conventional cemented carbide, which is the main reason HIP can increase flexural strength to a large degree but cannot increase toughness much. Hot pressing below liquid-phase-sintering temperature is not an effective method to eliminate microstructural defects for DC carbide because of the lower hot pressing temperature compared with liquid-phase sintering and its lower pressure compared with HIP. The microstructure defects include microcracks and porosity existing mainly inside the granule and at the granule/granule contact area. With higher cobalt-matrix levels, granule/granule contact area is reduced and defect density of DC carbide is reduced; therefore, the flexural strength increases. (The defect size in DC carbide can be estimated with the equation $K_{Ic} = \sigma\sqrt{\pi a}$. When the known toughness value, K_{Ic} , and flexural strength value, σ , for DC carbide are substituted, the defect size in DC carbide varies from 10 to 70 μm).

When the total cobalt content of DC carbide is considered, Fig. 22a becomes Fig. 22b, which shows that conventional cemented carbide has higher flexural strength than DC carbide at the same total cobalt content. With increasing total cobalt content, flexural strength of DC carbide increases first and decreases after the peak value.

Chou [53] developed the following metal-matrix-strength model for particle-strengthened composites:

$$\bar{\sigma}_t = \sigma_o + k_y (\bar{r}_m)^{-1/2} \quad (39)$$

where σ_o and k_y are constants and \bar{r}_m is the mean free path of the matrix.

Chou's [53] model (mean free path effect) shows the negative effect of mean free path of matrix, i.e., increased mean free path decreases strength of metal-matrix and the overall composite. The mean free path of metal-matrix for conventional cemented carbide is about several micrometers and for DC carbide can be as high as 40 μm , so the flexural strength difference between conventional cemented carbide and DC carbide is apparent according to eq (39). For both DC carbide and conventional cemented carbide, two factors contribute to the decrease of flexural strength. One is the defect (microcracks and pores) density and the other is the mean free path of metal-matrix. As shown in Fig. 22b, DC carbide strength increases with increased cobalt content at low matrix fractions when the defect effect plays the most important role. When cobalt content increases to a certain degree, the mean free path effect becomes more important, and strength begins to decrease with the increased cobalt content, as is apparent in the conventional cemented carbide data.

Fig. 23 compares the load-displacement curves between DC carbide and conventional cemented carbide with similar total cobalt contents. The DC carbide curve (Fig. 23a) shows ductility (displacement) similar to but no greater than ductility shown by the conventional cemented carbide curve (Fig. 23b) at similar loading. Compared with DC carbide (mean free path of metal-matrix is 37 μm), the mean free path of

conventional cemented carbide is much smaller (6 μm); therefore, the mean free effect leads to much higher flexural strength of conventional cemented carbide.

4.2.4. *Hardness*

Hardness, a basic property of materials, is often used to evaluate other characteristics such as wear resistance and strength. Measurement of DC carbide hardness is necessary for the mechanical property comparison between DC carbide and conventional cemented carbide.

Fig. 24a shows the effect of metal-matrix content and granule type on the hardness of the overall composite. For each granule type, the composite hardness decreases with increased metal-matrix content. At constant metal-matrix content, the harder granules (lower granule cobalt content) show higher composite hardness, as expected. It is also noticeable that the hardness difference between the curves for the hardest and softest granules is the greatest at the low-matrix end of the plot. This observation indicates that granule hardness has the greatest effect when there is little matrix and that increased matrix content reduces the effect of the granule reinforcement.

Fig. 24b illustrates the relationship between hardness and total cobalt content for both conventional cemented carbide and DC carbide. At the same total cobalt content, the conventional cemented carbide shows a slightly but consistently higher hardness than the DC carbide. This lower hardness of DC carbide is caused by the granular structure, with the cobalt matrix providing regions with relatively large mean free path compared to the conventional particulate structure.

4.2.5. Young's modulus

Young's modulus of DC carbide is shown in Fig. 24. Because Young's moduli of pure granules (100 vol.% granule) and cobalt matrix are known, Hashin-Shtrikman bounds for DC carbide [35] are set up, where lower bound is

$$E_1 = \frac{9K_1G_1}{3K_1 + G_1}$$

$$= \frac{9 \left(K_m + \frac{V_g}{[1/(K_g - K_m)] + [3V_m/(3K_m + 4G_m)]} \right) \left(G_m + \frac{V_g}{[1/(G_g - G_m)] + [6(K_m - 2G_m)V_m]/[5(3K_m - 4G_m)G_m]} \right)}{3 \left(K_m + \frac{V_g}{[1/(K_g - K_m)] + [3V_m/(3K_m + 4G_m)]} \right) + \left(G_m + \frac{V_g}{[1/(G_g - G_m)] + [6(K_m - 2G_m)V_m]/[5(3K_m - 4G_m)G_m]} \right)} \quad (40)$$

and the upper bound is

$$E_2 = \frac{9K_2G_2}{3K_2 + G_2}$$

$$= \frac{9 \left(K_g + \frac{V_m}{[1/(K_m - K_g)] + [3V_g/(3K_g + 4G_g)]} \right) \left(G_g + \frac{V_m}{[1/(G_m - G_g)] + [6(K_g - 2G_g)V_g]/[5(3K_g + 4G_g)G_g]} \right)}{3 \left(K_g + \frac{V_m}{[1/(K_m - K_g)] + [3V_g/(3K_g + 4G_g)]} \right) + \left(G_g + \frac{V_m}{[1/(G_m - G_g)] + [6(K_g - 2G_g)V_g]/[5(3K_g + 4G_g)G_g]} \right)} \quad (41)$$

where E, K and G are the Young's, bulk and shear moduli, respectively; V is the volume fraction; and subscripts g and m stand for granule and metal-matrix, respectively.

The relationships among Young's, bulk and shear moduli for an isotropic material are given [54]:

$$G = \frac{E}{2(1 + \mu)} \quad (42)$$

$$K = \frac{E}{3(1 - 2\mu)} \quad (43)$$

where μ is Poisson's ratio.

Young's modulus of cobalt is 211 GPa [37], and Young's modulus of the pure granules was measured directly. As a result, Fig. 25a shows Hashin-Shtrikman's [35] upper and lower bounds for DC carbide with different granules, demonstrating that this model is valid for DC carbide.

When the total cobalt content in DC carbide is considered, Hashin-Shtrikman [35] boundaries in Fig. 25b were calculated from elastic properties of pure WC and cobalt. The elastic modulus data for pure WC are given by Doi et al. [37]. Young's modulus of DC carbide fits well inside the Hashin-Shtrikman [35] boundaries, indicating that, compared with conventional cemented carbide, the double structure of DC carbide does not change the elastic property and that the total cobalt content is the most significant factor controlling Young's modulus.

4.2.6. Relationship between toughness and wear resistance of DC carbide

With the combination of Figs. 15 and 18, the relationship between toughness and high stress wear resistance of DC carbide is shown in Fig. 26, where, for both DC carbide and conventional cemented carbide, toughness and wear resistance are two conflictive properties, i.e. the gain of one property is the loss of the other, but DC carbide shows superior combination of toughness and high stress wear resistance over conventional cemented carbide. In the arrow direction in Fig. 26, the total cobalt content remains constant, DC carbide with harder granules (less cobalt content inside the granules) leads to larger mean free path of metal-matrix, and both toughness and high stress wear resistance increase simultaneously.

Fig. 27 shows the relationship between toughness and low stress wear resistance of both DC carbide and conventional cemented carbide. DC carbide still shows superior toughness over conventional cemented carbide but no better low stress wear resistance because of its double structure.

During the investigation of the effect of granule cobalt content, direct comparison between DC carbide and conventional cemented carbide was made. At the same total cobalt content, compared with conventional cemented carbide, DC carbide shows higher toughness and high stress wear resistance, as well as similar hardness, Young's modulus and low stress wear resistance, but lower flexural strength. In addition, DC carbide shows a superior combination of toughness and high stress wear resistance compared to conventional cemented carbide; the harder (lower granule cobalt content) the granules, the more apparent this advantage becomes.

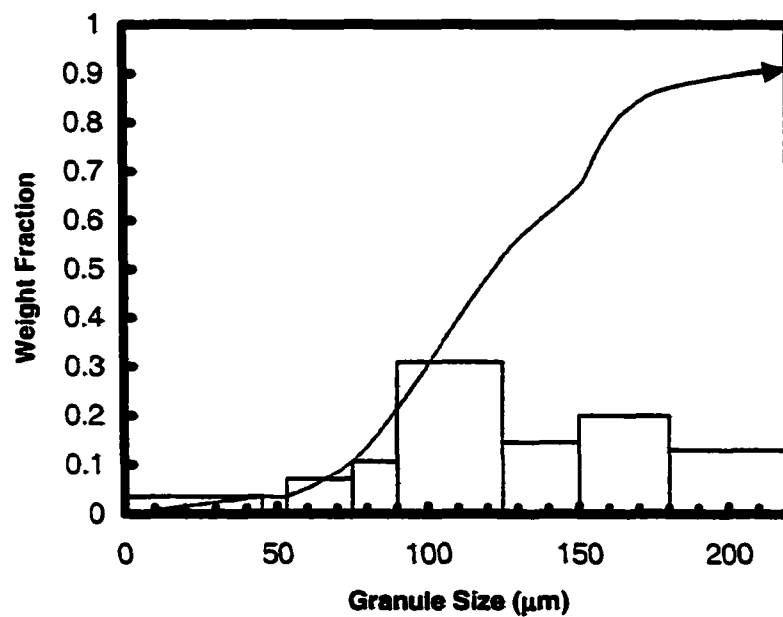


Fig. 12. Granule size histogram and cumulative curve for the 10 vol.% cobalt granule, typical of the three granule types with about 3 μm WC and 10, 18 and 25 vol.% cobalt.

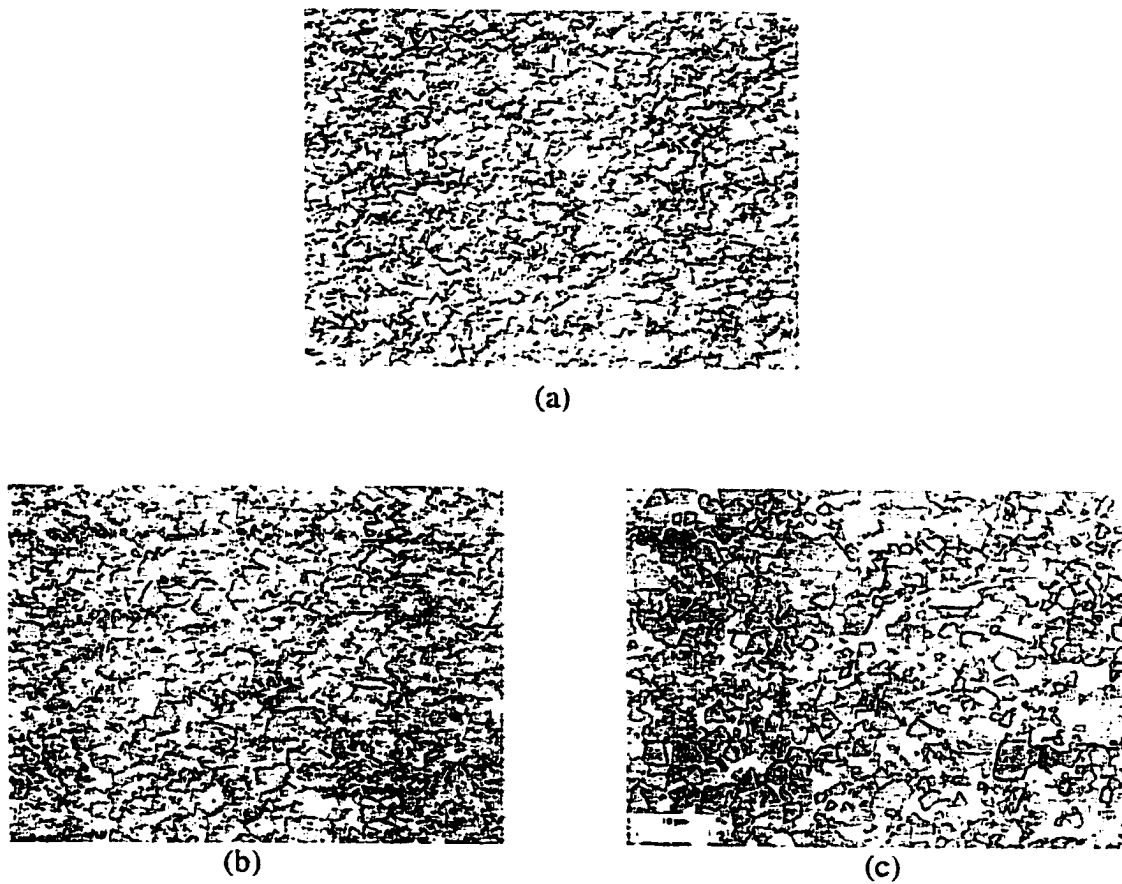


Fig. 13. Microstructure of granules with similar WC size ($3\text{ }\mu\text{m}$) but different cobalt content: (a) 10, (b) 18 and (c) 25 vol.%.

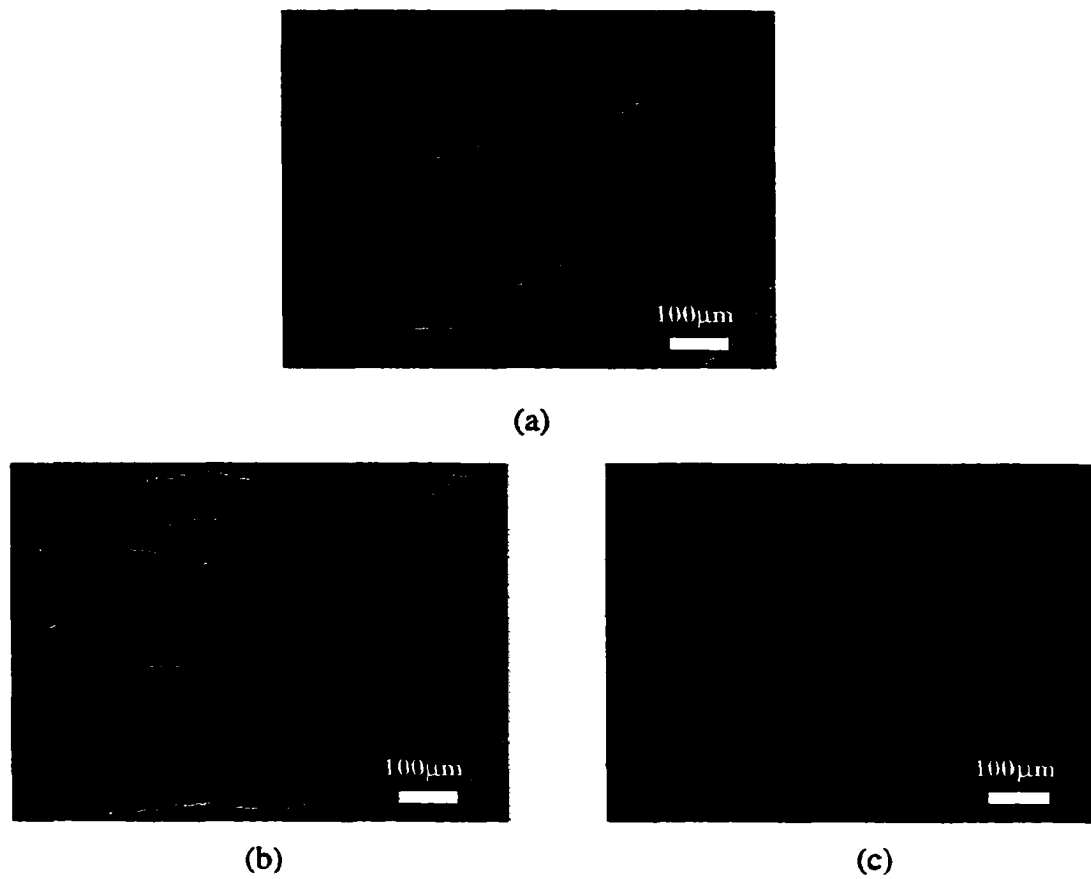
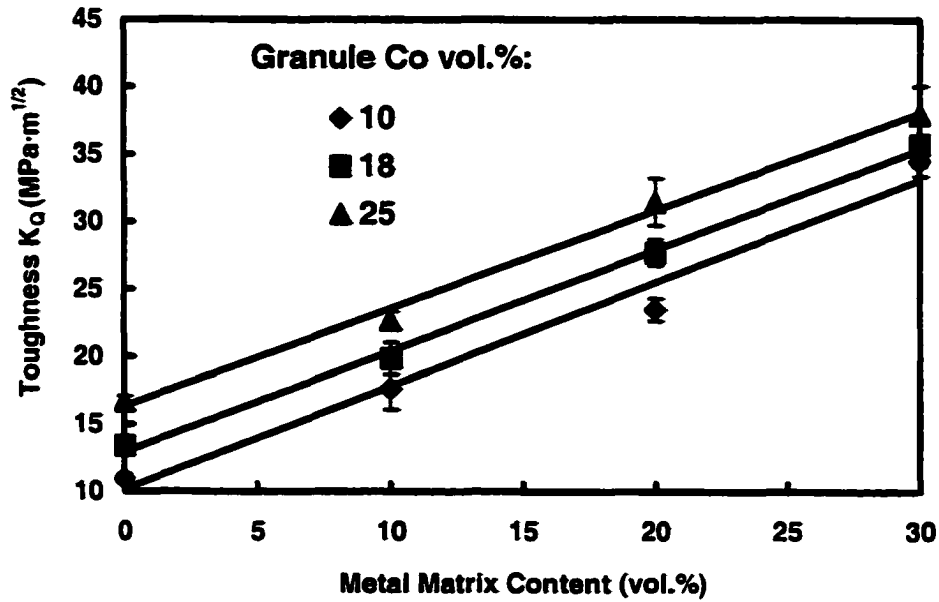
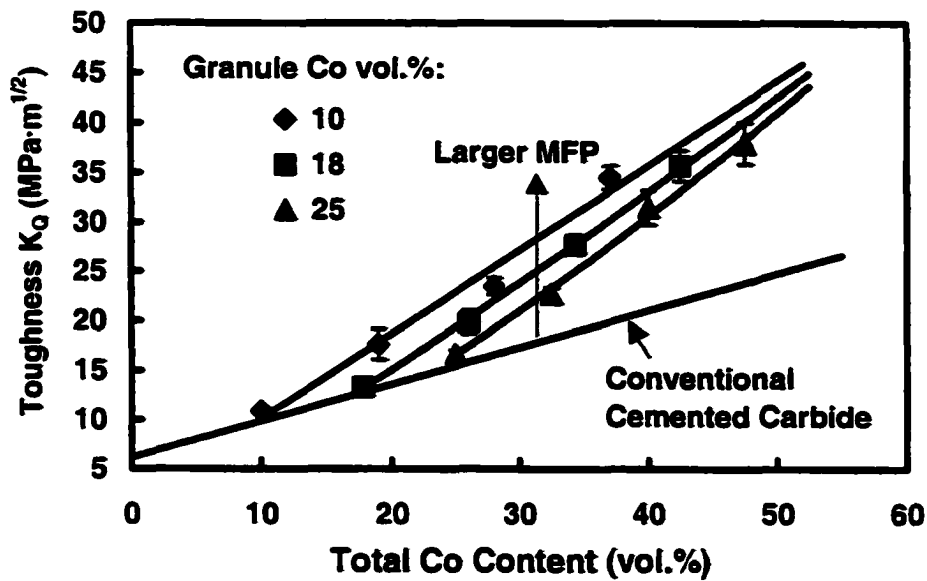


Fig. 14. Microstructure of DC carbide with (a) 70, (b) 80 and (c) 90 vol.% granule, granule cobalt content 10 vol.%, granule WC size 3 μm .



(a)



(b)

Fig. 15. Toughness of DC carbide with different granule cobalt contents but similar WC size (3 μ m) as a function of (a) cobalt metal-matrix content and (b) total cobalt content (including the cobalt inside the granule and the cobalt in the metal-matrix). "MFP" in (b) stands for mean free path of metal-matrix. Error bars are plus/minus one standard deviation.

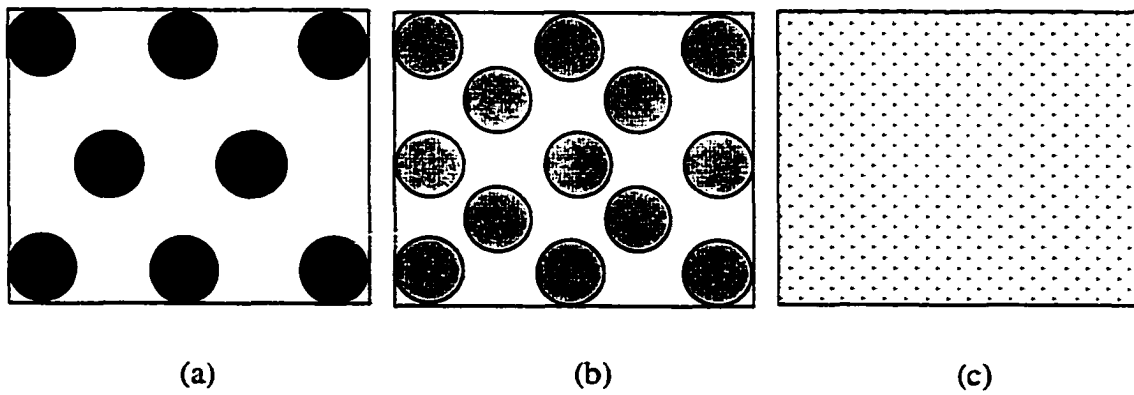


Fig. 16. Microstructure development from (a) DC carbide with low cobalt content granules to (b) DC carbide with high cobalt content granules to (c) conventional cemented carbide.

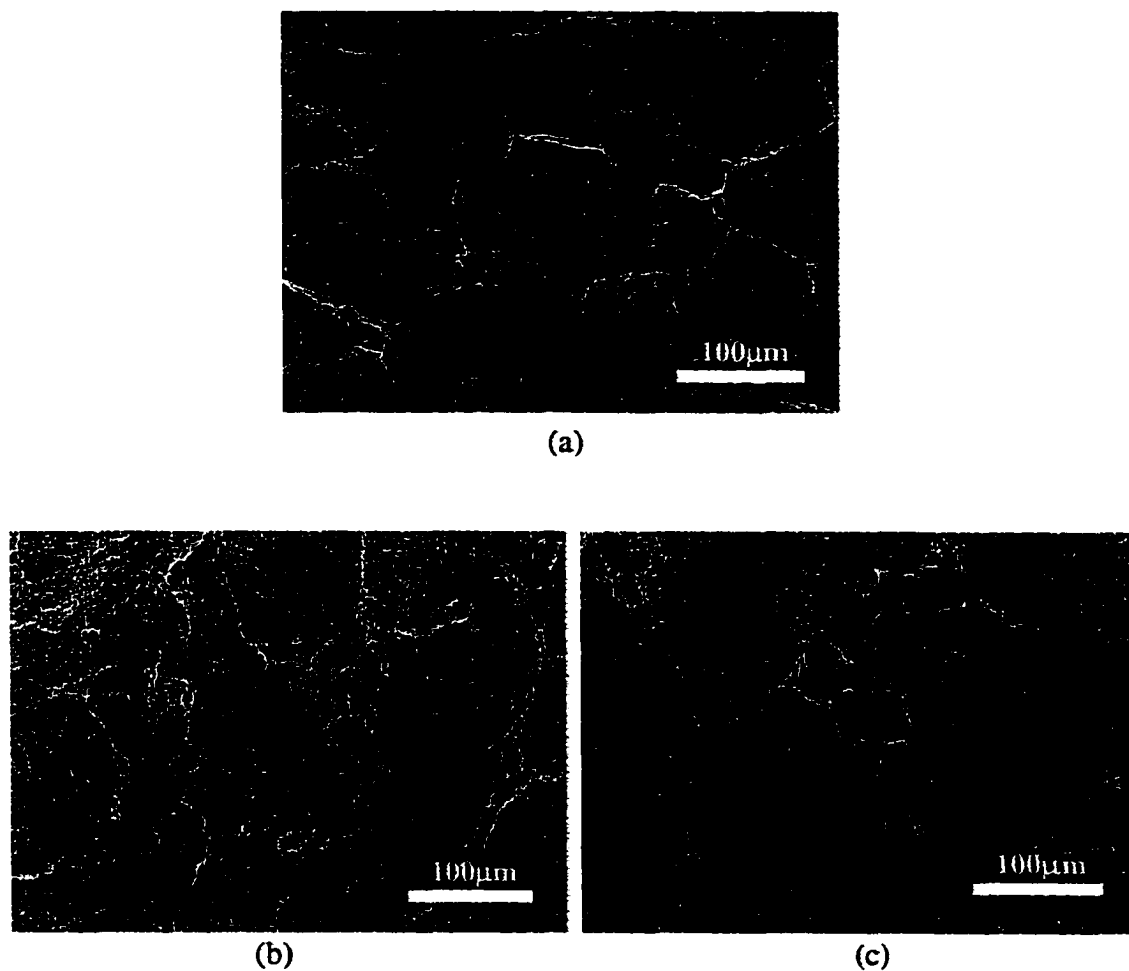
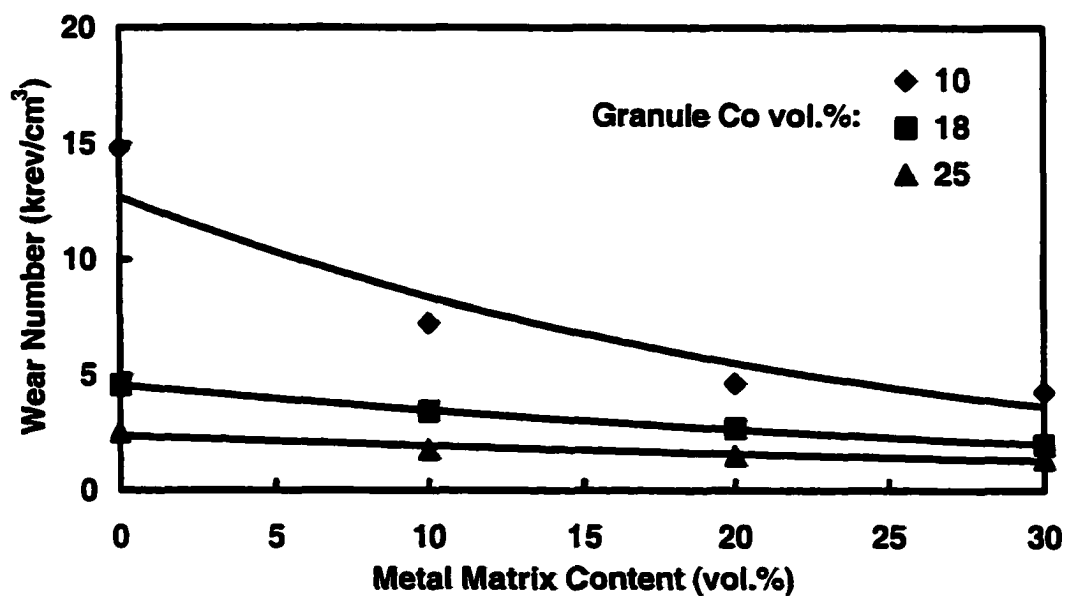
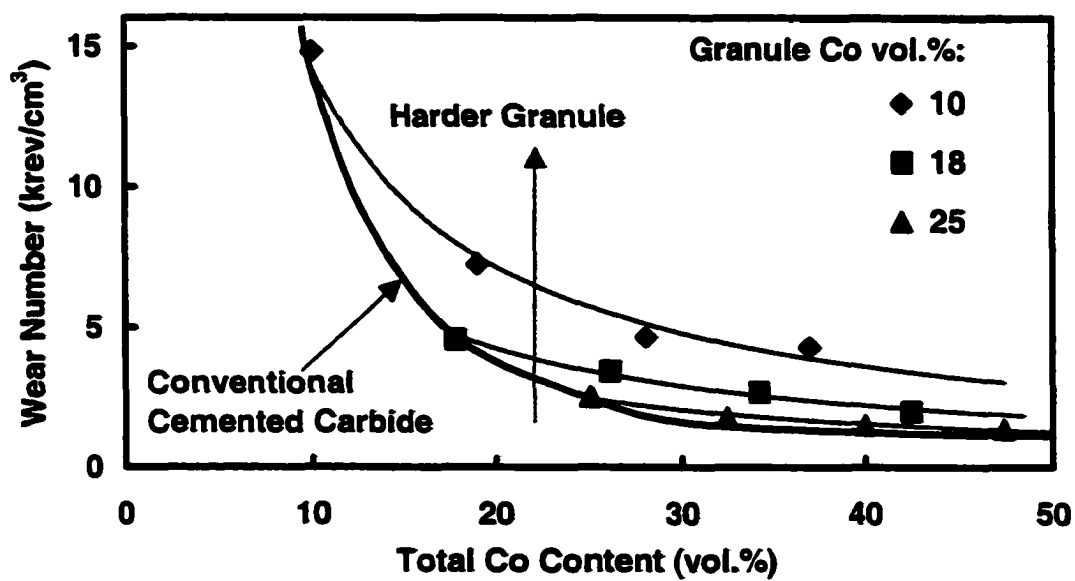


Fig. 17. Fracture surface of DC carbide with 10 vol.% granule cobalt and 3 μm WC but different metal-matrix content, (a) 30, (b) 20 and (c) 10 vol.% after toughness test, always showing flat fracture surface for DC carbide with different metal-matrix contents.



(a)



(b)

Fig. 18. Effect of (a) metal-matrix content and (b) total cobalt content on the high stress wear resistance of DC carbide with different granule cobalt content varying from 10 to 25 vol.% but the same WC size of 3 μm .

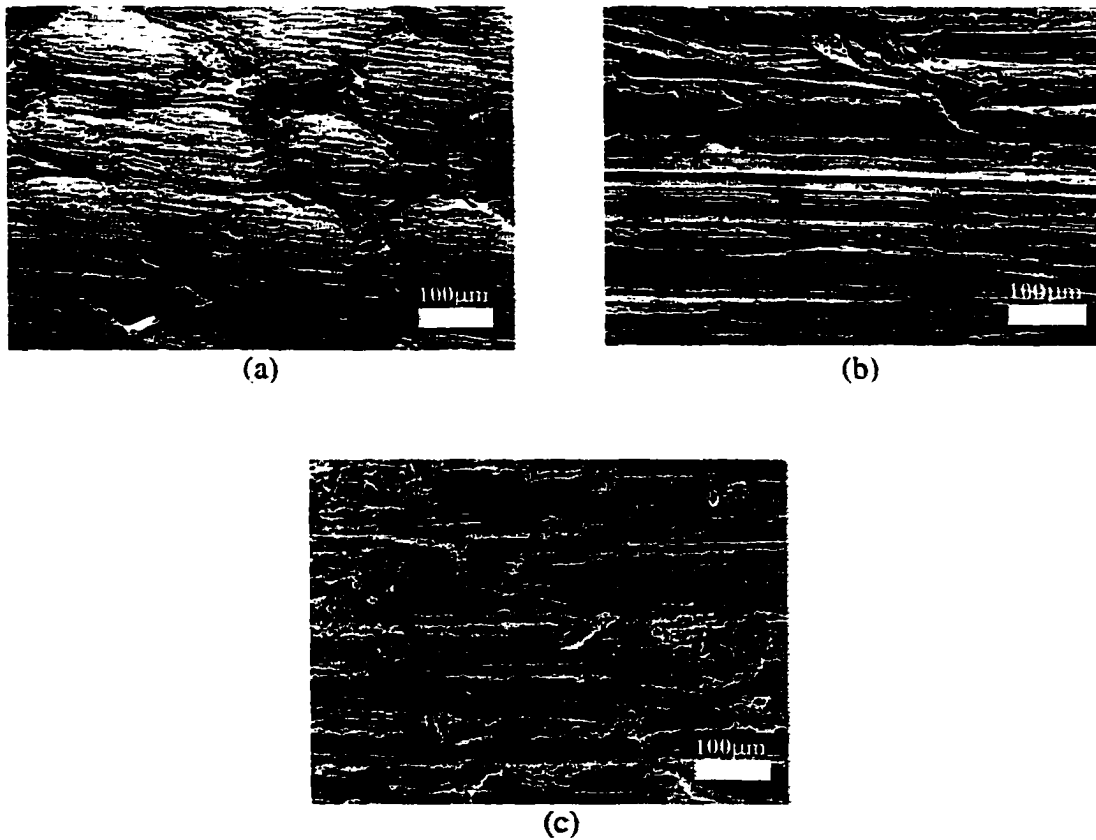
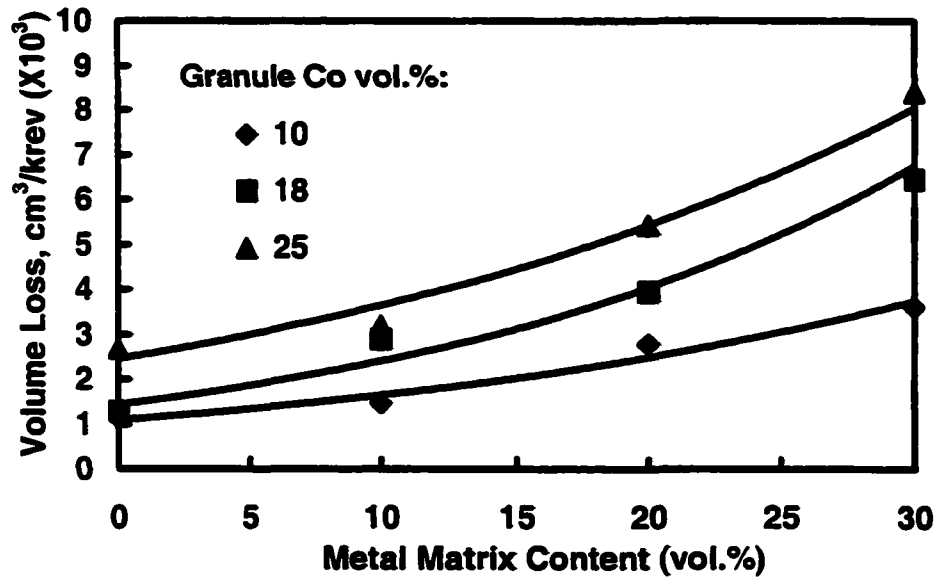
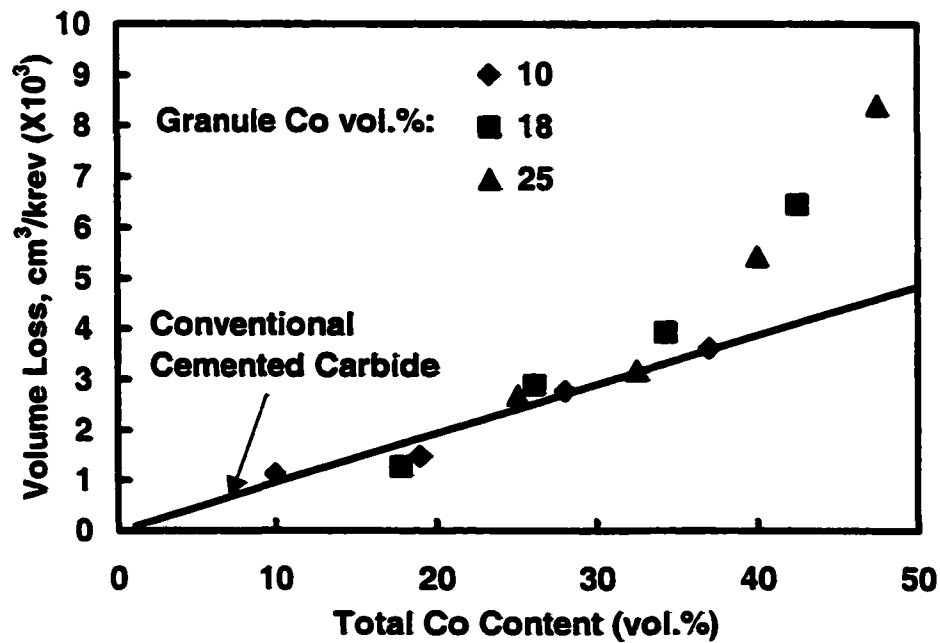


Fig. 19. Wear surface of DC carbide with 30 vol.% metal-matrix but different granules-(a) hard granules (10 vol.% cobalt in the granules) and (b) soft granules (25 vol.% cobalt in the granules)-and wear surface of (c) conventional cemented carbide with 30 vol.% cobalt, showing that the harder granule protrusion is the main reason DC carbide has higher high stress wear resistance than conventional cemented carbide.



(a)



(b)

Fig. 20. Effect of (a) metal-matrix content and (b) total cobalt content on the low stress wear resistance of DC carbide with different granule cobalt content varying from 10 to 25 vol.% but the same WC size of 3 μm . DC carbide has no advantage over conventional cemented carbide in low stress wear resistance.

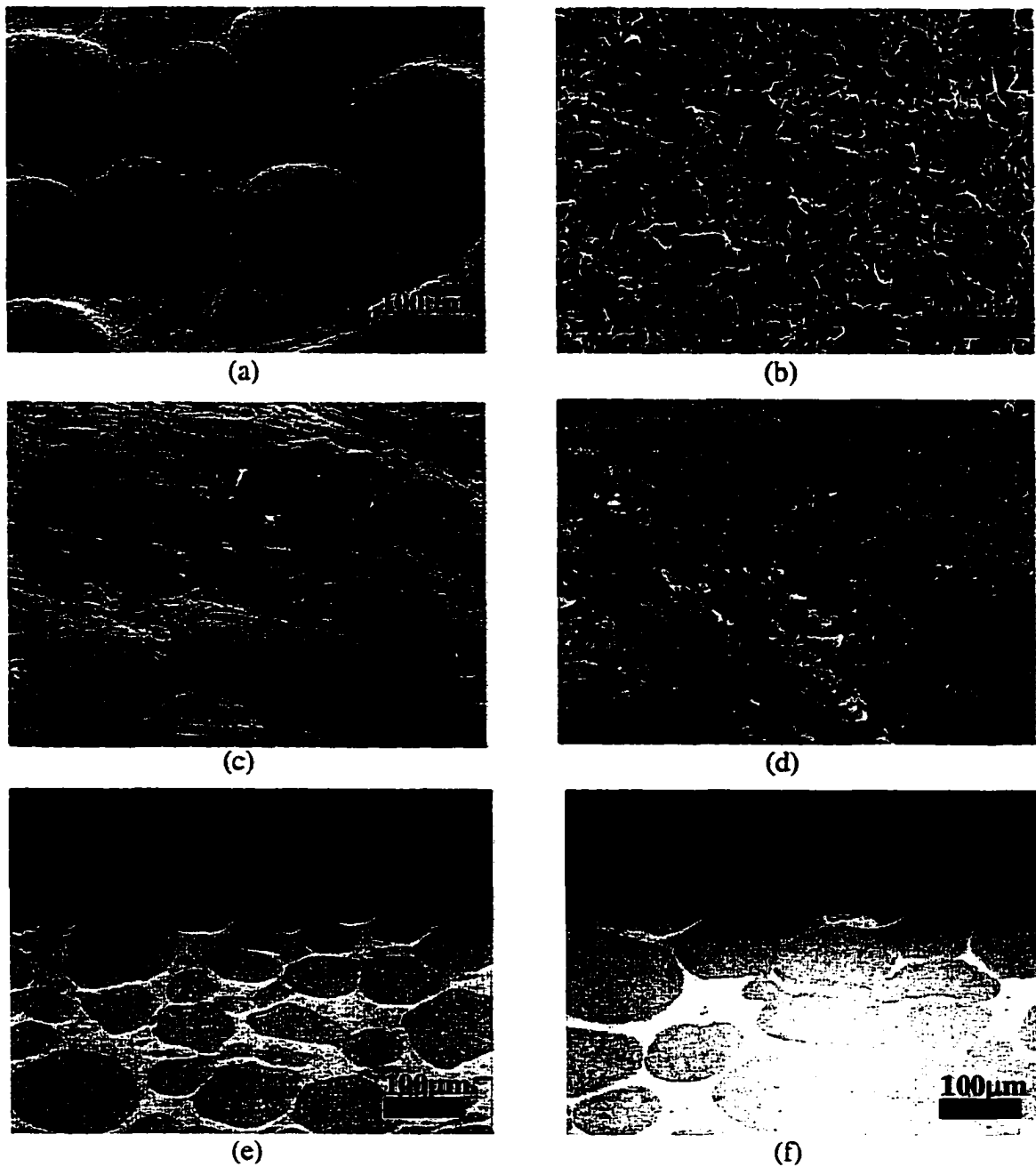
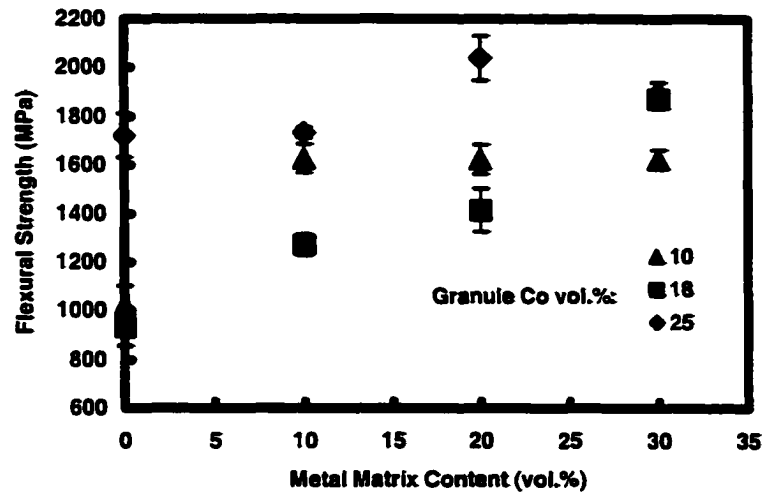
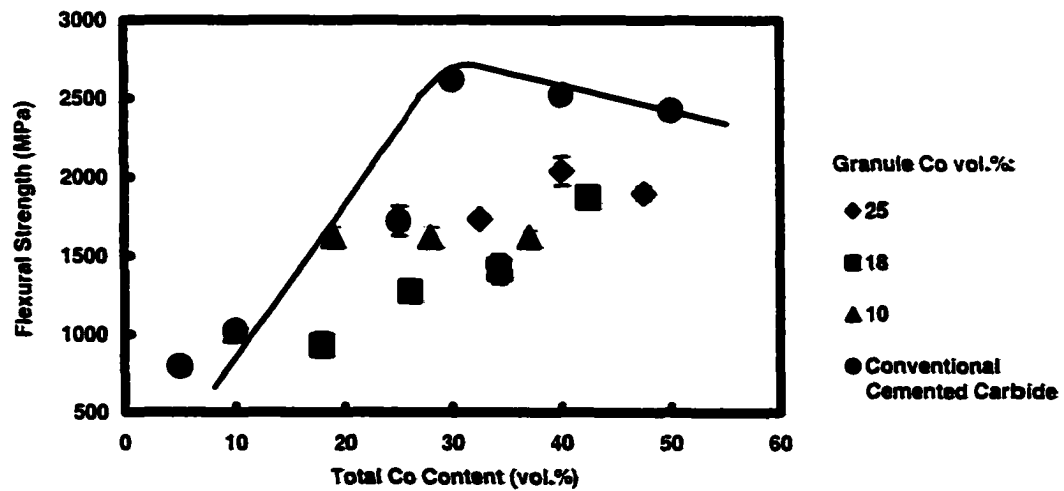


Fig. 21. Wear surface of DC carbide with 30 vol.% cobalt matrix, 10 vol.% granule cobalt and 3 μm WC. (a) Low stress wear surface of DC carbide, (b) low stress wear surface of granule, (c) high stress wear surface of DC carbide, (d) high stress wear surface of granule, (e) side view of high stress wear and (f) side view of low stress wear. The preferred metal-matrix and cobalt-binding-phase removal and granule cap fracture are the main low stress wear mechanism for DC carbide and the main reason DC carbide has no advantage over conventional cemented carbide in low stress wear resistance.

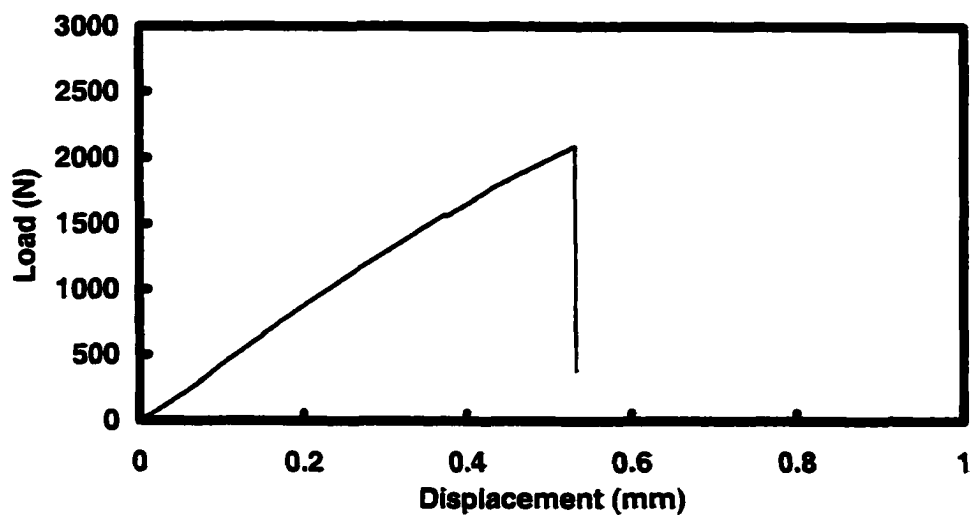


(a)

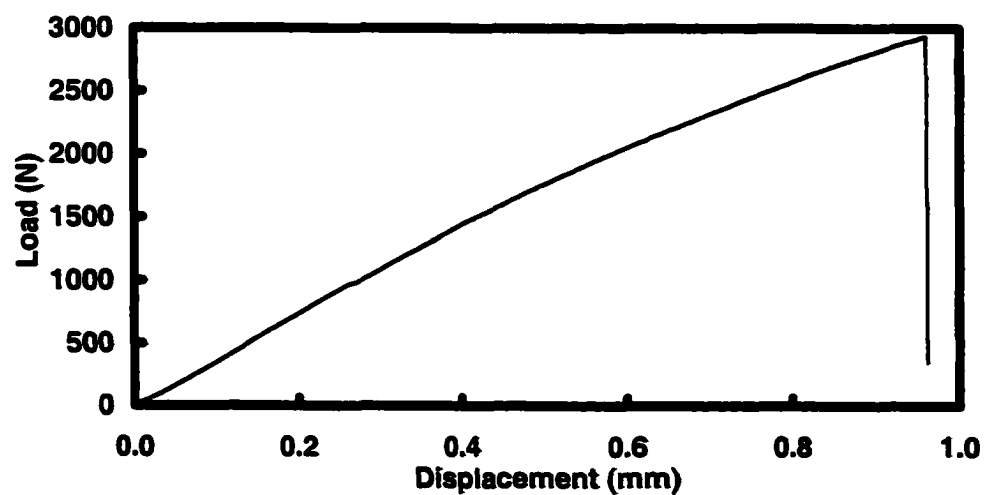


(b)

Fig. 22. Effect of (a) metal-matrix content and (b) total cobalt content on flexural strength of DC carbide with different granule cobalt content varying from 10 to 25 vol.% but the same WC size of 3 μm . Error bars are plus/minus one standard deviation.

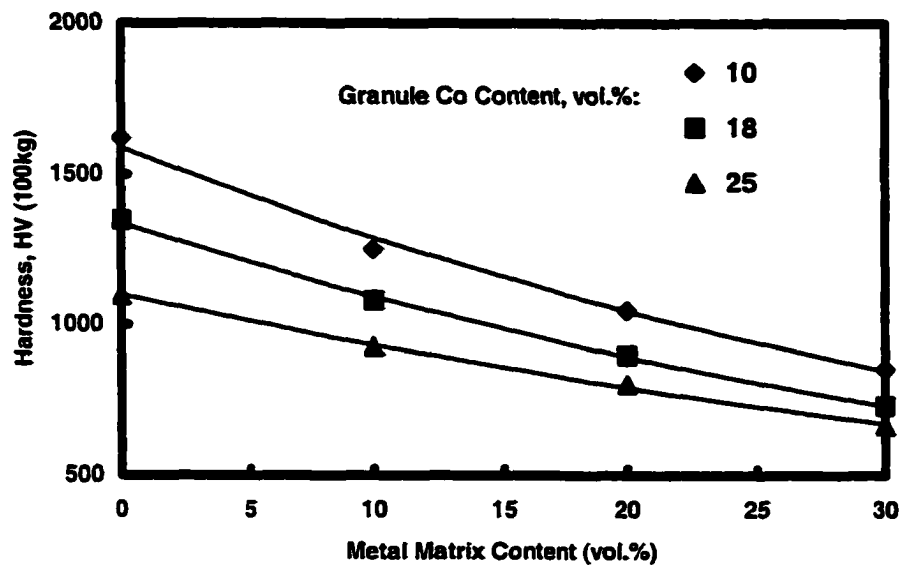


(a)

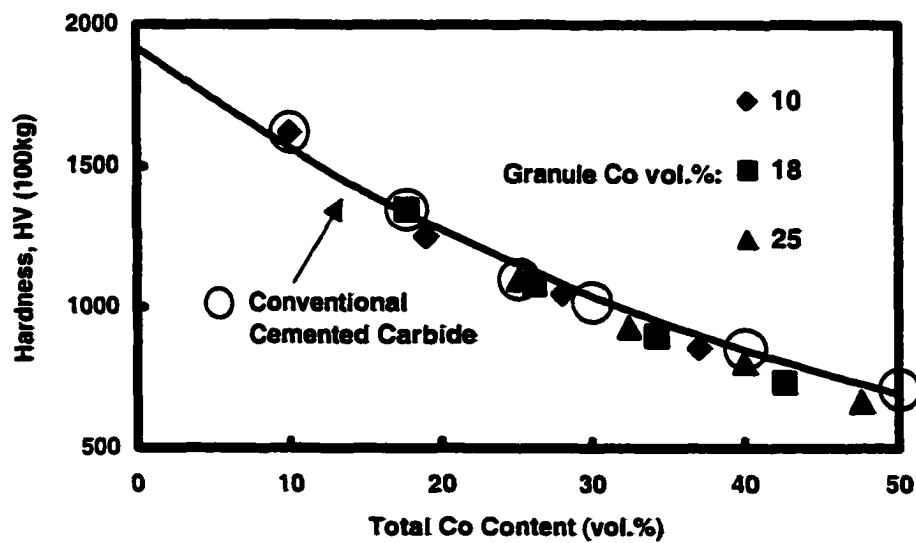


(b)

Fig. 23. Load-displacement curve of flexural strength test for (a) DC carbide with 30 vol.% cobalt matrix, 10 vol.% granule cobalt and 3 μm WC and (b) conventional cemented carbide with 40 vol.% cobalt and 3 μm WC.

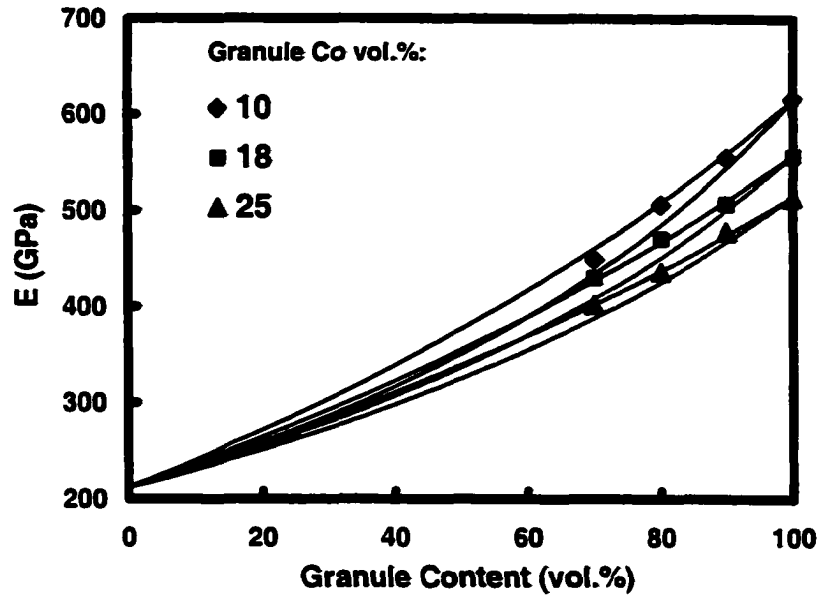


(a)

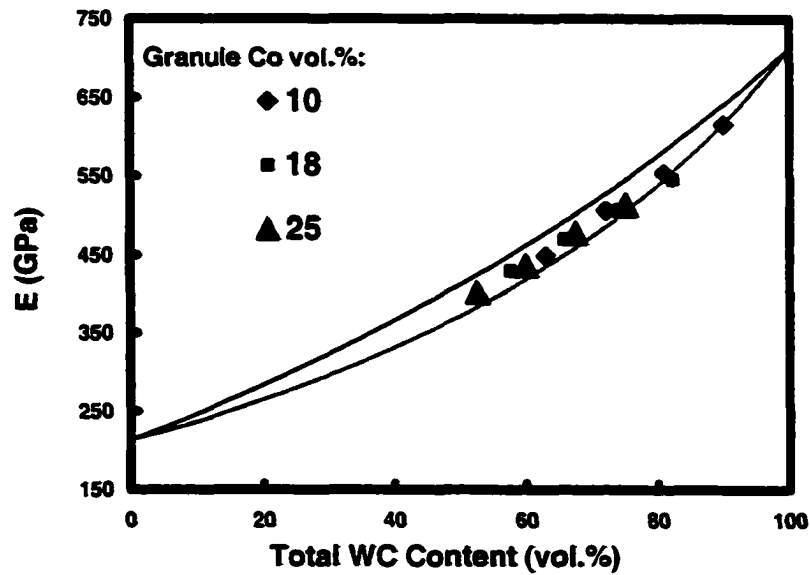


(b)

Fig. 24. Vickers hardness of DC carbide with 3 μm WC inside the granules but different granule cobalt content varying from 10 to 25 vol.% as a function of (a) metal-matrix content and (b) total cobalt content. Compared with conventional cemented carbide, DC carbide shows only slightly lower hardness.



(a)



(b)

Fig. 25. Young's modulus and Hashin-Shtrikman boundaries for DC carbide with different granule cobalt content (10-25 vol.%) but the same WC size ($3\ \mu\text{m}$) as a function of (a) granule content and (b) total WC content. The Hashin-Shtrikman model applies to DC carbide structure.

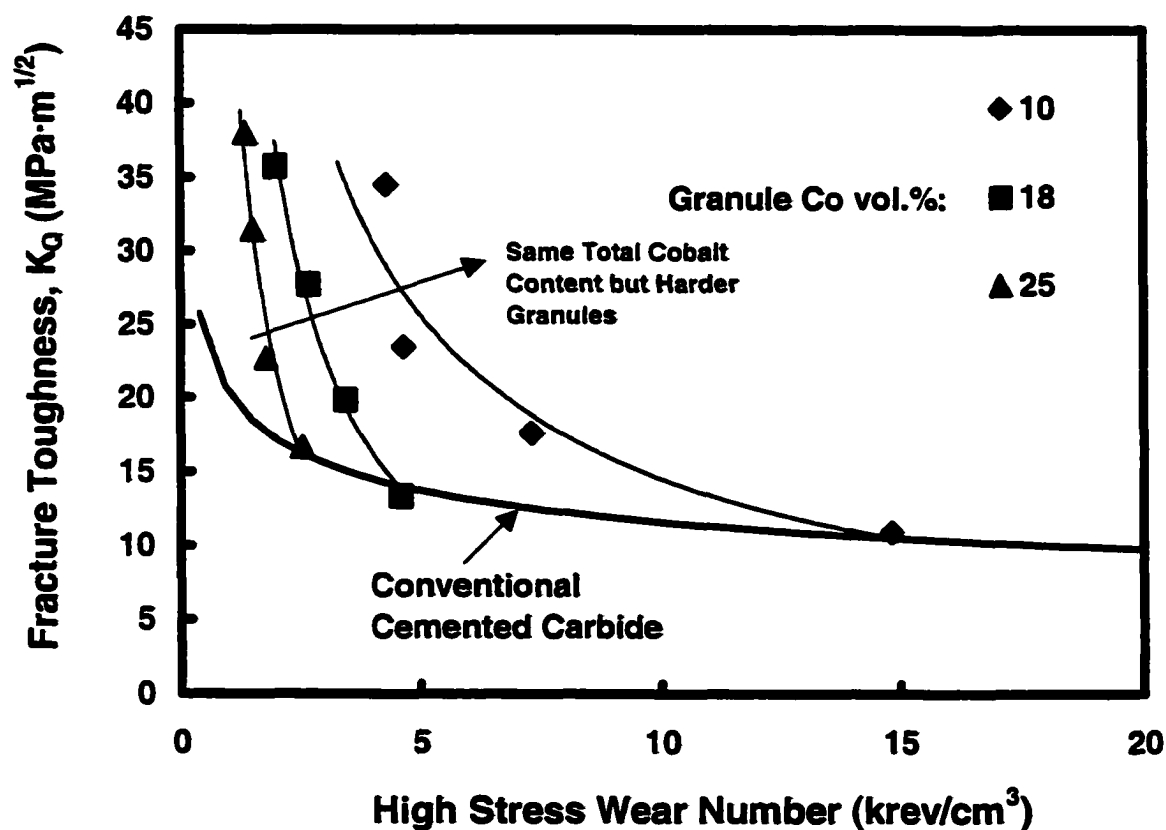


Fig. 26. Relationship between toughness and high stress wear resistance of DC carbide and conventional cemented carbide. Although toughness and high stress wear resistance are two properties with opposite dependencies for both DC carbide and conventional cemented carbide, DC carbide shows a superior combination of toughness and high stress wear resistance compared to conventional cemented carbide.

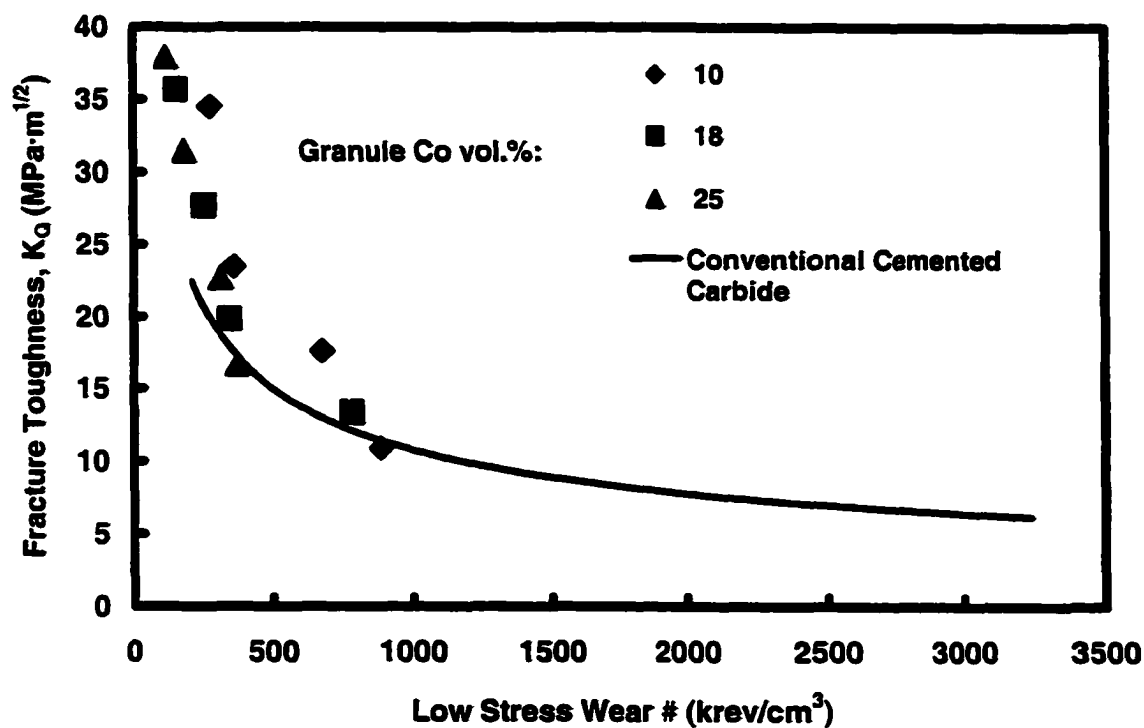


Fig. 27. Relationship between toughness and low stress wear resistance of DC carbide with 3 μ m WC inside the granules but different granule cobalt content varying from 10 to 25 vol.% compared with this relationship in conventional cemented carbide. DC carbide shows a better combination of toughness and low stress wear resistance than that of conventional cemented carbide to a limited degree only.

CHAPTER 5

EFFECT OF GRANULE WC SIZE ON MECHANICAL PROPERTIES OF DC CARBIDE

For conventional cemented carbide, WC particle size plays an important role in mechanical properties. At constant binder phase content, mean free path of binder phase increases with carbide particle size according to eq. (1) [19]. Along with the increase of carbide particle size, hardness decreases [31], toughness increases [20, 26, 28-30] and flexural strength reaches the maximum at a certain carbide particle size or mean free path of binder phase and then decreases (Fig. 4b) [31]. For DC carbide, changing WC particle size inside the granules will change mechanical properties of granules and finally change the overall properties of DC carbide. Four kinds of granules with different WC particle sizes (0.98, 1.56, 3.3, and 5.8 μm) and the same cobalt binder phase content (10 vol.%) were selected for this investigation. The granules were sieved, and only -80+120 mesh was used to eliminate granule size effect. The microstructure of granules is shown in Fig. 28, where increased WC particle size increases the mean free path of binding phase from less than 1 μm for granules with 0.98 μm WC to 3 μm for granules with 5.8 μm WC. Cobalt was again selected as the metal-matrix, the content of which is 0 (for pure granule property) and 30 vol.%.

5.1. *Toughness*

Fig. 29 shows the effect of WC particle size on the toughness of DC carbide. For DC carbide with pure granules, increased WC particle size increases the toughness slightly; however, for DC carbide with 70 vol.% granules, increased WC particle size increases the toughness of DC carbide even less, indicating that cobalt-matrix toughening effect makes granule WC size effect negligible.

5.2. *Wear resistance*

Fig. 30a shows the effect of WC particle size on high stress wear resistance of DC carbide. For both pure granule and DC carbide with 30 vol.% cobalt matrix, high stress wear resistance decreases with the increase of WC particle size. For low stress wear resistance of DC carbide, Fig. 30b gives similar trends. Along with the increase of WC particle size, low stress wear resistance decreases for both pure granules and DC carbide with 30 vol.% cobalt matrix. WC particle size shows a more significant effect on pure granules than DC carbide with 30 vol.% cobalt matrix, so the addition of cobalt matrix reduces the WC size effect on wear resistance. Fig. 31 shows the high stress wear surface of DC carbide with different WC particle sizes. Finer WC particle results in higher wear resistance of granule and hence more apparent granule protrusion and stronger hard facing effect, which yields higher wear resistance of DC carbide. Fig. 32 shows the low stress wear surface of DC carbide with different WC particle sizes, where finer WC particle gives smoother granule surface than coarser WC particle. In this investigation, all the DC carbides have similar granule size (-80+120 mesh) and the same metal-matrix content (30 vol.%); therefore, the DC carbides have similar mean free path of metal-

matrix and similar metal-matrix removal condition during low stress wear test. Finer WC particles inside the granule reduce the mean free path of the cobalt-binding phase, making the cobalt-binding-phase removal more difficult and the granule more wear resistant in the low stress wear test, which contributes to the increase of overall DC carbide wear resistance.

5.3. *Hardness and flexural strength*

Fig. 33a shows the effect of WC particle size on the hardness of DC carbide, where increased WC particle size decreases the hardness of both pure granules and DC carbide with 70 vol.% granules. Fig. 33b shows the effect of WC particle size on the flexural strength of DC carbide. The increased WC particle size increases the flexural strength of both pure granules and DC carbide with 70 vol.% granules. As mentioned in Section 4.2.3, two factors influence the flexural strength of cemented carbide, i.e. defect density and mean free path of metal-matrix. For pure granules, increased WC particle size increases mean free path of the cobalt-binding phase, which reduces the contiguity of WC particles and decreases the defect density (WC particle contact area is the main location where microcrack exists, and the main position crack first happens during deformation), hence increasing the flexural strength. For each WC particle size, DC carbide with 70 vol.% granules has higher flexural strength than pure granules because the addition of cobalt matrix decreases the defect density. For the 5.8 μm WC particle size, this increase is much less than the increase for the 0.98 μm WC particle size, indicating that the defect density for the pure granule with 5.8 μm WC particle size is

already low; therefore, the further addition of cobalt matrix introduces more mean free path effect, which decreases the strength of DC carbide according to eq. (39).

In this chapter, the effect of WC size within the granules was investigated. For both pure granule and DC carbide with 30 vol.% cobalt matrix, increased WC size decreases both high and low stress wear resistance and hardness and has no significant effect on toughness but decreases flexural strength.

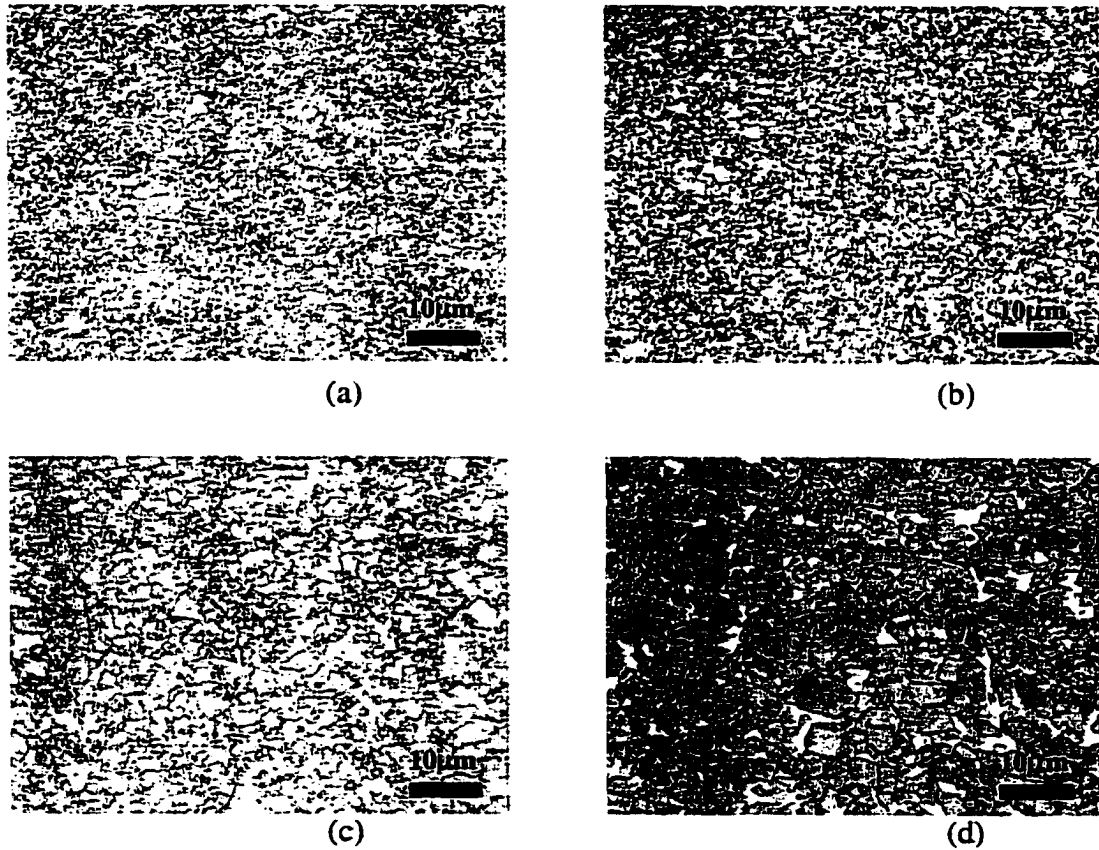


Fig. 28. Microstructure of granules with different WC particle sizes, (a) 0.98 μm , (b) 1.56 μm , (c) 3.3 μm and (d) 5.8 μm , but the same granule cobalt content, 10 vol.%. With increased WC particle size, mean free path of cobalt binding phase increases from sub-micrometer levels to about 3 μm .

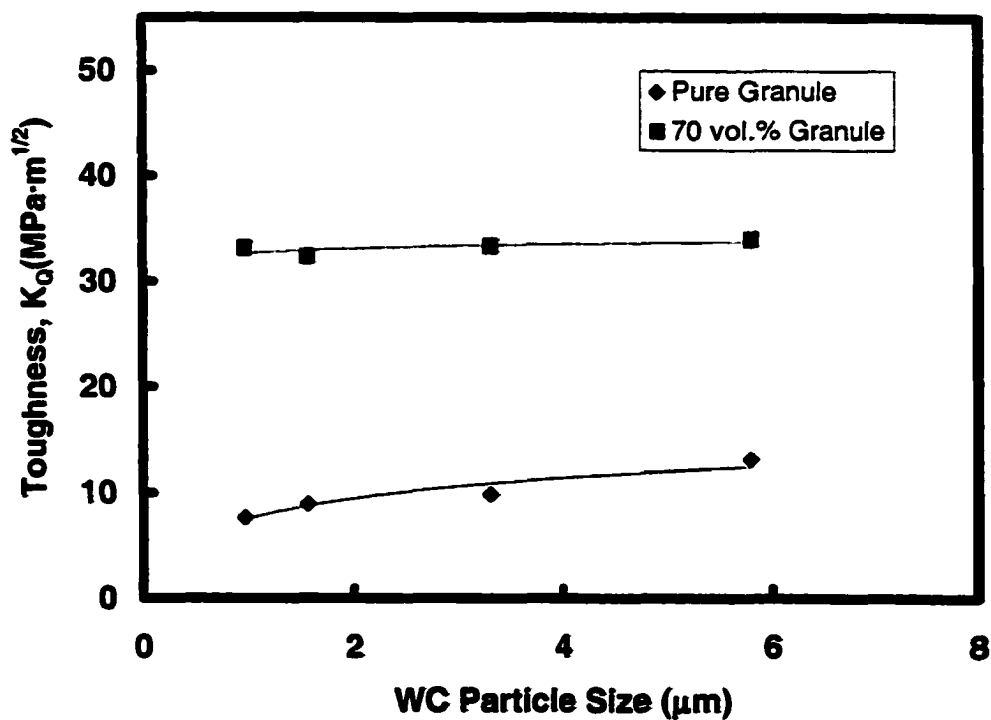
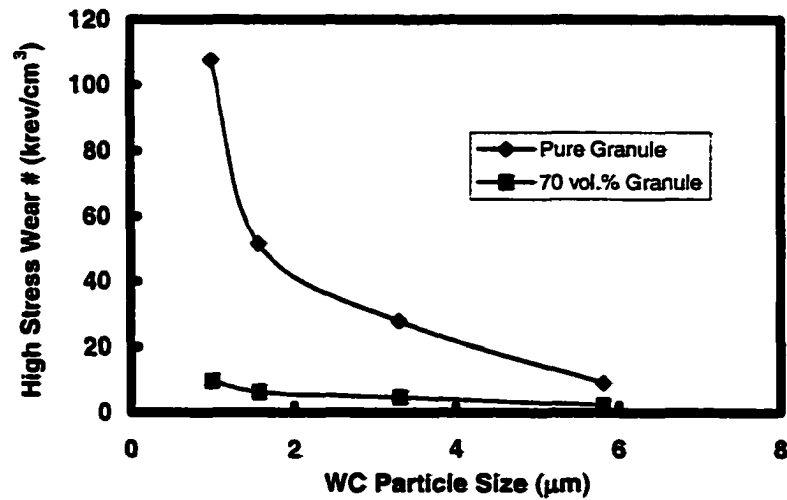
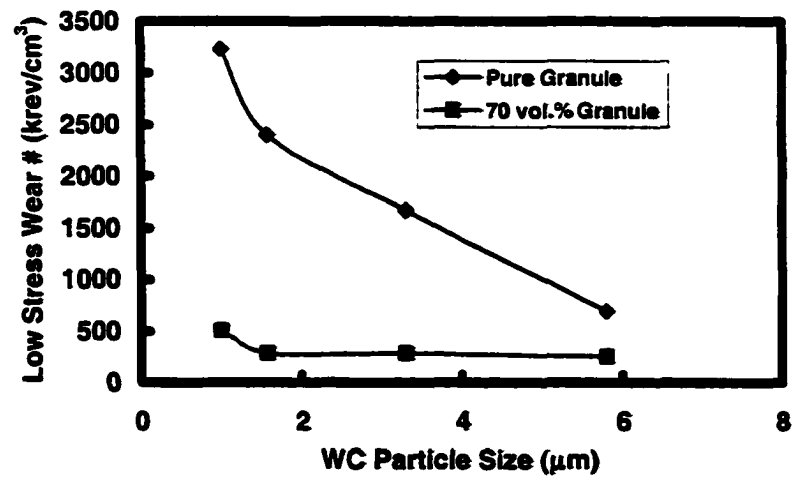


Fig. 29. Effect of WC particle size on the toughness of pure granule and DC carbide with 30 vol.% cobalt matrix, granule cobalt content 10 vol.% and granule size -80+120mesh. Increased WC particle size increases toughness of pure granule to a limited degree but has no apparent effect on the toughness of DC carbide with 30 vol.% metal-matrix.



(a)



(b)

Fig. 30. Effect of WC particle size on (a) high stress wear resistance and (b) low stress wear resistance of pure granule and DC carbide with 30 vol.% cobalt matrix, granule cobalt content 10 vol.% and granule size -80+120 mesh. Increased WC particle size increases both high and low stress wear resistance of both pure granule and DC carbide with 30 vol.% cobalt matrix.

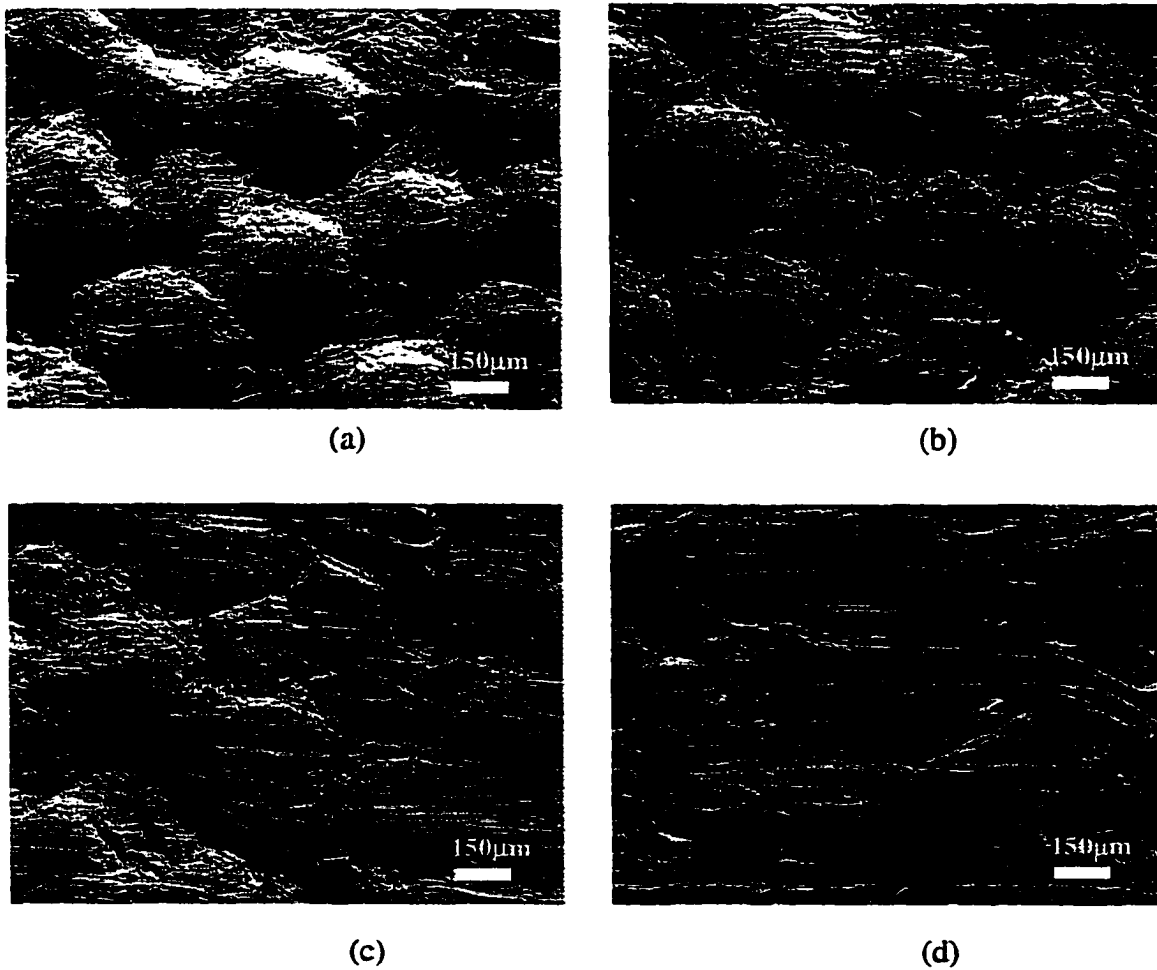


Fig. 31. High stress wear surface of DC carbide with 70 vol.% granule (granule cobalt content 10 vol.%, granule size $-80+120$ mesh) and 30 vol.% cobalt matrix, (a) WC size $0.98\ \mu\text{m}$, (b) WC size $1.56\ \mu\text{m}$, (c) WC size $3.3\ \mu\text{m}$ and (d) WC size $5.8\ \mu\text{m}$. Finer WC leads to harder granules and more granule protrusion, enhancing high stress wear resistance of DC carbide.

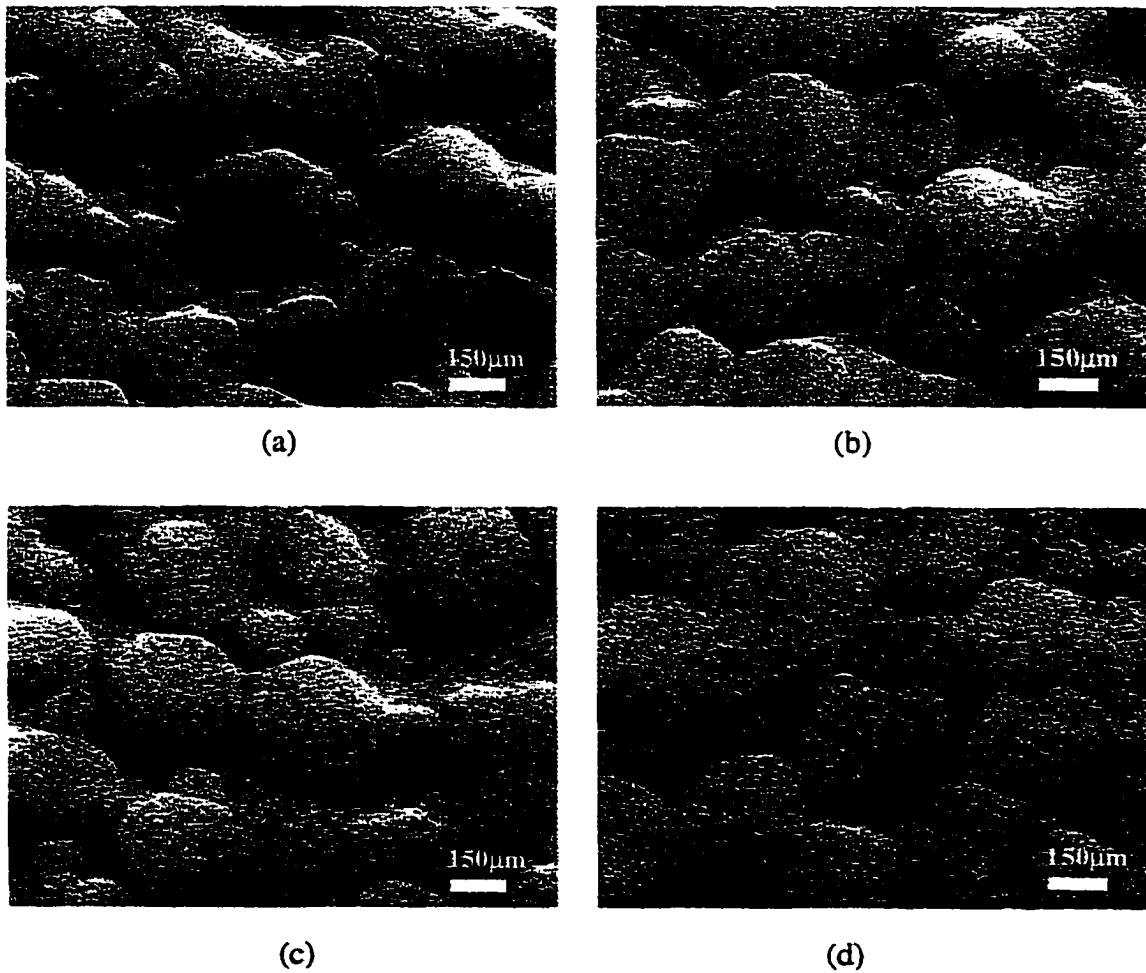
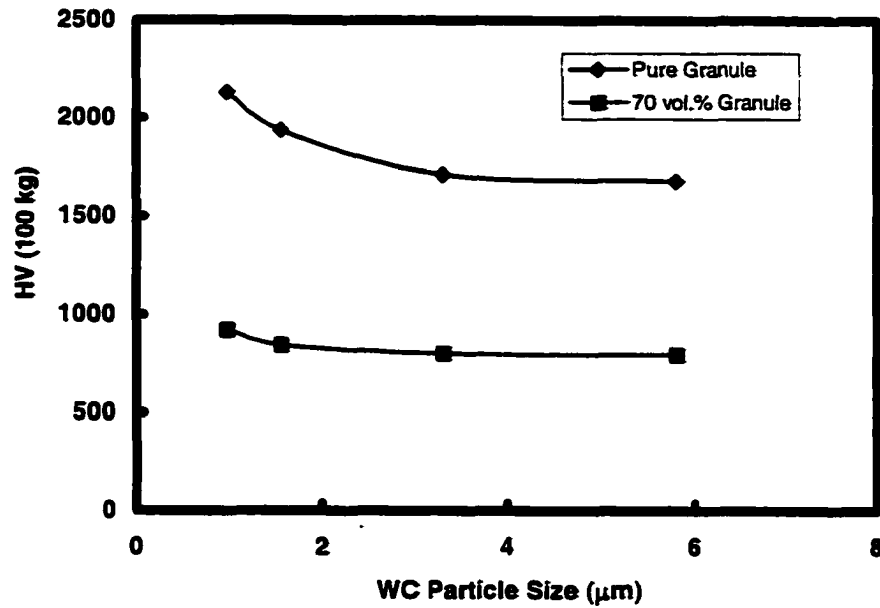
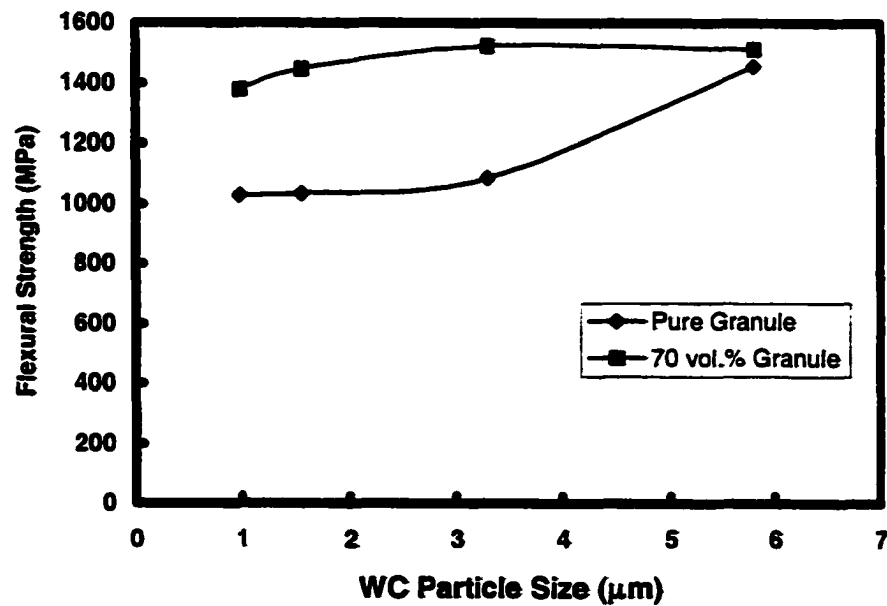


Fig. 32. Low stress wear surface of DC carbide with 70 vol.% granule (granule cobalt content 10 vol.%, granule size $-80+120$ mesh) and 30 vol.% cobalt; (a) WC size $0.98\ \mu\text{m}$; (b) WC size $1.56\ \mu\text{m}$; (c) WC size $3.3\ \mu\text{m}$; and (d) WC size $5.8\ \mu\text{m}$. Coarser WC softens granules and reduces the overall low stress wear resistance of DC carbide.



(a)



(b)

Fig. 33. Effect of WC particle size on (a) hardness and (b) flexural strength of pure granule and DC carbide with 30 vol.% cobalt matrix, granule cobalt content 10 vol.% and granule size $-80+120$ mesh. Increased WC size decreases hardness while increasing flexural strength.

CHAPTER 6

EFFECT OF GRANULE SIZE ON MECHANICAL PROPERTIES OF DC CARBIDE

When the granules or metal-matrix content in DC carbide is constant, changing granule size changes mean free path of metal-matrix directly according to eq. (1), leading to the variation of mechanical properties of DC carbide. For the investigation of granule size effect, the granule with 18 vol.% cobalt and 3 μm WC was sieved into five size classes, including +80 mesh ($>180\ \mu\text{m}$), -80+100 mesh (150-180 μm), -100+120 mesh (125-150 μm), -120+170 mesh (90-125 μm) and -170+270 mesh (53-90 μm). The morphologies of different size cuts of granules are shown in Fig. 34. Cobalt was again selected as the metal-matrix, with 30 vol.% in DC carbide. The microstructures of DC carbide with different granule sizes are shown in Fig. 35, where mean free path of metal-matrix increases from 16 to 41 μm with the increase of granule size.

6.1. *Toughness*

Fig. 36 shows the effect of granule size and mean free path of metal-matrix on the toughness of DC carbide. At the same metal-matrix content and the same total cobalt content, the toughness of DC carbide increases monotonically with granule size and mean free path of metal-matrix. A special toughness model, discussed in Chapter 7, applies to the relationship between toughness and granule size or mean free path of metal-matrix (Fig. 36).

Fig. 37 is the schematic microstructure development from typical DC carbide to conventional cemented carbide in the reverse direction of the x-axis of Fig. 36. The mean free path of metal-matrix decreases (from 40 μm for DC carbide to several micrometers for conventional cemented carbide) with the decrease of granule size. When the granule size decreases to a critical point, DC carbide becomes conventional cemented carbide with the small mean free path and hence the low toughness.

6.2. *Wear resistance*

6.2.1. *High stress wear resistance*

The effect of granule size on the high stress wear resistance of DC carbide is shown in Fig. 38, where the high stress wear resistance of DC carbide increases linearly with granule size. Wear surface observation in Fig. 39 manifests that larger granules (larger mean free path of metal-matrix) yield more apparent granule protrusion, which leads to the hard facing effect discussed in Section 4.2.1.

6.2.2. *Low stress wear resistance*

For low stress wear resistance of DC carbide, there is a critical granule size corresponding to the lowest resistance (Fig. 40). The critical granule size in Fig. 40 is about 80 μm , somewhat smaller than the abrasive particle size of 212-300 μm . The wear surface observation in Fig. 41 shows that DC carbide with larger granules has more apparent granule protrusion while finer granules produce a wear surface that is comparatively flat. Unlike the high stress wear test, where a steel wheel and large and hard Al_2O_3 abrasive particles are employed, the low stress wear test uses a rubber wheel

and smaller and softer SiO_2 particles, which means SiO_2 particles can dig deeply into the cobalt matrix. Especially when softer SiO_2 is broken into smaller pieces, this digging effect is more apparent. As discussed in Section 4.2.2, Fig. 41 shows that preferred cobalt removal and granule cap fracture are the two main low stress wear mechanisms for DC carbide. Both granule size and mean free path of metal-matrix have an important effect on low stress wear resistance of DC carbide. At the same metal-matrix content, larger granules are more difficult to be broken; therefore, low stress wear resistance increases with granule size. On the other hand, the mean free path of the cobalt-matrix increases with the granule size and the cobalt-matrix becomes more easily removed; as a result, the low stress wear resistance decreases with mean free path of the metal-matrix. The combined effects of granule size and mean free path of metal-matrix lead to the critical granule size or mean free path of metal-matrix for lowest wear resistance, which means that for a certain granule size or mean free path of metal-matrix, both granule cap fracture and metal-matrix removal effects are significant, leading to the lowest wear resistance.

6.3. *Flexural strength*

Fig. 42 shows that the flexural strength of DC carbide decreases monotonically with the increase of granule size or mean free path of metal-matrix. As discussed in Section 4.2.3, two factors have significant effect on the flexural strength of DC carbide, i.e. defect density and the mean free path of metal-matrix. In Fig. 41, DC carbides with the same granule cobalt content (18 vol.%), the same granule WC particle size (3 μm), and the same cobalt-matrix content (30 vol.%) are employed; therefore, the defect density for DC carbide, assumed to be intragranular porosity or cracks, is controlled to the similar

level; hence, the mean free path of metal-matrix becomes the main factor controlling the strength, which decreases the flexural strength with the increase of itself, as explained by eq. (39).

6.4. *Hardness*

The effect of granule size or mean free path of metal-matrix on the hardness of DC carbide is shown in Fig. 43. Although not greatly, hardness does decrease with the increase of granule size and mean free path. Because all the granules have the same cobalt content and WC particle size and therefore the same hardness, the decreased hardness is mainly caused by the increase of mean free path of metal-matrix, according to eq. (39).

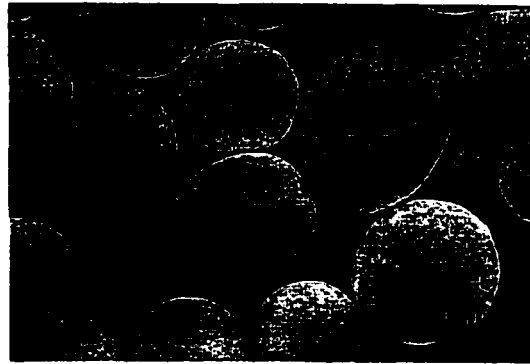
6.5. *Relationship between toughness and wear resistance of DC carbide*

Fig. 44 shows the relationship between toughness and wear resistance for both conventional cemented carbide and DC carbide with 30 vol.% cobalt matrix, 18 vol.% granule cobalt, 3 μm WC but granule size varying from 55 to 133 μm . For conventional cemented carbide, toughness and high stress wear resistance are two properties in contradiction, i.e. the gain of one property leads to the loss of the other property. For DC carbide with the same cobalt-matrix content and granule type, increased granule size increases both toughness and high stress wear resistance at the same time. The main reason is that the increased granule size increases the mean free path of metal-matrix, which increases the toughness, and enhances the granule protrusion effect, which

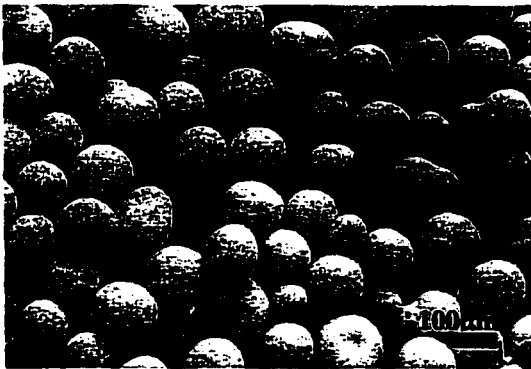
increases the high stress wear resistance. The larger granule is a critical DC carbide design concept for both toughness and high stress wear resistance.

Fig. 45 shows the relationship between toughness and low stress wear resistance for both conventional cemented carbide and DC carbide with 30 vol.% cobalt matrix, 18 vol.% granule cobalt content and 3 μm WC but with granule size varying from 55 to 133 μm . Similarly to Fig. 44, Fig. 45 shows that for conventional cemented carbide, low stress wear resistance and toughness are two properties in conflict, too. For DC carbide with the same cobalt-matrix content and granule type, increased granule size increases toughness but has no apparent effect on low stress wear resistance. In Fig. 45, DC carbide does not show superior low stress wear resistance compared to conventional cemented carbide because of the preferred cobalt matrix removal during the low stress wear test.

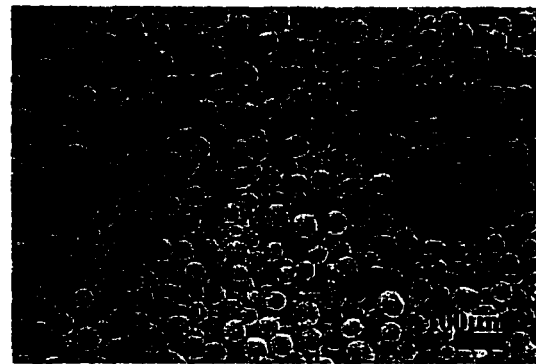
In this chapter, the effect of granule size was investigated. At the same cobalt-matrix content, increased granule size increases both toughness and high stress wear resistance but decreases hardness and flexural strength to a limited degree. There is a critical granule size corresponding to the lowest low stress wear resistance. During this investigation, DC carbide is related to conventional cemented carbide by the concept of mean free path of metal-matrix. Conventional cemented carbide can be regarded a special DC carbide with very small mean free path of metal-matrix.



(a)



(b)



(c)

Fig. 34: The morphology of granules with 18 vol.% cobalt and 3 μm WC but different granule sizes, (a) +80 mesh, (b) -120+170 mesh and (c) -325 mesh.

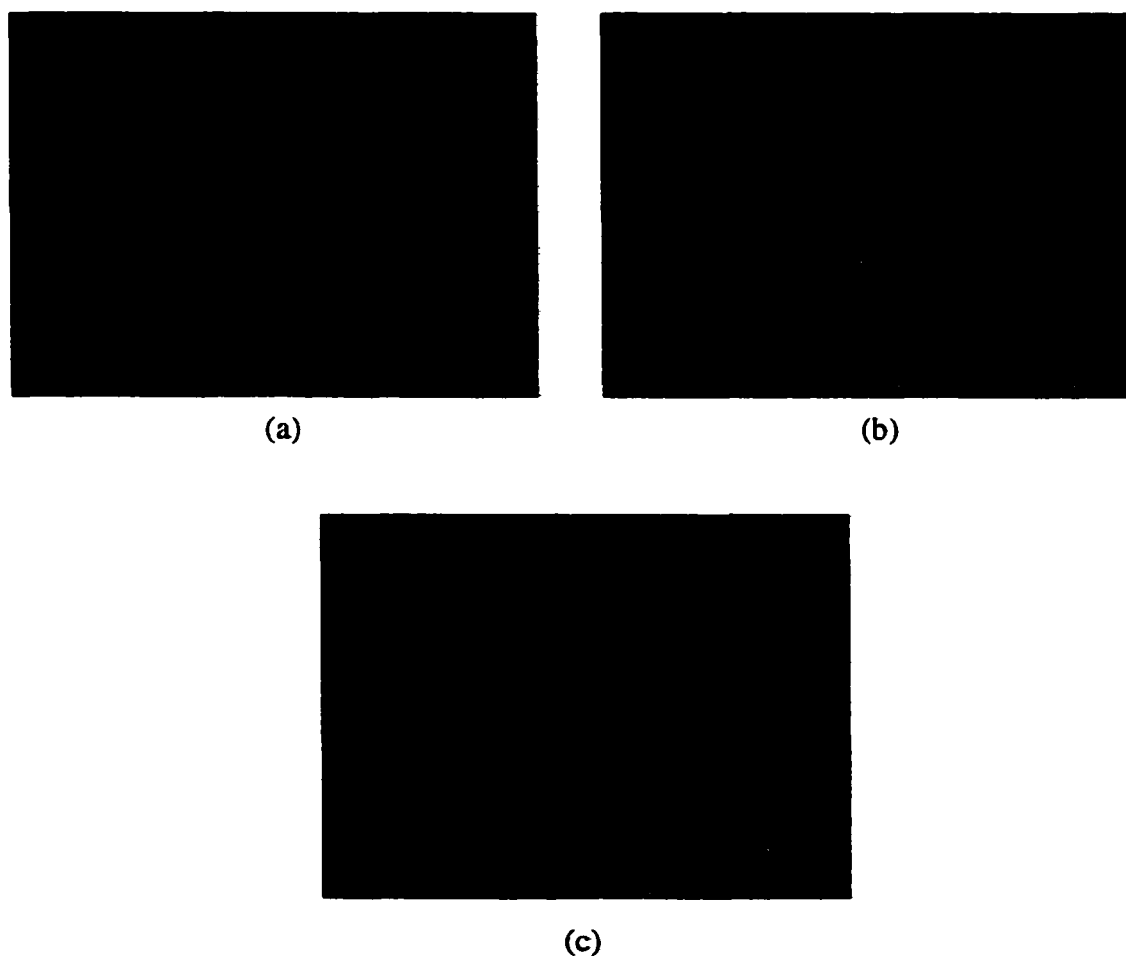
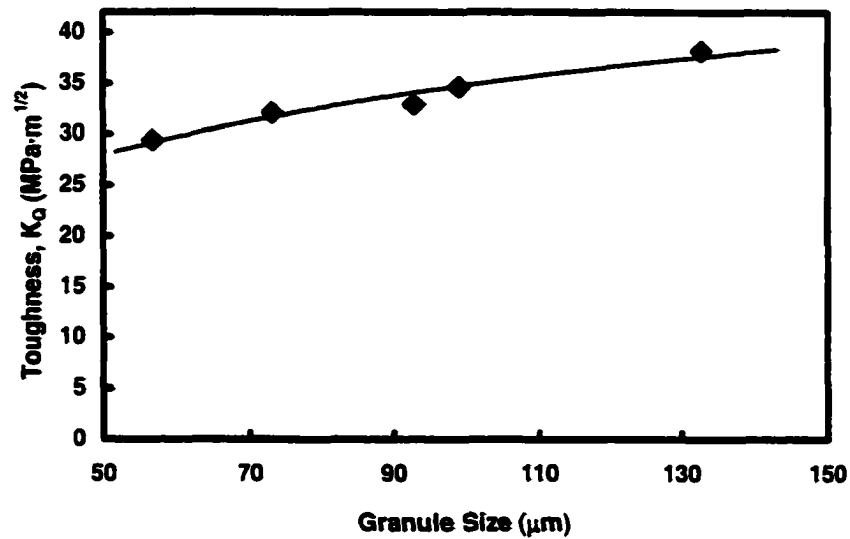
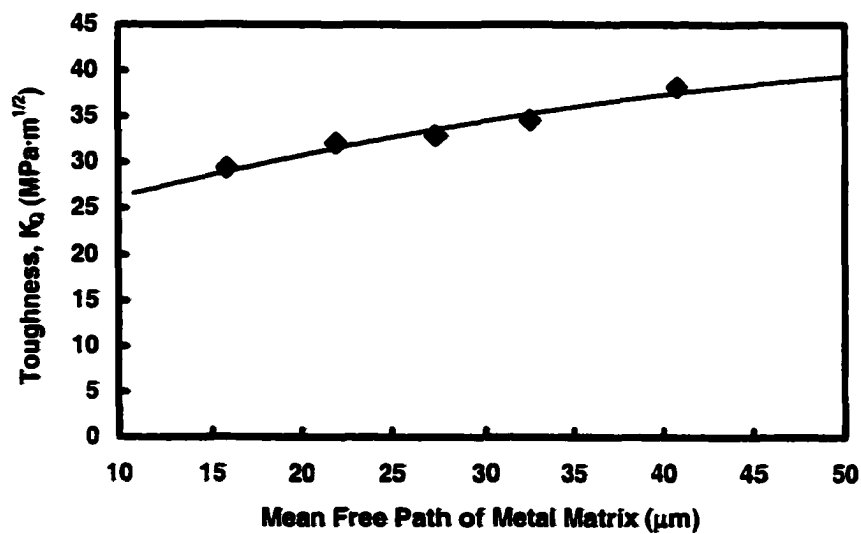


Fig. 35. The microstructure of DC carbide with 30 vol.% metal-matrix but different average granule size, (a) 130 μm , (b) 90 μm and (c) 60 μm ; granule cobalt content 18 vol.% and WC size 3 μm . Decreased granule size decreases the mean free path of metal-matrix from 41 to 16 μm .



(a)



(b)

Fig. 36. Effect of (a) granule size and (b) mean free path of metal-matrix on toughness of DC carbide with 30 vol.% cobalt matrix, granule cobalt content 18 vol.% and WC size 3 μm . Increased granule size or mean free path of metal-matrix increases toughness monotonically.

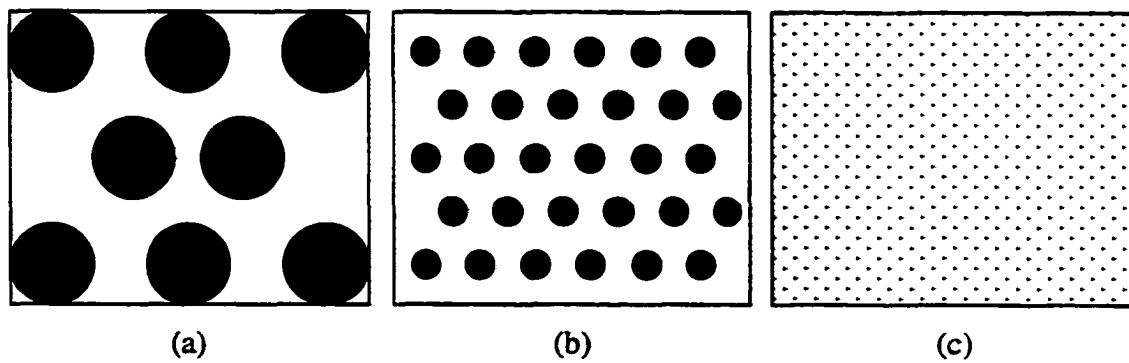


Fig. 37. Microstructure development of DC carbide from (a) large granule to (b) small granule to (c) conventional cemented carbide. Conventional cemented carbide can be regarded a special DC carbide with very short mean free path of metal-matrix and hence very low toughness.

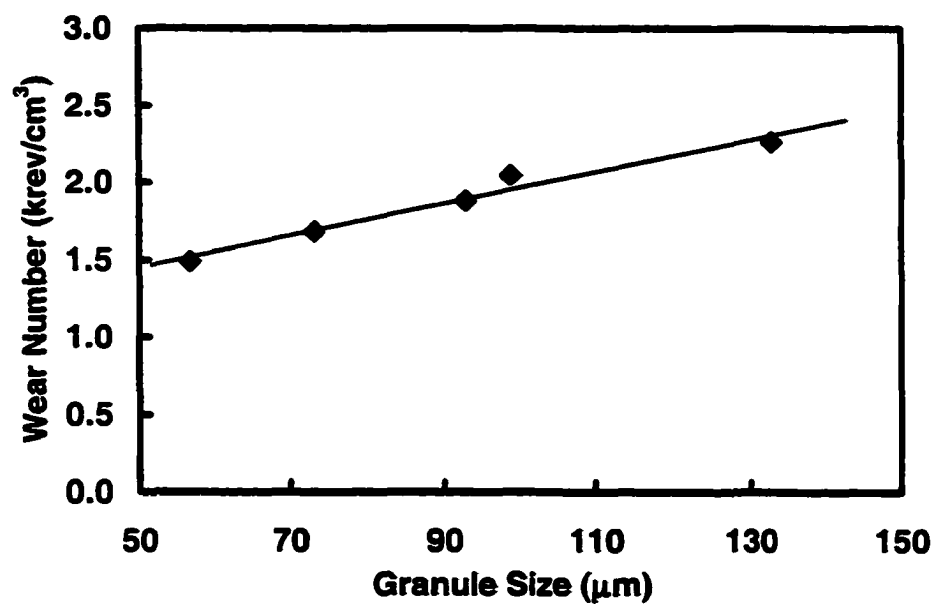


Fig. 38. Effect of granule size on high stress wear resistance of DC carbide with 70 vol.% granules (18 vol.% Co and 3 μm WC in granule). High stress wear resistance of DC carbide increases linearly with granule size.

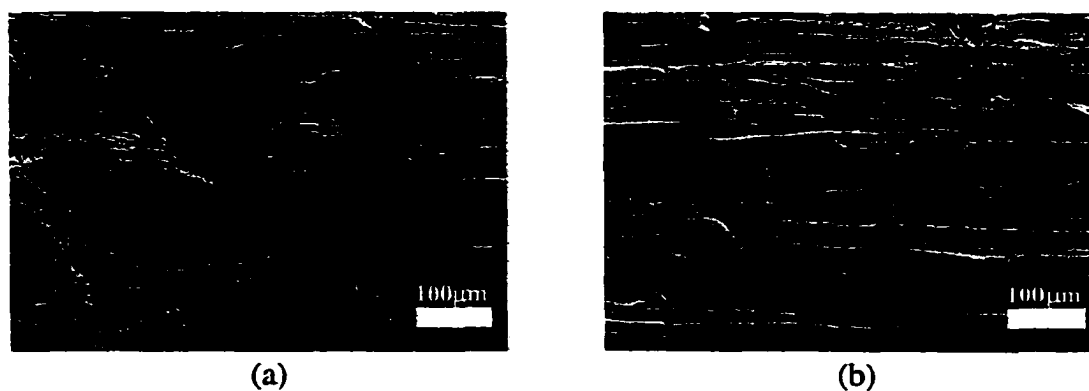


Fig. 39. Wear surface of DC carbide with 30 vol.% metal-matrix and 3 μm WC inside the granule but different granule sizes: (a) large granules (133 μm , 18 vol.% Co in granule) and (b) small granules (57 μm , 18 vol.% Co in granule). Larger granule size makes more granule protrusion, leading to greater high stress wear resistance.

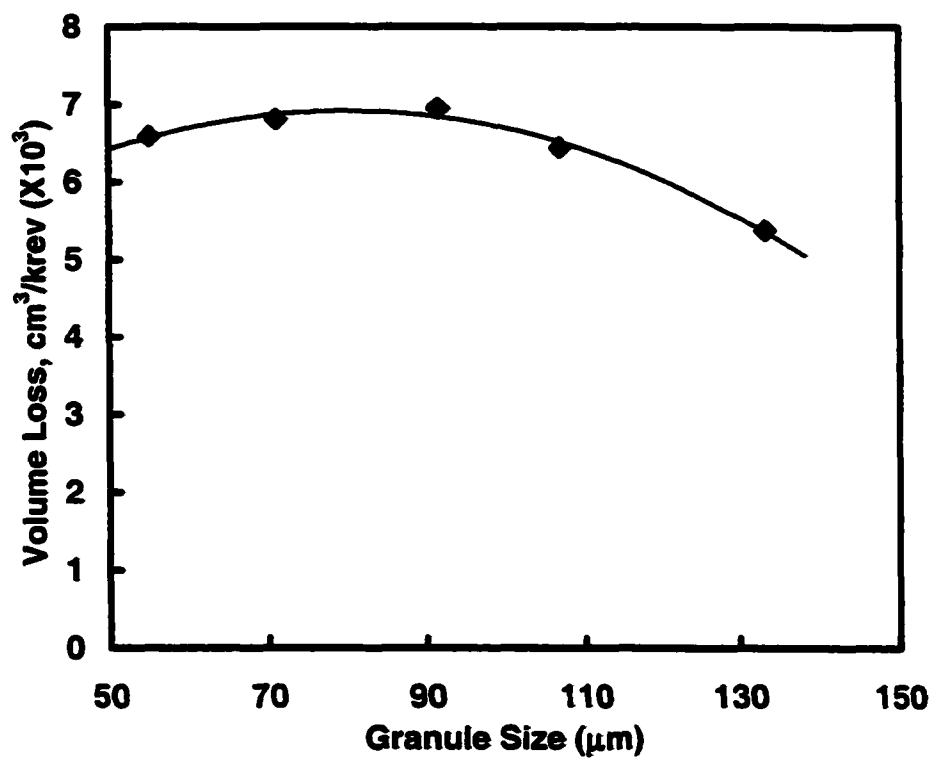


Fig. 40. Effect of granule size on low stress wear resistance of DC carbide. There is a critical granule size (about 80 μm) corresponding to the lowest low stress wear resistance.

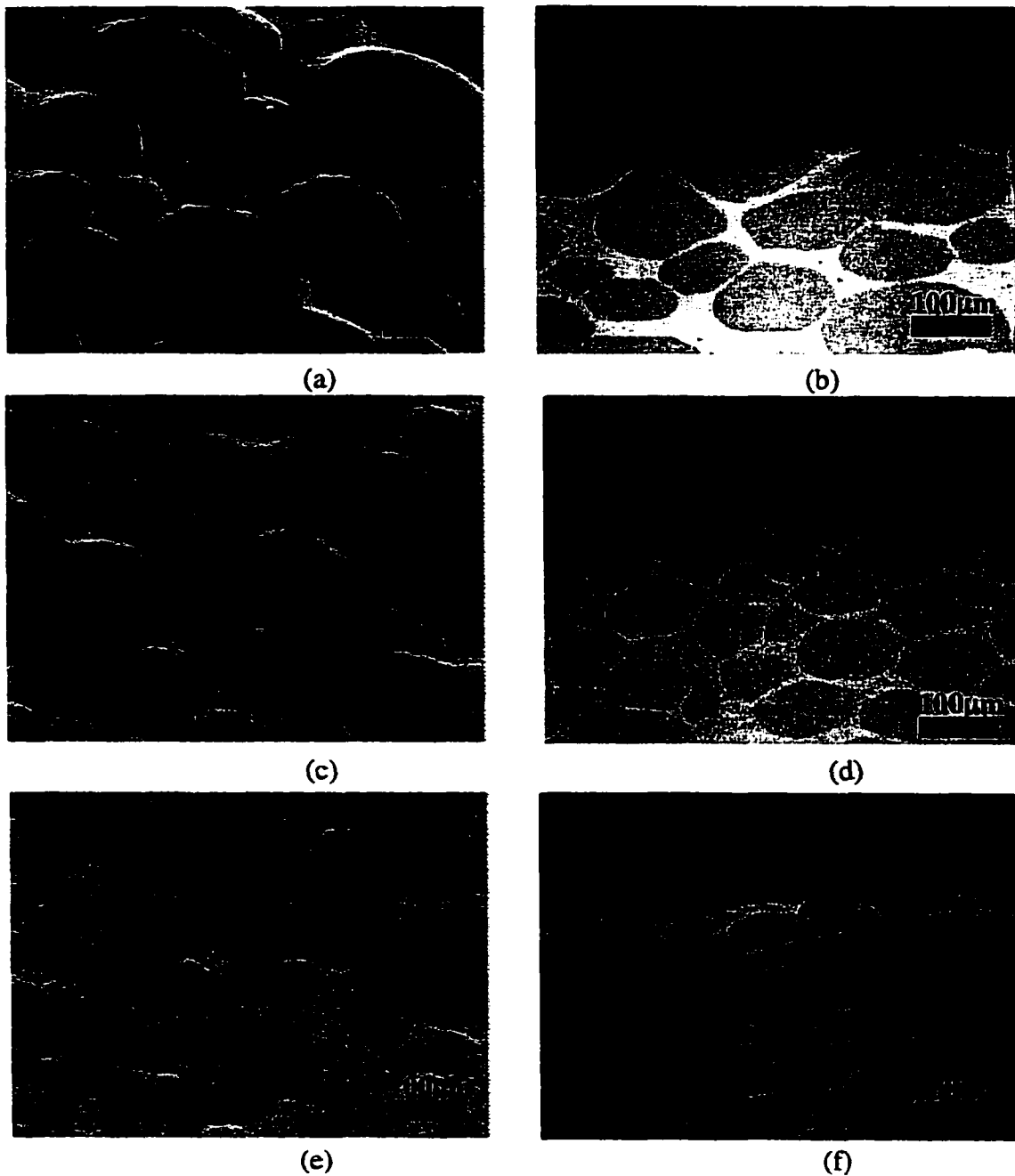
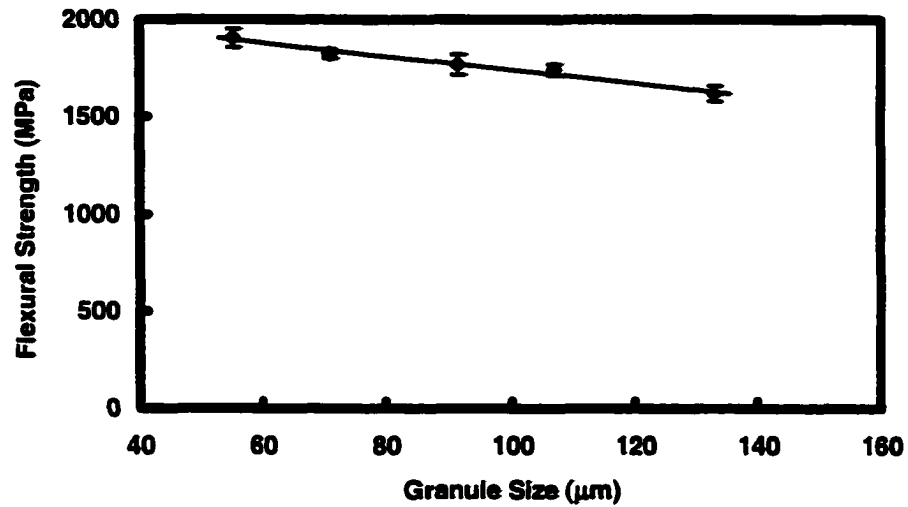
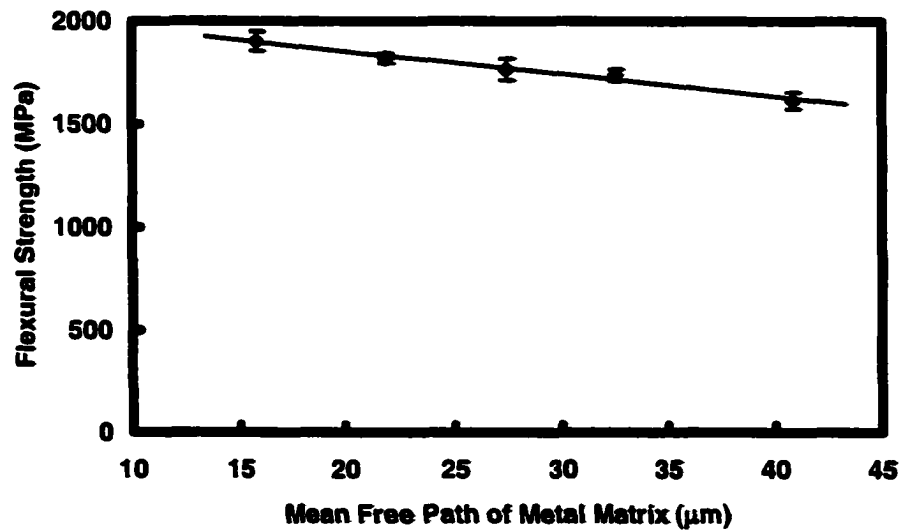


Fig. 41. Low stress wear surface of DC carbide with 30 vol.% cobalt matrix, 18 vol.% granule cobalt content and 3 μm WC but different granule sizes: (a) 130 μm , overview; (b) 130 μm , sideview; (c) 90 μm , overview; (d) 90 μm , sideview; (e) 60 μm , overview; and (f) 60 μm , sideview. Preferred cobalt matrix removal and granule cap fracture are two main low stress wear mechanisms for DC carbide.

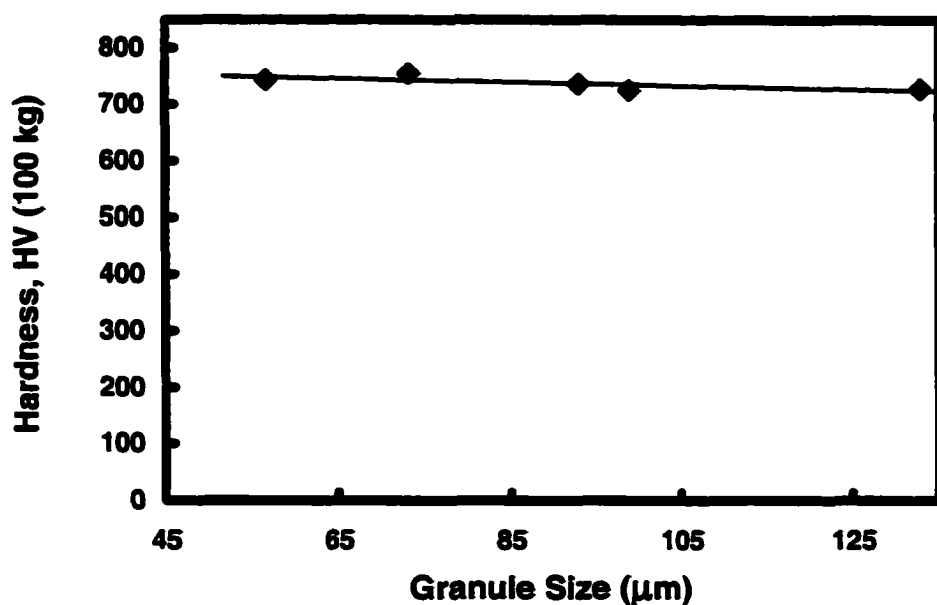


(a)

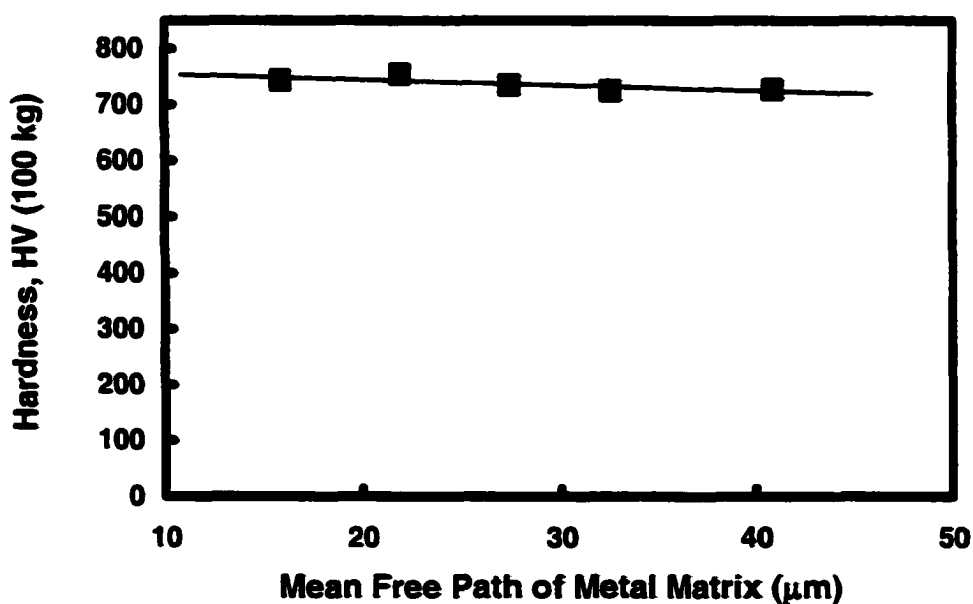


(b)

Fig. 42. Effect of (a) granule size and (b) mean free path of metal-matrix on flexural strength of DC carbide with 30 vol.% cobalt matrix, 18 vol.% granule cobalt content and 3 μm WC. Increased granule size or mean free path of metal-matrix decreases flexural strength slightly. Error bars are plus/minus one standard deviation.



(a)



(b)

Fig. 43. Effect of (a) granule size and (b) mean free path of metal-matrix on the hardness of DC carbide with 30 vol.% cobalt matrix, 18 vol.% granule cobalt content and 3 μm WC. Increased granule size or mean free path of metal-matrix decreases the hardness only slightly.

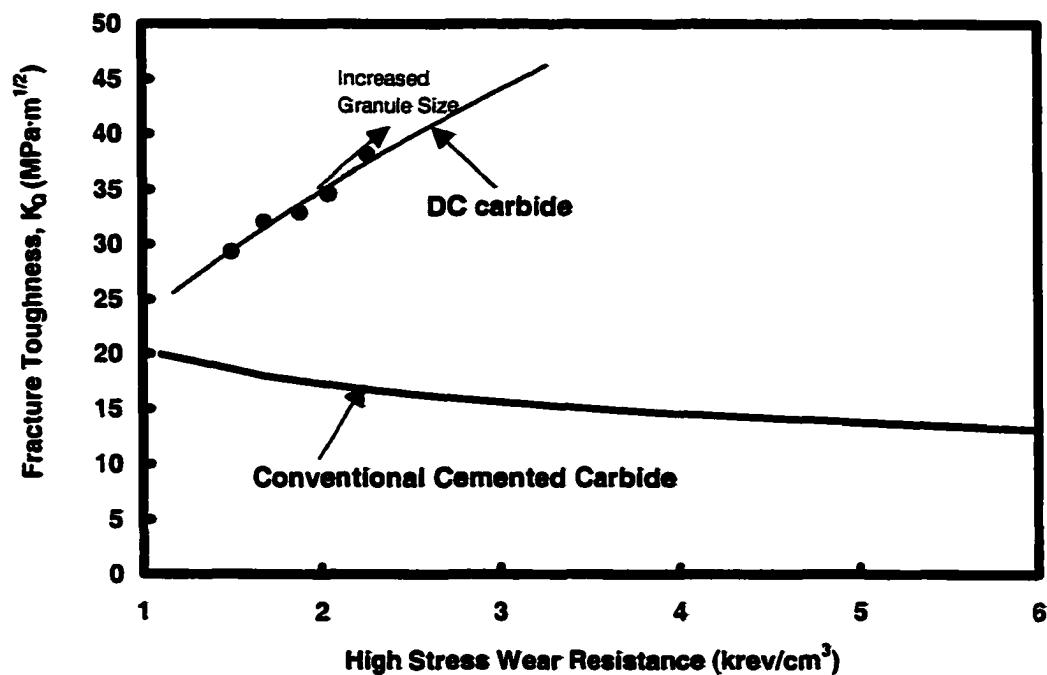


Fig. 44. Relationship between toughness and high stress wear resistance for both conventional cemented carbide and DC carbide with 30 vol.% cobalt matrix, 18 vol.% granule cobalt content and 3 μ m WC but granule size varying from 55 to 133 μ m. Increased granule size increases both toughness and high stress wear resistance at the same time.

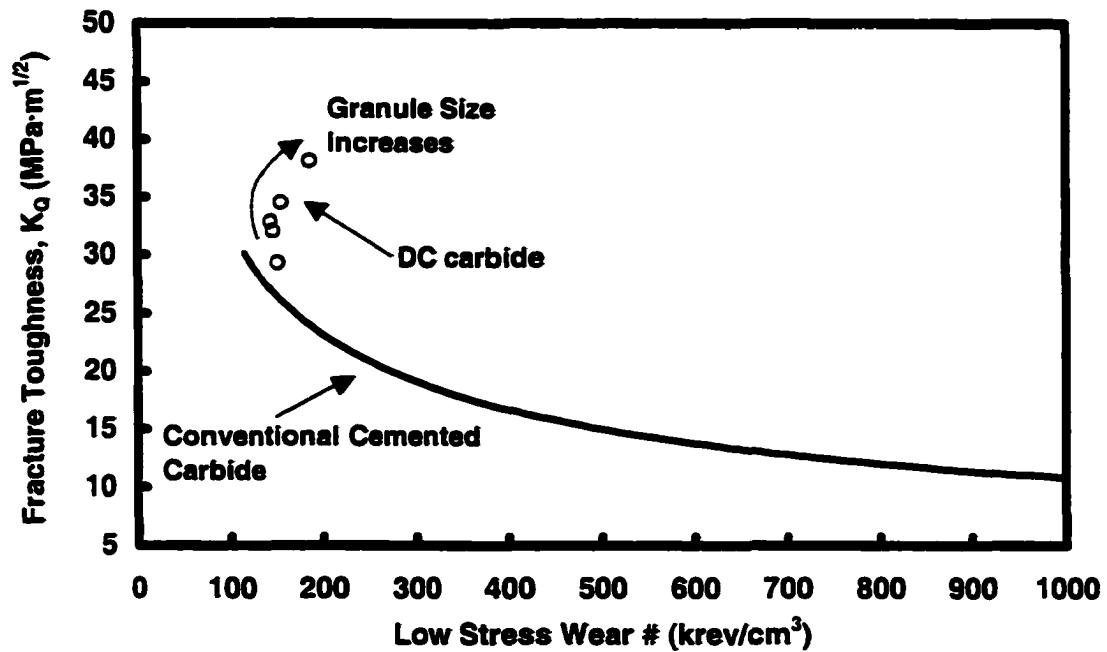


Fig. 45. Relationship between toughness and low stress wear resistance for both conventional cemented carbide and DC carbide with 30 vol.% cobalt matrix, 18 vol.% granule cobalt content and 3 μ m WC but granule size varying from 55 to 133 μ m. Although increased granule size increases toughness, DC carbide has no superior low stress wear resistance compared to conventional cemented carbide.

CHAPTER 7

WEAR MECHANISM AND TOUGHNESS MODELING OF DC CARBIDE

7.1. Wear resistance mechanism of DC carbide

As discussed in Chapter 4, DC carbide has a unique wear mechanism because of its specific microstructure. Because wear resistance is a functional rather than an intrinsic property of materials, which means both intrinsic properties and test conditions have an important role in the final results, the wear mechanisms discussed here are specific for the high (ASTM B611) and low (ASTM G65) stress wear test conditions.

7.1.1. High stress wear mechanism

As shown in Fig. 46, during the high stress wear test, the softer metal-matrix is removed first by abrasive particles, producing granule protrusion. Coarse abrasive particles then have a greater chance to contact granules than the metal-matrix; hence, the granule protrusion acts as a discontinuous hard facing, which enhances the wear resistance of DC carbide. At the same total cobalt content (cobalt in granule plus cobalt in metal-matrix), DC carbide has greater high stress wear resistance than conventional cemented carbide because of the granule protrusion effect. Granule properties (controlled by WC particle size, cobalt content inside the granule and granule size) and metal-matrix properties both have direct influence on the granule protrusion effect and hence the wear resistance of DC carbide. Finer WC particles within the granules produce harder and more wear resistant granules; hence, the granule protrusion effect is more apparent,

which leads to greater high stress wear resistance. At the same metal-matrix content, larger granules result in a larger mean free path of metal-matrix and more apparent granule protrusion effect, which results in higher high stress wear resistance.

7.1.2. Low stress wear mechanism

The low stress wear test employs a rubber wheel and finer and softer SiO_2 abrasive particles compared to the steel wheel and coarser and harder Al_2O_3 abrasive in the high stress wear test. As shown in Fig. 47, in the low stress wear test, the abrasive particles can dig into the metal-matrix much more easily than in the high stress test; metal-matrix removal is an important wear mechanism for DC carbide. During the wear test, soft SiO_2 is easily broken into smaller particles, making metal-matrix removal easier. SiO_2 is so soft that it can only remove cobalt inside the granules and the metal-matrix around the granules. The WC particle inside the granules is pulled out when the cobalt binding phase cannot hold the particle. When the granules are worn to a certain size, granule fracture becomes another mechanism for low stress wear of DC carbide.

Both granule and metal-matrix properties have a significant effect on low stress wear resistance. Finer WC particle size or lower cobalt content inside the granules increases the hardness and wear resistance of the granules and consequently increases the low stress wear resistance of DC carbide. Granule size effect is complicated because both metal-matrix removal and granule fracture have an effect. For small granules, although the mean free path of the metal-matrix is small, the granules are easily broken; for large granules, although the mean free path of the metal-matrix is larger and therefore the metal-matrix is

more easily removed, the granules are difficult to fracture. The combined metal-matrix removal and granule fracture effects cause a critical granule size or mean free path of metal-matrix for the lowest wear resistance.

7.2. Toughness modeling

Many efforts have been made to develop the toughness models of conventional cemented carbide [26-28]. Most efforts demonstrate that the mean free path of the metal-matrix is the critical factor influencing the toughness. Ravichandran gave a typical expression of the toughness for conventional cemented carbide [27]:

$$G_C = (1 - V_f)G_m + V_f\sigma_o\lambda\chi \quad (44)$$

where G_C and G_m are the critical strain energy release rates of cemented carbide and WC phase, respectively; V_f , σ_o and λ are the volume fraction, the bulk flow stress and the mean free path of the metal-matrix, respectively; and χ is the work of rupture parameter varying from 4 to 16, which accounts for the constrained flow behavior of the metal-matrix.

In fact, the term $\sigma_o\chi$ can be considered as the valid flow stress of the metal-matrix constrained by WC particles. Different models have different expressions for this term. Sigl and Fischmeister [19] regarded that Chou's Hall-Petch type model [53] for soft phases in two-phase composites takes an important role in the flow stress of metal-matrix in cemented carbide:

$$\sigma_y = \sigma_y^0 + k_y\lambda^{-1/2} \quad (45)$$

where σ_y is the flow stress of metal-matrix, σ_y^0 and k_y are constants and λ is the mean free path of metal-matrix.

When the terms for the WC phase in eq. (44) are changed directly into terms for the granules in DC carbide, Ravichandran's [27] model for conventional cemented carbide is transformed into the toughness model for DC carbide:

$$G_{lc} = V_v^g G_{lc}^g + V_v^m \lambda \bar{\sigma}_f \quad (46)$$

where G_{lc}^g is the critical strain energy release rate of granule; V_v^g and V_v^m are the volume fractions of granule and metal-matrix, respectively; λ is the mean free path of metal-matrix; and $\bar{\sigma}_f$ is the flow stress of metal-matrix.

When both Chou's [53] and Ravichandran's [27] models for flow stress of metal-matrix are considered, the flow stress of metal-matrix in DC carbide can be expressed as:

$$\bar{\sigma}_f = \sigma_f^0 + k_y \lambda^{-1/2} \quad (47)$$

Combining eqs. (46) and (47) gives

$$G_{lc} = V_v^g G_{lc}^g + V_v^m \lambda \sigma_f^0 + V_v^m k_y \lambda^{1/2} \quad (48)$$

Because the stress intensity factor of DC carbide, K_{lc} , is already known from toughness testing, the critical energy release rate of DC carbide, G_{lc} , can be calculated as [54]:

$$G_{lc} = K_{lc}^2 (1 - \mu_c^2) / E_c \quad (49)$$

where μ_c is the Poisson's ratio and E_c is Young's modulus of DC carbide. Here, isotropic elastic properties of DC carbide are assumed, Poisson's ratio comes directly

from Koopman et al. [50], and Young's modulus comes from experimental measurements in Section 4-2-5.

Every term is known in eq. (48) except σ_f^0 and k_y ; therefore, multiple linear regression was made to determine these two constants, which yields $\sigma_f^0 = 18.8 \text{ MPa}$ and $k_y = 1.37 \text{ MNm}^{-3/2}$; the coefficient of determination for this regression is 0.95, which is quite close to 1, indicating the validity of eq. (48). For a typical cobalt phase in conventional cemented carbide, Sigl and Fischmeister gave $\sigma_f^0 = 480 \text{ MPa}$ and $k_y = 1.35 \text{ MNm}^{-3/2}$ [19]. The k_y value is quite close to the result of DC carbide, while the σ_f^0 value is different between DC carbide and conventional cemented carbide. The main reason is the high residual tensile stress existing in the cobalt matrix. Although direct residual stress measurement is not available at present, finite element analysis for DC carbide shows that the residual tensile stress of cobalt matrix is around 500 MPa [55]; therefore, the valid σ_f^0 value should be the *difference* between the value for the unstressed state and the residual tensile stress of the cobalt matrix. This difference is near zero, similar to the regression result. Table 4 compares K_{Ic} calculated from eqs. (48) and (49) and the experimental data, demonstrating that eq. (48) is a valid toughness model predicting DC carbide toughness.

Fig. 48 shows the relationship between toughness and mean free path of metal-matrix. All these five curves are produced by eq. (48) at the same total cobalt content. The three fine curves stand for the DC carbide with the same granule cobalt content but different granule sizes (hence the different mean free path of the metal-matrix). The two coarse curves stand for the DC carbide with the same granule size but different granule

cobalt content. The decreased mean free path of the metal-matrix decreases the toughness of these five curves and finally makes the curves meet at a common point corresponding to the toughness of conventional cemented carbide. The arrow in Fig. 48 means that at the same total cobalt content, harder granules lead to larger mean free path of metal-matrix and yield higher toughness, which is consistent with the arrow in Fig. 15b.

Table 4. Toughness comparison between experimental data and calculation from eqs. (48) and (49)

| Granule Toughness ($\text{MPa}\cdot\text{m}^{1/2}$) | Granule vol. % | Matrix Type | Matrix vol. % | Mean Free Path of Metal-Matrix (μm) | Experimental Toughness ($\text{MPa}\cdot\text{m}^{1/2}$) | Toughness Calculated from eqs. (48) and (49) ($\text{MPa}\cdot\text{m}^{1/2}$) |
|---|----------------|-------------|---------------|--|--|--|
| 16.7 | 70 | Co | 30 | 29.4 | 37.9 | 34.5 |
| 16.7 | 80 | Co | 20 | 23.4 | 31.5 | 29.1 |
| 16.7 | 90 | Co | 10 | 16.2 | 22.7 | 23.0 |
| 13.4 | 70 | Co | 30 | 26.9 | 35.7 | 33.9 |
| 13.4 | 80 | Co | 20 | 20.9 | 27.7 | 28.1 |
| 13.4 | 90 | Co | 10 | 14.8 | 19.9 | 21.2 |
| 10.9 | 70 | Co | 30 | 37.3 | 34.5 | 36.9 |
| 10.9 | 80 | Co | 20 | 21.4 | 23.5 | 28.3 |
| 10.9 | 90 | Co | 10 | 17.9 | 17.6 | 21.3 |
| 13.4 | 70 | Co | 30 | 40.8 | 38.2 | 37.7 |
| 13.4 | 70 | Co | 30 | 32.5 | 34.6 | 35.8 |
| 13.4 | 70 | Co | 30 | 27.4 | 32.9 | 33.9 |
| 13.4 | 70 | Co | 30 | 21.9 | 32.1 | 32.0 |
| 13.4 | 70 | Co | 30 | 15.8 | 29.4 | 29.6 |

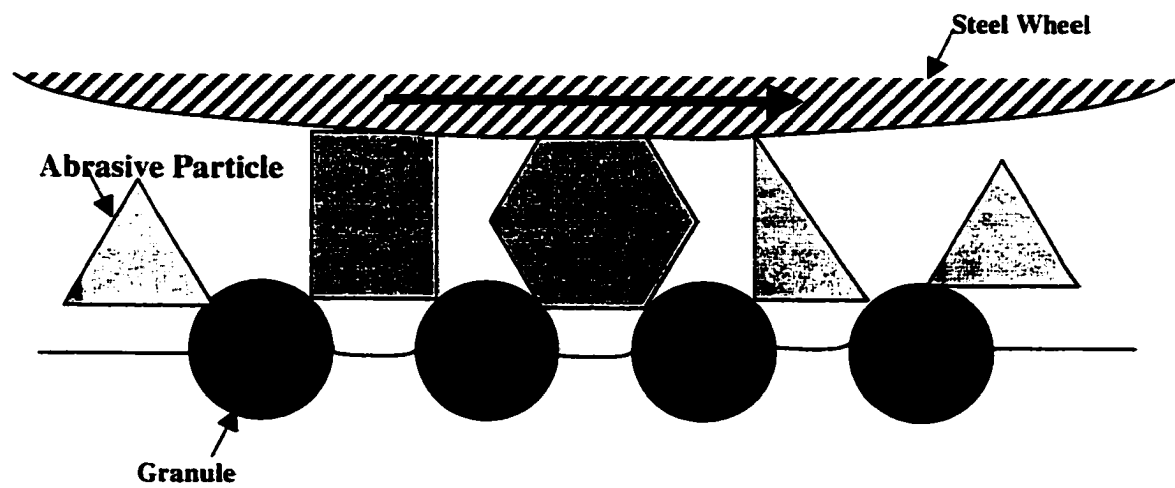


Fig. 46. High stress wear mechanism of DC carbide.

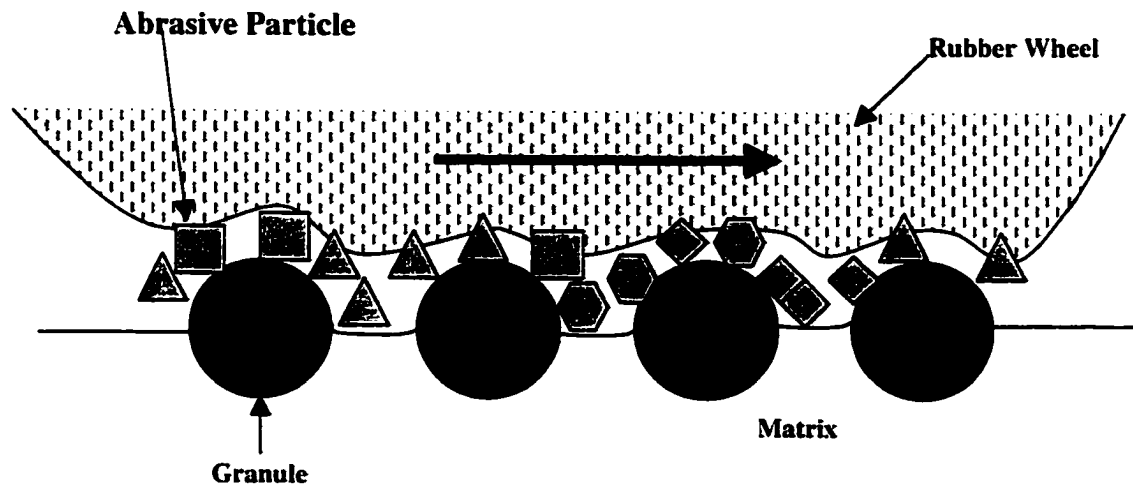


Fig. 47. Low stress wear mechanism of DC carbide.

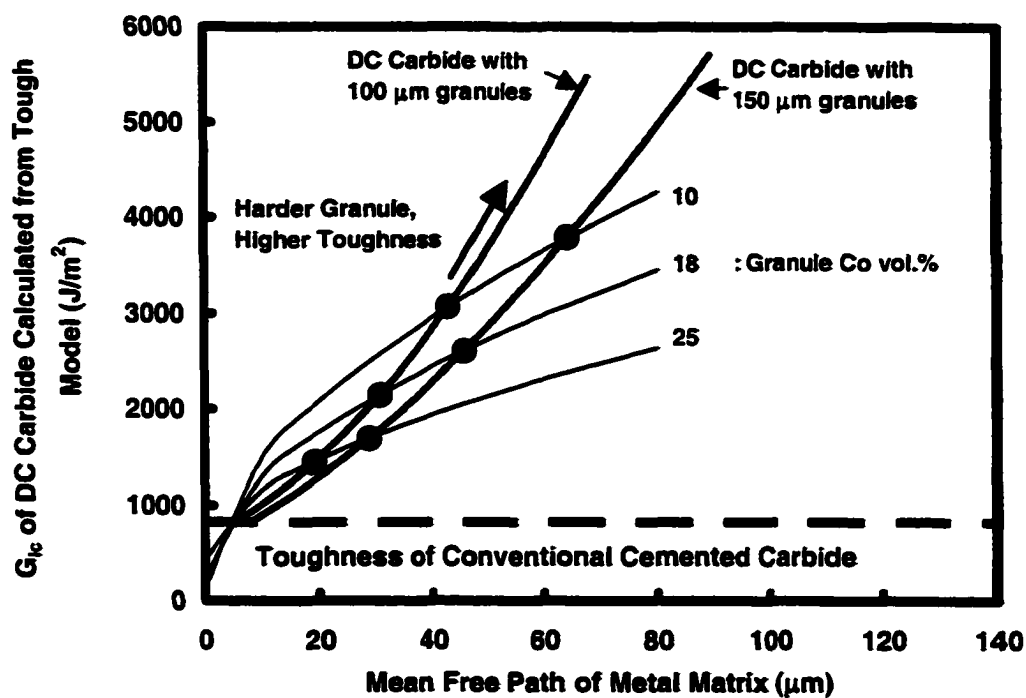


Fig. 48. Critical energy release rate as a function of mean free path of metal-matrix.

CHAPTER 8

CONCLUSIONS

Based on the discussion in Chapters 1-7, the following conclusions can be drawn:

1. DC carbide is a promising dual composite due to both its superior mechanical property combination over conventional cemented carbide and the flexibility of composite design.
2. Mechanical properties of granule and metal-matrix are the two main factors controlling mechanical properties of DC carbide. WC particle size and cobalt content inside the granules control the mechanical properties of the granules.
3. At the same total cobalt content, DC carbide with cobalt matrix demonstrates higher toughness and high stress wear resistance but lower hardness and flexural strength than conventional cemented carbide.
4. Granule size influences mechanical properties of DC carbide by changing mean free path of metal-matrix. Toughness and high stress wear resistance decrease, while flexural strength and hardness increase with the decrease of granule size. There is a critical granule size or mean free path of metal-matrix corresponding to the lowest low stress wear resistance.
5. Mean free path of metal-matrix is a critical factor controlling the toughness of DC carbide and relating conventional cemented carbide and DC carbide. Conventional cemented carbide can be considered a special case of DC carbide with very fine granule size and very short mean free path of metal-matrix.

6. Granule protrusion is the main mechanism for high stress wear resistance, enabling DC carbide to have greater high stress wear resistance than conventional cemented carbide. For low stress wear resistance, preferred metal-matrix removal and granule fracture are two important mechanisms.

7. Defect density and mean free path of metal-matrix are two significant factors influencing flexural strength of DC carbide, which makes DC carbide have lower flexural strength than conventional cemented carbide.

LIST OF REFERENCES

1. Schroeter K. U.S. Patent 1,549,615, 1925.
2. Krall J, Olsson A. U.S. Patent 5,423,899, 1995.
3. Fischer U, Waldenstrom W, Hartzell T. U.S. Patent 5,856,626, 1999.
4. Fang Z, Albert SJ. U.S. Patent 5,880,382, 1999.
5. Fang Z, Lockwood G, Griffio A. Metall Mater Trans A 1999; 30A:3231.
6. Brookes KJA. Metal Powder Report 1995;50:22.
7. Doi H. In: Almond EA, Brookes CA, Warren R, editors. Science of Hard Materials. Bristol: Adam Hilger Ltd; 1986. p. 489-523.
8. Suzuki H, Taniguchi Y, Hayashi K. J Jpn Powder Metall 1982;29:25.
9. Chaochen Y. In: Kaysser WA, Huppmann WJ, editors. Horizon in Powder Metall. Part I. Freiburg: Verlag-Schmid GmbH; 1986. p. 289-292.
10. Tracy VA, Hall NRV. Powder Metall Int 1980;12:132.
11. Moskowitz P, Ford MJ, Humenik Jr M. Int J Powder Metall 1970; 6: 55.
12. Prakash L. In: Kaysser WA, Huppmann WJ, editors. Horizon in Powder Metall. Part I. Freiburg: Verlag-Schmid GmbH; 1986. p. 261-264.
13. Farooq T, Davies T. J. Int J Powder Metall 1991;27:347.
14. Prakash L. In: Bildstein H, Eck R, editors. Proceedings 13th International Plansee Seminar Reutte, Austria; 1993. vol. 2, p. 80-109.
15. Larsen-Basse J. In: Viswanadham RK, Rowcliffe DJ, and Gurland J, editors. Science of Hard Materials. New York: Plenum Press; 1983. p. 797-813.
16. Santhanam AT, Tierney P, Hunt JL. In: Davis JR, et al, editors. ASM Handbook. 10th edition. Materials Park (OH): ASM Intl.; 1990. Vol. 2, p. 950-977.

17. Cooper R. In: Viswanadham RK, Rowcliffe DJ, Gurland J, editors. *Science of Hard Materials*. New York: Plenum Press; 1983. p. 341-355.
18. Brookes Kenneth JA. *Hardmetals and Other Hard Materials, International Carbide Data*. Hertfordshire (UK); 1992.
19. Sigl LS, Fischmeister HF. *Acta metall* 1988;36:887.
20. Gurland J. *Trans AIME* 1958;212:452.
21. Upadhyaya GS. *Cemented Tungsten Carbides-Production, Properties, and Testing*. Westwood (NJ): Noyes Publications, 1998.
22. Hack TA, Peters CT. In: Bildstein H, Ortner HM, editors. *Proceedings of the 11th International Plansee Seminar Reutte, Austria*; 1985. vol. 2, p. 799-813.
23. Larsen-Basse J. *J Metals* 1983;Nov:35.
24. Wayne SF, Baldoni JG, Buljan ST. *Tribology Trans* 1990;33:611.
25. Fang Z, Griffio A, White B, Lockwood G, Belnap D, Hilmas G, Bitler J. *Int J Refract Metals Hard Mat* 2001;19:453.
26. Sigl LS, Exner HE. *Metall Trans A* 1987;18A:1299.
27. Ravichandran KS. *Acta metall mater* 1994;42:143.
28. Nakamura M, Gurland J. *Metall Trans A* 1980;11A:141.
29. Pickens JR, Gurland J. *Mater Sci Eng* 1978;33:135.
30. Hong J, Schwarzkopf P. In: Underwood JH, Freiman SW, Baratta RI, editors. *Chevron-Notched Specimens: Testing and Stress Analysis*, ASTM STP 855. Philadelphia (PA): American Society for Testing and Materials; 1984. p. 297-308.
31. Gurland J, Bardzil P. *Trans AIME* 1955;203:311.
32. Chermant JL, Osterstock F. *Powder Metall Int* 1979;11:106.
33. Lee HC, Gurland J. *Mater Sci Eng* 1978;33:125.
34. Liu B, Zhang Y, Ouyang S, *Materials Chemistry Physics* 2000;62:35.
35. Hashin Z, Shtrikman S. *J Mechanics Physics Solids* 1963;11:127.
36. Paul B. *Trans AIME* 1960;218:36.

37. Doi H, Fujiwara Y, Miyake K, Oosawa Y. *Metall Trans* 1970;1:1417.
38. Jaensson BO, Sundstrom BO. *Mater Sci Eng* 1972;9:217.
39. Nardone VC, Strife JR. *Metall Trans A* 1991; 22A: 183.
40. Nardone VC. *Metall Trans A* 1992;23A:563.
41. Nardone VC, Strife JR, Prewo KM. *Metall Trans A* 1991; 22A:171.
42. Zok F, Jansson S, Evans AG, Nardone V. *Metall Trans A* 1991;22A:2107.
43. Angers R, Champagne B, Fiset M, Chollet P. In: Aqua EN, Whitman CI. editors. *Modern Developments in Powder Metallurgy*. (NJ): Metal Powder Industries Federation; 1985. Vol. 17, p. 159-175.
44. Champagne B, Angers R, Fiset M. *Int J Refract Hard Met* 1987;6:155.
45. Wu Shang-Xian. In: Underwood JH, Freiman SW, and Baratta RI. editors. *Chevron-Notched Specimens: Testing and Stress Analysis*, ASTM STP 855. Philadelphia (PA): American Society for Testing and Materials; 1984. p. 176-192.
46. ASTM Standard B611. In: Allen RF, et al., editors. *Annual Book of ASTM Standards*, Vol. 02.05. West Conshohocken (PA): American Society for Testing and Materials; 1999. p. 327-328.
47. ASTM Standard G65. In: Allen R. F., et al., editors. *Annual Book of ASTM Standards*, Vol. 03.02. West Conshohocken (PA): American Society for Testing and Materials; 1999. p. 245-256.
48. ASTM Standard C1161. In: Azara JC, et al., editors. *Annual Book of ASTM Standards*, Vol. 15.01. West Conshohocken (PA): ASTM; 1997. p. 309-315.
49. ASTM Standard E1876. In: Azara JC, et al., editors. *Annual Book of ASTM Standards*, Vol. 15.01. West Conshohocken (PA): American Society for Testing and Materials; 1997. p. 1046-1054.
50. Koopman M, Chawla KK, Coffin C, Patterson BR, Deng X, Patel BV, Fang Z, Lockwood G. *Advanced Engineering Materials* 2002;4:37.
51. Hilliard JE. In: Dehoff RT, Rhines FN. editors. *Quantitative Microscopy*. New York: McGraw-Hill Book Company; 1968. p. 45-76.
52. Underwood EE. In: Dehoff RT, Rhines FN. editors. *Quantitative Microscopy*. New York: McGraw-Hill Book Company; 1968. p. 151-200.

53. Chou YT. *J Appl Phys* 1966;37:2425.
54. Meyers MA, Chawla KK. *Mechanical Behavior of Materials*. Upper Saddle River (NJ): Prentice Hall; 1999. p. 359.
55. Patel BV. Unpublished data.

**GRADUATE SCHOOL
UNIVERSITY OF ALABAMA AT BIRMINGHAM
DISSERTATION APPROVAL FORM
DOCTOR OF PHILOSOPHY**

Name of Candidate Xin Deng

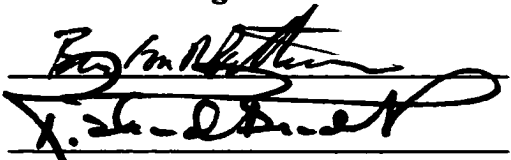



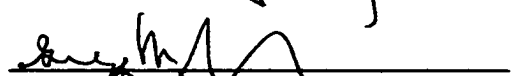

Graduate Program Materials Engineering

Title of Dissertation Double Cemented Carbide:

Microstructure-Property Relationships

I certify that I have read this document and examined the student regarding its content. In my opinion, this dissertation conforms to acceptable standards of scholarly presentation and is adequate in scope and quality, and the attainments of this student are such that he may be recommended for the degree of Doctor of Philosophy.

Dissertation Committee:

| Name | Signature |
|------------------------------------|--|
| <u>Burton R. Patterson</u> , Chair |  |
| <u>Richard Bradt</u> |  |
| <u>Krishan K. Chawla</u> |  |
| <u>Alan W. Eberhardt</u> |  |
| <u>Zhigang Fang</u> |  |
| <u>Gregg M. Janowski</u> |  |

Director of Graduate Program Berry Anderson

Dean, UAB Graduate School Joan Loden

Date 2/5/2003